Triplet Superfluidity in Quasi-one-dimensional Conductors and Ultra-cold Fermi Gases

A Thesis
Presented to
The Academic Faculty

by

Wei Zhang

In Partial Fulfillment
of the Requirements for the Degree
Doctor of Philosophy

School of Physics
Georgia Institute of Technology
December 2006

Triplet Superfluidity in Quasi-one-dimensional Conductors and Ultra-cold Fermi Gases

Approved by:

Professor Carlos Sá de Melo, Advisor
School of Physics
Georgia Institute of Technology

Professor T. A. Brian Kennedy
School of Physics
Georgia Institute of Technology

Professor Dragomir Davidovic
School of Physics
Georgia Institute of Technology

Professor Chandra Raman
School of Physics
Georgia Institute of Technology

Professor Stavros Garoufalidis
School of Mathematics
Georgia Institute of Technology

Date Approved: September 7, 2006

To my beloved wife Liu,

and my parents, Fan and Ping,

for their constant encouragement and support over the years.

ACKNOWLEDGEMENTS

First, I would like to thank my advisor Prof. Carlos Sá de Melo, and other members in my thesis committee: Prof. Dragomir Davidovic, Prof. T. A. Brian Kennedy, Prof. Chandra Raman in School of Physics, and Prof. Stavros Garoufalidis in School of Mathematics.

It is always my pleasure to pursue my graduate studies in Georgia Tech, where I had the opportunity to work directly with and learn from a group of very talented scientists. In particular, Carlos provided me with an exceptional model of a theoretical physicist. Carlos is a great thinker. His abilities allow him to generate many interesting ideas and possible pathways towards them almost simultaneously, as well as to debug some technical difficulties in a mess of formulae. Carlos is also a very good advisor. He provides me time to clear my mind and room for creativity such that I always had a say in what I was working on. As a graduate student of Carlos, I shall never forget the time he spent to teach me how to think, work, and talk as a physicist. In addition, my master advisor in mathematics Prof. Stavros Garoufalidis helps me a lot about mathematics, which is invaluable for a theoretical physicist. Most importantly, his rigorous working style shows me a perfect example of how to organize ideas, works, as well as my office.

I would like to thank the other two graduate students in our group, Sergio Botelho and Menderes Iskin. Although we did not collaborate in a same research topic, the numerous discussions with them are always delightful and helpful. In addition, Sergio helped me a lot on computer and programming problems. I still feel sorry for knocking his office door three times in a same day to ask the same command in Linux just because I kept forgetting it. I also thank Miles Stoudemire, Robert Cherng and Philip Powell for their collaboration and discussion. They are very gifted students and I am sure they will do great work in their graduate studies.

Georgia Tech is full of so many other people that I have come to know well, I could not list all their names. However I would like to single out Jiang Xiao. Jiang is my classmate

since 1997. We are very good friends and had a lot of discussions about physical and non-physical problems. Jiang is also a very good listener of my presentation. After explaining my research to him and answering all his questions, I finally realized an invited talk is not so hard.

I would also like to express my thanks to the ones who are important to me, but are not directly related to my graduate studies. My parents and my wife constantly encourage me to pursue my goals and support my own decisions. They shared with all my experience in the past five years. I always feel their generous love. Most responsible for stimulating my interests about physics was Long Han, my physics teacher in Yaohua High School. I always appreciate his effort of delicately planning curriculum, designing experiments, and setting up observatory. I would also like to thank Han Zhang, my undergraduate advisor in Peking University. He taught me a lot about condensed matter experiments, which are proved to be very useful for a theorist to build a common sense about what can be done in the real world.

Finally, I would like to thank Gilbert F. Amelio for his generosity to provide me financial support. Research discussed in this thesis are supported by National Science Foundation (Grant No. DMR-0304380).

TABLE OF CONTENTS

LIST OF FIGURES

SUMMARY

This thesis presents theoretical investigations of triplet superfluidity (triplet superconductivity) in quasi-one-dimensional organic conductors and ultra-cold Fermi gases. Triplet superfluidity is different from its s-wave singlet counterpart since the order parameter is a complex vector and the interaction between fermions is in general anisotropic. Because of these distinctions, triplet superfluids have different physical properties in comparison to the s-wave case. The author discusses in this thesis the interplay between triplet superconductivity and spin density waves in quasi-one-dimensional organic conductors, and proposes a coexistence region of the two orders. Within the coexistence region, the interaction between the two order parameters acquires a vector structure, and induces an anomalous magnetic field effect. Furthermore, the author analyzes the matter-wave interference between two p-wave Fermi condensates, and proposes a polarization effect. For a single harmonically trapped p-wave Fermi condensate, the author also shows that the expansion upon release from the trap can be anisotropic, which reflects the anisotropy of the p-wave interaction.

CHAPTER I

INTRODUCTION

1.1 Brief History of Superfluidity

The original observation of the phenomenon known as *superfluidity* in liquid Helium-4 was made in 1938 by Kapitza in Moscow [1], and Allen and Misener in Cambridge [2]. Stimulated by measurements that seemed to show that below a characteristic temperature ($\sim$2.17 K, known as the *lambda* temperature) the heat flow was not simply proportional to the temperature gradient, Kapitza, as well as Allen and Misener, decided to measure the resistance to the flow of liquid helium clamped in narrow channels and subjected to a pressure drop. They found that liquid Helium-4 flowed so easily below the lambda temperature that the viscosity would be at least a factor of 1500 smaller than its value above the lambda temperature. It was this peculiar behavior for which Kapitza coined the term *superfluidity* [1].

Only a few months after the experimental observations, Fritz London suggested that the anomalous properties of liquid helium below the lambda temperature (the so-called He-II phase) could be related to the degeneracy of particles obeying Bose statistics at low temperatures [3]. This low temperature degeneracy was first studied by Bose [4] and Einstein [5] in non-interacting gases. They found that below a critical temperature which depends on the mass and density, a finite fraction of all the atoms (and at zero temperature, all of them) should occupy a single quantum state. This quantum degeneracy is known nowadays as Bose-Einstein condensation (BEC). Very soon thereafter Laszlo Tisza [6] pushed the idea a step further by suggesting that the anomalous flow behavior seen in the He-II phase could be qualitatively understood within a "two-fluid" model in which the "condensate" (i.e., those atoms which occupy the single quantum state) behaves like a frictionless liquid, while the rest behaves like an ordinary liquid.

This qualitative "two-fluid" model was improved by Lev Landau [7] in a seminal paper published in 1941. In this paper, Landau classified the excitations of the Bose liquid into

two types: sound waves or "phonons" with linear dispersion relation ($\epsilon = cp$, c is the speed of sound), and "rotons" which corresponds to rotational motion. In order to understand the flow and thermodynamic properties of He-II, Landau assumed that it consisted of two components: the "superfluid" component, which was the part of the liquid that remained in its ground state, and a "normal" component, which corresponded to excitations. The superfluid component was conceived as carrying zero entropy and having irrotational flow, while the normal component behaved like any other viscous liquid. From these minimal postulates Landau derived a theory of two-fluid hydrodynamics, which explained, and most remarkably predicted many experimental results quantitatively.

Needless to say, Landau's theory of two-fluid hydrodynamics provided a landmark in the understanding of superfluidity. However, the theory is phenomenological in the sense that both the properties of the superfluid component and the nature of the excitation spectrum were postulated in an intuitive way instead of being derived from a microscopic model. Along this path, F. London [3] suggested that the superfluidity in ^{4}He might be related to BEC, but microscopic calculations were lacking until the seminal paper published in 1947 by N. N. Bogoliubov [8]. In that paper, Bogoliubov considered a dilute gas of atoms obeying Bose statistics and interacting via an interatomic potential, which was weakly repulsive. Assuming the existence of BEC in such an interacting Bose system, he showed that the energy spectrum for large momentum p corresponded approximately to the simple excitation of free atoms from the condensates [$\epsilon(p) = p^2/2m$], while at smaller momenta it had precisely the phonon-like form $\epsilon(p) = cp$ postulated by Landau. However, in Bogoliubov's work there is no obvious trace of the second, "roton" branch of the excitation spectrum postulated by Landau.

While Bogoliubov's results were very suggestive, they referred to a dilute system, which was rather far from the condition in real-life liquid helium. This gap is filled in 1956 by Feynman and Cohen [9], who predicted that the excitation spectrum of real liquid He-II should crossover from the "phonon-like" behavior at small momenta to a "roton-like" form $\epsilon(p) = \Delta + (p - p_0)^2/2m$ at larger momenta. Actually, this dispersion relation first postulated by Landau was seen in neutron scattering experiment of the early 1950s [10].

Another key point in Bogoliubov's paper was that he assumed *a priori* that an interacting Bose system would undergo BEC like the non-interacting ideal Bose gas. However, the interacting Bose problem is far more complicated then he assumed. First, for a general Bose system, there is no systematic method (at least to my knowledge) to predict whether there would be macroscopic occupation of *any* quantum state at zero temperature, i.e., the zero-temperature phase diagram of ^{4}He of interacting strength is still an open question. In fact, one can start from the BEC state of the non-interacting ideal Bose gas and perform perturbation theory in the interatomic interactions to derive a finite value (generally less than 100%) of the condensate fraction in thermal equilibrium. However, this approach is apparently limited. Another question is why, given that macroscopic occupation occurs, it occurs only in a *single* quantum state. It can be shown that at least within the Hartree-Fock approximation, macroscopic occupation of more than one state is always energetically unfavorable provided the effective low-energy interaction is *repulsive*, as is believe to be the case for ^{4}He. However, For the case of an attractive interaction the problem is complicated.

All the above theoretical progresses, as well as other important advances made thereafter, provide the our current understanding of the liquid Helium-4 below the lambda temperature. However, that is not the end of the story. In 1972 it was discovered that the light isotope of helium (^{3}He) possesses two anomalous phases (known as ^{3}He-A and ^{3}He-B) below the temperature of 3 mK [11, 12]. Each of the two phases displays most of the properties expected of a superfluid, so these phases are collectively described as "superfluid helium-3". In this case, since the ^{3}He atom obeys Fermi rather than Bose statistics, the mechanism of superfluidity cannot be simply BEC as in ^{4}He. Rather, just as in metallic superconductors, the fermions pair up to form "Cooper pairs", having characteristic size which is much larger than the typical interatomic distance.

The connection between superfluidity and superconductivity was initially suggested before the discovery of superfluid ^{3}He, and was clearly stated in F. London's two-volume book "*Superfluidity*" (1950), where both superfluidity and superconductivity are discussed [13]. Very soon after the papers of Bardeen, Cooper, and Schrieffer (1957) [14] and Bogoliubov (1958) [15] where a microscopic theory of superconductivity is proposed, it was realized that

the phenomenon of Cooper pairing should not be restricted to electrons but could well occur in other highly degenerate systems of fermions, e.g., liquid ^{3}He. However, since ^{3}He atoms are neutral, they could not show anomalous electrical properties like the zero resistance and Meisner effect in superconductors; but they should show the corresponding anomalous mass flow properties, i.e., the superfluidity. Moreover, the BCS theory of electrons in superconductors describes pairs with relative angular momentum zero, while in ^{3}He this would be prevented by the strong hard-core repulsions, and therefore Cooper pairing was likely to be in a state with finite angular momentum. Such a state would have an anisotropic pair wave function and thus anisotropic properties. This expectation was proved soon after the discovery of the A and B phases of superfluid ^{3}He, and further experimental investigation strongly supported the idea that the Cooper pairs are in a triplet state, instead of a singlet state in the ordinary BCS theory of superconductors. In this triplet state, the Cooper pairs have an additional internal degrees of freedom, as well as their center-of-mass degree of freedom. For instance, they possess total spin $S = 1$ and also "intrinsic" orbital angular momentum $L = 1, 3...$, which corresponds to p-wave, f-wave, etc. The corresponding order parameter thus acquires a vector form. This internal degree of freedom is absent for the Cooper pairs in *conventional* superconductors with $L = S = 0$. However, it was suggested that a triplet state can be found in some *unconventional* superconductors including ruthenates and organic conductors, which will be discussed next.

1.2 Triplet Superconductors

After the discovery of superfluid liquid ^{3}He in the early 1970's the search for triplet superconductivity was intensified. Experimentalists and theorists have looked at several possibilities including heavy fermion, oxide, and organic superconductors. Here, I concentrate on organic superconductors of the Bechgaard salt family. Excellent reviews exist in the literature regarding triplet superconductivity in heavy fermion [16, 17], and oxide (Sr_2RuO_4) [18] systems.

Just after the discovery of the first organic superconductor $(TMTSF)_2PF_6$ by Jerome *et al.* [19] in 1980, it became clear that quasi-one-dimensional (quasi-1D) organic materials

$(TMTSF)_2X$ and $(TMTTF)_2X$ (where $X = PF_6, ClO_4 \ldots$ is an anion), known as Bechgaard salts, were very unusual materials. A couple of years later, it was found that superconductivity in these compounds was rapidly destroyed by non-magnetic defects [20, 21, 22, 23, 24]. Soon after these experiments, Abrikosov [25] pointed out that the strong suppression of the critical temperature in the presence of non-magnetic defects could be reasonably explained under the assumption of triplet pairing. This initial suggestion by Abrikosov was later reinforced by Gorkov and Jerome [26] in their analysis of upper critical field measurements by Brussetti *et al.* [27], and Ishiguro *et al.* [28]. Gorkov and Jerome suggested that the upper critical field along the **a** direction $H_{c_2}^a$ seemed to exceed the Pauli paramagnetic limit [29, 30] $\mu_B H_P(T=0) \approx 1.84 T_c(H=0)$ by a factor of 2. This opened the possibility of triplet superconductivity, because the spin-orbit coupling in these systems was too small to account for a large violation of the Clogston limit. Further experimental evidence of unusual behavior in these systems was reported in 1987 by Takigawa *et al.* [31]. They reported the absence of the Hebel–Slichter peak [32] in the proton spin-lattice relaxation time $(1/T_1)$ data of $(TMTSF)_2ClO_4$ and a $1/T_1 \propto T^3$ temperature dependence in the region of $T_c/2 < T < T_c$. These early results were interpreted by Hasegawa and Fukuyama [33] as evidence for the existence of zeros of the superconducting order parameter on the quasi-1D Fermi surface. Hasegawa and Fukuyama also emphasized that these early experiments probed essentially the orbital part of the order parameter, and could not directly distinguish between singlet or triplet pairing.

An early suggestion by Lebed [34], Burlachkov, Gorkov and Lebed (BGL) [35], and later by Dupuis, Montambaux, and Sá de Melo (DMS) [36], indicated that singlet and triplet pairing in quasi-1D superconductors could be tested in a measurement of upper critical fields. These authors found that the upper critical field for a triplet superconductor would exceed substantially the Pauli paramagnetic limit and produce a reentrant phase at high fields. This reentrant phase has increasing critical temperature with magnetic field, and is paramagnetic instead of diamagnetic [37, 38]. Lee *et al.* [39] started a systematic experimental search for triplet superconductivity in $(TMTSF)_2ClO_4$ via resistive measurements of $H_{c_2}(T)$ for fields parallel to the $\mathbf{b}'$ direction. Their results suggested (i) the survival of

superconductivity beyond the Pauli paramagnetic limit, and (ii) possible reentrant superconductivity at high magnetic fields without a magnetic superconductor [40]. Intrigued by these exciting possibilities, Lee *et al.* [41] decided to explore the phase diagram of another quasi-1D superconductor, the sister compound $(TMTSF)_2PF_6$.

Unlike $(TMTSF)_2ClO_4$, $(TMTSF)_2PF_6$ is not superconducting at ambient pressure, instead it undergoes a metal–insulator transition at 12 K. The insulating phase can be suppressed through the application of hydrostatic pressure above 5 kbar. The system then becomes superconducting with a maximum T_c around 1.2 K. (Various insulator–superconductor transition pressures were reported by different groups, due to experimental details of pressure cell calibration.) Keeping an optimized pressure of 6 kbar (or 9 kbar from another experimental group [19]) in order to maximize the superconducting critical temperature, Lee *et al.* [41] established that the upper critical fields along the $\mathbf{a}$ and $\mathbf{b}'$ directions (i) present a strong upward curvature, (ii) well exceed the Pauli paramagnetic limit, and (iii) have an unusual anisotropy inversion around 1.6 T. In addition to these upper critical field measurements, Belin and Behnia [42] measured the thermal conductivity of $(TMTSF)_2ClO_4$ at zero and low magnetic fields. The thermal conductivity seemed to be exponentially activated at low temperatures indicating the existence of a full gap in the quasiparticle excitation spectrum. Assuming that similar physics holds for $(TMTSF)_2ClO_4$ and $(TMTSF)_2PF_6$, these initial experiments combined were suggestive of a triplet superconducting phase with a fully gapped quasiparticle excitation spectrum.

After these experiments further theoretical studies were necessary to explain the experimental data. From the observation of a strong upward curvature in $H_{c_2}(T)$ for $(TMTSF)_2ClO_4$ and $(TMTSF)_2PF_6$ when the magnetic field was applied along the $\mathbf{b}'$ direction, it seemed natural to make a connection to the theory of Klemm, Luther, and Beasley (KLB) [43]. In this theory, the strong upward curvature of H_{c_2} when a magnetic field is aligned parallel to the layers in a layered superconductor is explained by a temperature-induced dimensional crossover (TIDC). The upward curvature is most pronounced when spin-orbit scattering is severe ($\gamma_{so} = \tau_{so} T_c \ll 1$), and the interlayer coupling is weak, $r \geq 1$, with $r = 2c/\pi\xi_\perp(0)$. The theory of KLB was applied successfully to layered superconductors [44] such as TaS_2,

$TaSe_2$, and $NbSe_2$. However, this theory may not be applicable to the $(TMTSF)_2X$ system, where the layer spacing $c \approx 13.5$ Å is smaller than the coherence length $\xi_\perp(0) \approx 20$ Å. In addition, spin-orbit effects are very small in $(TMTSF)_2X$ ($X = ClO_4, PF_6$) leading to $\gamma_{so} \approx 100$ (see References [45, 46, 28]), a value at least three orders of magnitude too large. Furthermore, the KLB theory does not include the effects of the quantum ("Landau") level structure in the electronic motion, which are thought to be very important for the existence of superconductivity in $(TMTSF)_2X$ [34, 35, 36, 38] at high magnetic fields and low temperatures.

Although the $H_{c_2}(T)$ measurements in $(TMTSF)_2ClO_4$ [39] and $(TMTSF)_2PF_6$ [41] suggest a triplet pairing state in quasi-1D Bechgaard salts, the singlet possibility cannot be completely ruled out, since no reentrant phase has been observed for these materials. The absence of the theoretically predicted reentrant phase in high magnetic fields could also suggest an spatially inhomogeneous s-wave singlet state discussed by DMS [36], Dupuis and Montambaux (DM) [47], and Dupuis [37], like the one discussed by Larkin and Ovchinikov [48], and Fulde and Ferrel [49] (LOFF). However, Lebed [50] showed that the LOFF state in quasi-1D superconductors is paramagnetically limited for magnetic fields applied along the $\mathbf{b}'$ axis when a more realistic dispersion relation was used. Thus it seems that a triplet state should be favored at least at intermediate and high magnetic fields when considered in competition to singlet (s-wave) spatially inhomogeneous states like the LOFF state.

The triplet state is also favored by Knight shift measurements in $(TMTSF)_2PF_6$ for a magnetic field applied along the $\mathbf{b}'$ axis [51]. These experiments implied that the spin susceptibility is essentially the same as the normal state value. Following these experimental results, Lebed, Machida and Ozaki (LMO) [52] implicitly assumed strong spin-orbit coupling and proposed that the triplet order parameter $\mathbf{d}(\mathbf{k})$ at zero magnetic field is frozen into the crystalline lattice in such a way to produce, at zero temperature, $\chi_{b'}(0) = \chi_n$, and $\chi_a(0) \ll \chi_n$, where χ_n is the normal state uniform susceptibility. A different proposal assuming weak spin-orbit coupling was suggested by Duncan, Vaccarella and Sá de Melo (DVS) [53], and Duncan, Cherng and Sá de Melo (DCS) [54], where the spin susceptibility

tensor and other thermodynamic quantities were calculated for various order parameter symmetries within the orthorhombic group [although $(TMTSF)_2PF_6$ is really a triclinic crystal]. The support for a weak spin-orbit coupling theory in these systems is rooted in the fact that the heaviest element in the material is selenium, and early estimates for the spin-orbit coupling strength are several orders of magnitude smaller [55] than the values required to fit the critical temperature of $(TMTSF)_2PF_6$ [52, 56], for instance, at low magnetic fields. Based on this analysis, DVS and DCS concluded that the fully gapped triplet state $^3B_{3u}(a)$ ("p_x-wave") would produce an experimentally measured spin susceptibility always close to χ_n, which implies that the diagonal components of the uniform spin susceptibility tensor are $\chi_a = \chi_{b'} = \chi_{c^*} \approx \chi_n$, for magnetic fields strong enough to overcome the pinning effect.

The full nature of the superconducting state in Bechgaard salts is yet to be revealed. There are pending issues that still need to be addressed. For instance, the exact symmetry of the superconducting order parameter and the pairing mechanism for superconductivity are still not understood. In a recent effort, Kuroki, Arita and Aoki (KAA) [57] examined the influence of charge and anisotropic spin fluctuation exchanges in the pairing stability for $(TMTSF)_2PF_6$, and proposed an f-wave triplet state with **d**-vector perpendicular to the quantization axis. In contrast, Shimahara [58] proposed a nodeless d-wave state for $(TMTSF)_2ClO_4$ based in part on the thermal conductivity measurements of Belin and Behnia [42]. These two proposals, combined with the suggestions of triplet superconductivity of Lebed [34], BGL [35], and DMS [36], add to the debate about the symmetry of order parameter and the mechanism of superconductivity in quasi-1D Bechgaard salts. *Prima facie* the symmetry of the order parameter should be the same for both compounds, given the strong electronic and structural similarities. However, there are neither thermal conductivity measurements in $(TMTSF)_2PF_6$ nor NMR experiments in $(TMTSF)_2ClO_4$ up to now, and direct evidence from phase sensitive experiments like the ones performed in high-T_c cuprate superconductors [59, 60, 61] is still lacking. In order to fulfill this gap, Sengupta *et al.* [62], and Vaccarella, Duncan and Sá de Melo (VDS) [63] suggested that tunneling experiments (both single and paired electron processes) could be used to distinguish order parameter symmetries. Although there was a recent attempt to perform tunneling

experiments in $(TMTSF)_2ClO_4$ bi-crystals [64], a direct comparison is still hard to make.

The issue of the angular dependence of the upper critical field is another important question. LMO [52] proposed that the anisotropy inversion in the upper critical fields seen in $(TMTSF)_2PF_6$ was due to a **d**-vector flop transition when an external magnetic field was applied along the **a** direction. However, a theoretical estimate [54] gives a value of the flopping field to be about 0.22 T, nearly one order of magnitude smaller than the anisotropy inversion field $H^* \sim 1.6$ T observed experimentally [41]. Furthermore, NMR experiment [65] also suggested that the flop transition should happen at a magnetic field $H < 1.43$ T $< H^*$. Another possibility is that the anisotropy inversion in $(TMTSF)_2PF_6$ was due to the disappearance of closed orbits present only for fields along the **a** direction, and to a reduction in the degeneracy of states when open-orbit contributions start to dominate. In this case, the anisotropy inversion would be purely orbital in nature, instead of a spin effect as proposed by LMO [52]. However, the angular dependence of the upper critical field of Bechgaard salts in the **a**-**b**$'$ plane at high magnetic fields has not been calculated yet.

In addition to the symmetry of superconducting states in Bechgaard salts $(TMTSF)_2ClO_4$ and $(TMTSF)_2PF_6$, there are more recent experimental works which suggest a possible coexistence region of spin density waves (SDW) and superconductivity in $(TMTSF)_2PF_6$. Some earlier measurements [66, 67] indicated the presence of an inhomogeneous state in the vicinity of critical pressure P_c. Specifically, Azevedo *et al.*[66] found that the quenching of the SDW state was a slow function of pressure from measurements of the Knight shift in ^{77}Se. This was interpreted as an indication of the coexistence of the SDW and metallic states. Lee *et al.* [67] assumed the presence of macroscopic domains of superconducting and insulating SDW states to explain an unusual upper curvature of $H_{c2}^{c^*}(T)$. Recently, transport measurements by Vuletić *et al.* [68] and Kornilov *et al.* [69], and a simultaneous NMR and electrical transport measurements by Lee *et al.* [70] in $(TMTSF)_2PF_6$ all suggest an "inhomogeneous" coexistence region of SDW and Metal (Superconductivity) orders. This coexistence region can be related to existing theoretical proposals. For instance, strictly one dimensional theories invoking SO(4) symmetry [71] or negative interface energies [72] have allowed for coexisting triplet superconductivity and SDW. However, Zhang and Sá

de Melo [73] showed that these theories are not directly applicable to three-dimensional but highly anisotropic Bechgaard salts, where the SO(4) symmetry is absent, and negative interface energies are not necessary conditions for the coexistence.

Setting other Bechgaard salts aside, I believe it is fair to say that the observation of unusual behavior in the upper critical fields [41] and the measurement of the spin susceptibility [65, 51] in $(TMTSF)_2PF_6$ strongly suggest the existence of a non-uniform triplet pairing superconducting state in a magnetic field. This state would reduce at zero field to a triplet phase similar to A-phase [74] of superfluid ^{3}He, apart of course from the group theoretical differences concerning lattice and time reversal in a magnetic field [53, 54]. However, as mentioned above, experiments in these systems are hard to perform so that quantitative comparisons between theoretical and experimental results are still lacking. In fact, this obstacle exists in nearly all solid state or condensed matter systems, where the degrees of freedom of a typical sample are around $10^{19} \sim 10^{23}$ and the controllability is very limited. However, recent experimental realization of Bose and Fermi condensates have allowed for studies of very clean strongly correlated systems with much higher controllability in comparison to standard solid state systems, as will be discussed next.

1.3 Superfluidity in Ultra-Cold Atomic Gases

Although superfluidity in ^{4}He, ^{3}He and superconductors have been extensively studied after their discoveries, a direct observation of BEC in a controllable laboratory system was not made until 1995. BEC was firstly observed in dilute gases of alkali metal atoms [75, 76], and later in dilute hydrogen gases [77], which were confined in magnetic and optical traps. More recently, Fermi superfluids were also realized in ultra-cold alkali gases [78, 79, 80, 81, 82], and were extensively studied.

1.3.1 Bose Systems

The techniques for trapping and cooling atoms had been developed and improved gradually since 1980s (see review articles by Chu [83], Cohen-Tannoudji [84], and Phillips [85]). With current technology, the typical maximum densities of atoms in traps range from $\sim 10^{11}$ to $\sim 10^{16}$ cm^{-3}, which is many orders of magnitude less than the atomic density of ^{4}He-II

(about 2×10^{22} cm^{-3}). Moreover, the atomic masses of the alkalis are much higher than for helium, especially for heavy alkali atoms ^{39}K and ^{87}Rb. Considering the BEC critical temperature T_c for an ideal Bose gas [86]

$$T_c = \frac{2\pi\hbar^2}{k_b m}\left(\frac{n}{2.612}\right)^{2/3}, \tag{1.1}$$

one expects T_c values $10^6 - 10^8$ times smaller than that for ^{4}He. In other words we expect $T_c \sim 10$ nK $- 1$ μK. It is remarkable that the techniques for cooling and trapping atoms with lasers and magnetic traps can now achieve such ultra-low temperatures in laboratory.

Alkali metal and hydrogen atoms are in the first column of the periodic table. They have a single valence electron in the outermost s-orbital, for example $1s$ for hydrogen, $2s$ for lithium, $3s$ for sodium, $4s$ for potassium, or $5s$ for rubidium. The other electrons are in completely full shells (except for H), and as a result they have a total orbital angular momentum and total spin of zero. The only other contribution to the total spin of the atom is the nuclear spin. Thus, if the nuclear isotope is one with an odd number of protons and neutrons it will have a net half-integer spin. For example, ^{7}Li, ^{23}Na, and ^{87}Rb all have $I = 3/2$ nuclei. In these cases, the total spin of an atom, which is the sum of the nuclear spin and the valence electron spin, will be an integer. According to the sum rule of two angular momenta, the total spin of these alkali atoms is either $F = 2$ or $F = 1$. If we can prepare the gas such that only one of these types of states is present, then this will be a gas of identical Bose particles. On the other hand, if atoms in both $F = 2$ and $F = 1$ quantum states are present, then this is effectively a mixture of two different species of bosons, since the two types of atoms are distinguishable from each other.

In order to see how the alkali atoms can be confined in a magneto-optical trap we must understand how the atom interact with electric and magnetic fields. For the interaction with electric fields, the most important effect one needs to consider (in the regime where most experiments are performed) is dipole interaction between the laser field and the electric dipole moment it induces on the atom. Considering only one excited state (usually $2p$ or $3p$ for alkali atoms and $2s$ for hydrogen) and ignoring the fine and hyperfine structures, the

change in energy of the atom in the laser field can be expressed as [87]

$$\Delta E_{\rm laser}(\mathbf{r}) = \frac{I(\mathbf{r})}{I_0}\frac{\Gamma^2}{\Delta}, \tag{1.2}$$

where $I(\mathbf{r})$ and I_0 are laser intensity at position $\mathbf{r}$ and infinity, respectively. Here, $\Gamma = \hbar/\tau$ is the inverse of the excited state life-time τ, and

$$\Delta = \hbar\omega - (E_{np} - E_{ns}) \tag{1.3}$$

is the detuning of the $ns \rightarrow np$ transition frequency. Therefore, a region of high laser intensity provides an attractive potential for $\Delta < 0$ and a repulsive potential for $\Delta > 0$. Using two counter-propagating laser beams, one can produce a potential that varies on the scale of half the lase wavelength, i.e., ~ 3000 Å.

For the interaction with magnetic fields, the energy levels of atoms can also be affected via the hyperfine-Zeeman interactions. For definiteness, here I consider only the alkali atoms who have an spin $I = 3/2$ nucleus. For the states with maximum total spin $F = 2$, there are five different states labeled by their z-component of total spin given by quantum number $M_F = 2, 1, 0, -1, -2$. The wave functions corresponding to these states are [88]

$$\begin{aligned}
|F=2, M_F=2\rangle &= \left|\frac{3}{2}, \frac{1}{2}\right\rangle, \\
|F=2, M_F=1\rangle &= \frac{1}{2}\left[\sqrt{3}\left|\frac{1}{2}, \frac{1}{2}\right\rangle + \left|\frac{3}{2}, -\frac{1}{2}\right\rangle\right], \\
|F=2, M_F=0\rangle &= \frac{1}{\sqrt{2}}\left[\left|\frac{1}{2}, -\frac{1}{2}\right\rangle + \left|-\frac{1}{2}, \frac{1}{2}\right\rangle\right], \\
|F=2, M_F=-1\rangle &= \frac{1}{2}\left[\sqrt{3}\left|-\frac{1}{2}, -\frac{1}{2}\right\rangle + \left|-\frac{3}{2}, \frac{1}{2}\right\rangle\right], \\
|F=2, M_F=-2\rangle &= \left|-\frac{3}{2}, -\frac{1}{2}\right\rangle,
\end{aligned} \tag{1.4}$$

where the notation $|m_I, m_S\rangle$ is used to denote the state where the nuclei is in state m_L and the electron is in state m_S. Similarly, there are three different states with total spin $F = 1$, corresponding to $M_F = 1, 0, -1$ with the wave functions

$$\begin{aligned}
|F=1, M_F=1\rangle &= \frac{1}{2}\left[\left|\frac{1}{2}, \frac{1}{2}\right\rangle - \sqrt{3}\left|\frac{3}{2}, -\frac{1}{2}\right\rangle\right], \\
|F=1, M_F=0\rangle &= \frac{1}{\sqrt{2}}\left[\left|\frac{1}{2}, -\frac{1}{2}\right\rangle - \left|-\frac{1}{2}, \frac{1}{2}\right\rangle\right], \\
|F=1, M_F=-1\rangle &= \frac{1}{2}\left[\left|-\frac{1}{2}, -\frac{1}{2}\right\rangle - \sqrt{3}\left|-\frac{3}{2}, \frac{1}{2}\right\rangle\right].
\end{aligned} \tag{1.5}$$

In zero magnetic field the $F = 2$ and $F = 1$ states have slightly different energies due to the weak hyperfine interaction between the nucleus and the valence electron, while within each group the states with different M_F values are degenerate. The application of a finite magnetic field produces the Zeeman coupling which split these degenerate states as shown in the second term of the following effective Hamiltonian,

$$\mathcal{H} = A\hat{\mathbf{I}} \cdot \hat{\mathbf{S}} + g\mu_B \hat{S}_z B_z, \tag{1.6}$$

where A is the hyperfine interaction, g is the gyromagnetic factor of the valence electron, $\mu_B = e\hbar/2m_e$ is the Bohr magneton, and B_z is the magnetic field which is assumed to be along the z-direction. In writing this Hamiltonian the Zeeman coupling to the magnetic moment of the nucleus was neglected, since it is much smaller than that of the valence electron. The energies of the various hyperfine states of this Hamiltonian are given as functions of the magnetic field B. It is convenient to choose the zero of energy to be the average of zero-field $E(F = 2)$ and $E(F = 1)$ energies, and it is not difficult to show that the zero-field splitting $E(F = 2) - E(F = 1)$ is $2A$. By introducing a characteristic hyperfine "crossover" field $B_{\rm hf} = A/|\mu_B|$, the energies of the various levels are given as follows [89]

$$\begin{array}{ccc} M_F & F & E(B) \\ 2 & 2 & A(1 + B/B_{\rm hf}), \\ 1 & \left\{ \begin{array}{c} 2 \\ \\ 1 \end{array} \right\} & \pm A[1 + B/B_{\rm hf} + (B/B_{\rm hf})^2]^{1/2}, \\ 0 & \left\{ \begin{array}{c} 2 \\ \\ 1 \end{array} \right\} & \pm A[1 + (B/B_{\rm hf})^2]^{1/2}, \\ -1 & \left\{ \begin{array}{c} 2 \\ \\ 1 \end{array} \right\} & \pm A[1 - B/B_{\rm hf} + (B/B_{\rm hf})^2]^{1/2}, \\ -2 & 2 & A(1 - B/B_{\rm hf}), \end{array} \tag{1.7}$$

where the plus sign corresponds to $F = 2$ and the minus sign to $F = 1$. A graph of these eigenvalues versus B is shown in Fig. 1.1.

This magnetic field dependence of the energies can be exploited in a magnetic atom trap. Since a magnetic field $\mathbf{B}(\mathbf{r})$ is curl-free and divergence-free in a region of free space,

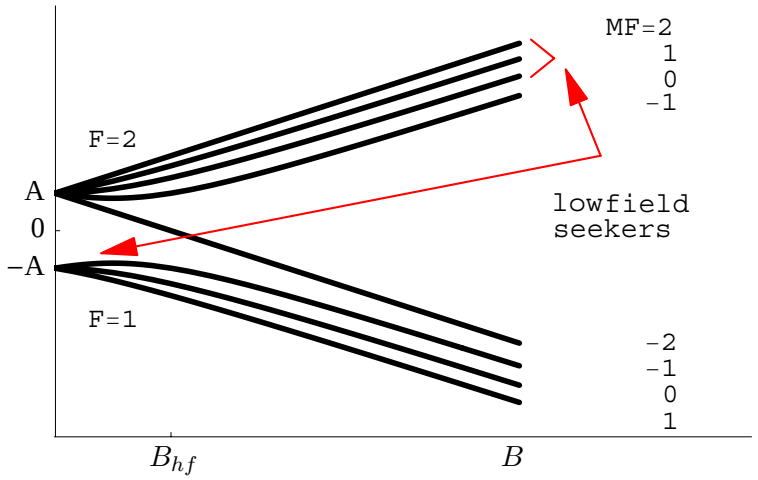

Figure 1.1: The energies of different hyperfine states as a function of magnetic field.

(i.e., no source present), it is forbidden that the magnitude of the magnetic field to have a global maximum or minimum. Furthermore, the magnetic analog of Earnshaw's theorem forbids the magnitude of $|\mathbf{B}(\mathbf{r})|$ to have a local maximum. Fortunately, nothing forbids the occurrence of a local minimum, and various methods can be used to provide such a minimum, for example, the "time-orbiting potential" and Ioffe-Pritchard traps [90, 91]. Thus, if we prepare an atom in a quantum state such as $(F = 2, M_F = 2)$, then it will lower its energy by moving toward a region of smaller magnetic field and thus be attracted into the magnetic trap, which will appear to the atom as a local minimum in potential energy. Notice that this potential well is only a local minimum, so atoms which have too much kinetic energy, that is, are too "hot", will not be bound by the trap and will escape; while atoms have less kinetic energy, that is, are "cold", will be bound.

Up to date, most non-laser-assisted magnetic traps used in BEC experiments have axial symmetry and a finite offset field, i.e., with an appropriate choice of a cylindrical polar coordinate system the magnitude of field has the form

$$|\mathbf{B}(\mathbf{r})| = B_0 + \frac{1}{2}\alpha\rho^2 + \frac{1}{2}\beta z^2. \tag{1.8}$$

Furthermore, in most BEC experiments the fields used are much less than $B_{\rm hf}$ in the relevant region of space. Then it is usually legitimate to linearize Eq. (1.7) in B, leading to

$$E(B) \approx \pm\left[A + \frac{1}{2}|\mu_B|M_F B\right], \tag{1.9}$$

where the $+(-)$ sign refers to the $F = 2$ ($F = 1$) states. Thus in a field configuration of the form (1.8), the states ($F = 2,\ M_F = -2, -1$) and ($F = 1,\ M_F = 1, 0$) will be expelled from the trap. On the other hand, the states ($F = 2, M_F = 2, 1, 0$) and ($F = 1, M_F = -1$) will be attracted to the origin and are called "low-field seekers" [89].

Unlike the ideal Bose gas, the alkali atoms in a magneto-optical trap do interact with each other. In fact the interactions can be quite strong, since the atoms strongly repel each other at short distances. Also, at large interatomic distances there is a van der Waals attraction force between the atoms, which would eventually lead trapped atoms to bind together into atomic clusters. But fortunately the rate at which this happens is very slow, since collisions between the atoms are almost entirely *two-body* collisions between pairs of atoms, and these elastic collisions cannot form bound states. Binding can only be possible in a *three-body* collision in which one pair of atoms could form a bound state, while the excess kinetic energy is carried off by the third atom. However, in a typical BEC experiment, the trapped Bose gas is so dilute that the three-body process is extremely rare, and it is possible to maintain the atoms in the trap for a reasonably long time from a few seconds to a few minutes. For comparison, experiments are usually done in a micro-second scale, which is much shorter than the system's life-time.

On the other hand, the two-body collisions between particles are not entirely negligible. First, it is important to note that the two-body collisions do not allow transitions between the different hyperfine quantum states in Fig. 1.1. Therefore particles prepared in one of the low-field seeker states will remain in the same state. Second, the interparticle interactions contribute to the overall potential energy of the atoms in the trap, and have non-trivial effect on the BEC properties [92]. Finally, pairwise interparticle interactions are also necessary to establish thermal equilibrium within the timescale of the experiment.

The interatomic pair interactions can be treated by the standard scattering theory [93]. In the limit where the interaction range is much smaller than the interparticle separation, which is valid in most BEC experiments, the interaction potential can be approximated by a Dirac-delta function

$$V(\mathbf{r}_1 - \mathbf{r}_2) \approx g\delta(\mathbf{r}_1 - \mathbf{r}_2). \tag{1.10}$$

Here, g is the characteristic strength and can be expressed in terms of the two-body s-wave scattering length a_s through the relation

$$g = \frac{4\pi a_s \hbar^2}{m}. \tag{1.11}$$

An amazing experimental achievement is that this interatomic interactions can be tuned [94, 95]. Thus, the ultra-cold alkali gases are ideal laboratory systems to study theoretical problems. For example, a phase transition to the highly-correlated Mott insulator state was observed through studies of quantum gases in optical lattices [96]. This controllability, however, is rarely existed in solid state materials.

1.3.2 Fermi Systems

More recently, the techniques used to create alkali BECs were applied to Fermi systems. To create a Fermi gas of atoms, the same cooling techniques as those used to achieve BEC were applied to particles obeying Fermi statistics. For instance, the isotopes ^{6}Li and ^{40}K are commonly used in current experiments. However, due to the Fermi statistics the s-wave collisions required for evaporative cooling are not present at ultra-cold temperatures in a gas of identical fermions. The solution to this problem was to introduce a second particle for the evaporative cooling, either another state of the fermionic atom or another species of particles. The first gas of fermionic atoms to enter the quantum degenerate regime was created at JILA in 1999 using ^{40}K [97]. In the next couple of years, many more Fermi gas experiments followed using a variety of cooling techniques [98, 99, 100, 101, 102, 103, 104, 105, 106].

After the realization of ultra-cold Fermi gases, the next goal was to achieve superfluidity of paired fermions. In conventional superconductors, the s-wave pairing process happens between spin-up and spin-down electrons with the same Fermi energy. Presumably, the same pairing process could also occur with the creation of a two-component atomic gas with equal Fermi energies. Such a two-component gas can be realized using an equal mixture of alkali atoms in two different hyperfine states. Thus, s-wave superfluidity could emerge if the temperature of this two-component gas was cold enough as well as the interaction strength between fermions is sufficiently attractive. However, for typical interactions within the

temperature required to reach the superfluidity was far too low compared to the achievable temperature at that time. In order to overcome this experimental difficulty, Stoof *et al.* noted that the interaction between ^{6}Li atoms was large compared to typical values ($|a| \approx 2000a_0$), as well as attractive, bringing the BCS transition temperature closer to realistic temperatures [107, 108]. It was then recognized that a type of scattering resonance, known as a Feshbach resonance, could allow arbitrary changes in the interaction strength [109, 110, 111].

Feshbach resonances were first predicted theoretically in the ^{6}Li and in the ^{40}K systems [112, 113], and were observed experimentally by many groups [114, 115, 116, 117]. Using these s-wave Feshbach resonances, experimentalists can reversibly convert Fermi gases into systems of diatomic molecules [118, 119, 120, 121]. The observation that these molecules were surprisingly long-lived created many opportunities for further study [119, 120, 121, 122]. Eventually, condensates of these diatomic molecules were achieved [78, 79, 80, 81, 82], and were extensively studied including measurements of collective excitations [123, 124, 125], thermodynamic properties [104, 81, 126, 127], the nature of the pairs [82, 128, 129], and the vortex structure [130].

In addition to the condensate of s-wave paired fermions, which is in analogy to the conventional superconductors, in principle, Fermi systems can also form another kind of condensate corresponding to unconventional superconductors. For instance, the fermions can be paired through the non-zero angular momentum channel such as p-wave ($L = 1$) and d-wave ($L = 2$), and possibly form a p-wave or d-wave Fermi condensate. As in the s-wave case, the Feshbach resonance for p-wave pairing was observed in ^{6}Li and ^{40}K systems [117, 131, 132, 133, 134]. For Feshbach resonances currently tried, the molecules were not long-lived and atom losses were significant due to dipole interaction and three body processes. However, other unexplored Feshbach resonances may show less dramatic losses and lead to the possibility of surpassing these experimental difficulties.

Although p-wave Fermi condensates are not available so far, there exists already some theoretical investigations about this "unconventional" superfluidity in ultra-cold Fermi

gases. For instance, it was shown that the so-called BCS–BEC evolution becomes a second order phase transition in p-wave (and actually all non-zero angular momentum) Fermi condensates, while it is only a crossover in the s-wave case [135, 136, 137, 138, 139, 140].

The research of ultra-cold Fermi gases is partially motivated from the idea of creating a very clean strongly correlated Fermi system with the controllability which is absent in solid state samples. In principle the density and two-fermion interactions can be fully controlled, and as a result, physics properties can be studied as a function of density and interaction strength. Further details of ultra-cold Fermi gases would be described in Chap. 2.

1.4 Summary

Superfluidity, superconductivity and Bose-Einstein condensation are among the most fascinating phenomena in nature. Their strange and often surprising properties are direct consequences of quantum mechanics. However, while most other quantum effects only appear in matter on the atomic or subatomic scale, superfluids and superconductors show the effects of quantum mechanics acting on the bulk properties of matter on a large scale. In essence they are macroscopic quantum phenomena. As discussed in the previous sections, superconductivity, superfluidity in ^{3}He, and in atomic Fermi condensates have a great deal in common with each other. Therefore, I will denote these phenomena by the same term "superfluidity" throughout this thesis, as used in the title.

Although for systems discussed in this thesis (quasi-one-dimensional superconductors and interacting Fermi gases), superfluidity, superconductivity and BEC of paired fermions are related phenomena, it should be stated clearly that BEC and superfluidity are actually independent concepts. In particular, it can be shown that BEC in an ideal Bose gas (no interaction) is not a superfluid. When there are no interactions the critical velocity for superfluid flow is zero. It is only when the interactions are finite that it becomes possible to sustain a true superfluid state, for example, to have a liquid that can flow with zero viscosity and sustain persistent currents which are unaffected by external perturbations. On the other hand, it is well known that superfluidity can be held in two-dimensional systems (Berezinskii-Kosterlitz-Thouless phase [141, 142, 143]), where a true BEC cannot

appear.

In this thesis, I will discuss superfluidity in quasi-1D organic conductors and atomic Fermi condensates, where the fermion pairing happens most likely in the triplet channel. As we shall see, this "unconventional" superfluid behaves very differently from the singlet BCS state. For quasi-1D organic conductors, I will discuss the possibility of coexistence of spin density waves and triplet superconductivity. For atomic Fermi gases, I will show the polarization effect of matter-wave interference, and the anisotropy of a single cloud expansion.

The overall plan of the thesis is as follows. In Chapter 2, I present a general background about superconductivity and introduce the singlet BCS pairing and the generalized triplet unconventional pairing states. Some of the experimental evidence in favor of triplet superconductivity in quasi-1D organic conductors are discussed in Chapter 3, together with theoretical investigations about the possibility of a coexistence phase of spin density waves and triplet superconductivity in Bechgaard salt $(TMTSF)_2PF_6$. Furthermore, I discuss triplet superfluidity in atomic Fermi gases, especially emphasize the polarization effect in matter-wave interference and anisotropic expansion in p-wave Fermi condensate in Chapter 4. Finally, conclusions are presented in Chapter 5, while some detailed technical information are included in Appendices.

CHAPTER II

BACKGROUND

The microscopic description of superfluid Fermi liquids dates back to 1957, when J. Bardeen, L. Cooper, and J. Schrieffer [14] created the successful theory of superconductivity (hereafter labeled by the BCS theory). This theory is based on Cooper's theorem about the instability of the ground state of an electron gas with an arbitrarily small attraction against formation of bound states. In many superconductors, the attraction between electrons is sufficient to overcome the direct Coulomb repulsion because a retardation effect generated by interaction between electrons and vibrations of the crystal lattice (phonons). This attractive interaction is almost isotropic, so that Cooper pairs are formed in a state with zero orbital angular momentum (s-wave pairing). This situation is quite different in superfluid ^{3}He, where Cooper pairing might be due to the interaction between nuclear spins of Helium-3 atoms and fluctuations of the liquid magnetization (paramagnons). The interaction mediated by paramagnons is essentially anisotropic and leads to formation of Cooper pairs with orbital angular momentum $L = 1$ (p-wave pairing). For atomic Fermi gases confined in magneto-optical traps, the interaction strengths in s-wave and p-wave channels can be controlled in laboratory, so that singlet and triplet paired Fermi superfluidity can be selectively created in principle. In this chapter, I will introduce the Cooper problem, the pairing states in singlet and triplet channels, and the Ginzburg–Landau theory of a generalized BCS Hamiltonian.

2.1 Cooper Pairing

Although the nature of attraction between particles may vary considerably, Cooper pairing is a common mechanism responsible for formation of superfluid states in various Fermi systems. The basic idea is that even for a very weakly attractive interaction, the ground state of two fermions above the Fermi sea is unstable against the formation of a bound state. This instability manifests itself as a negative pair binding energy $\Delta < 0$.

Following Cooper [144], I consider the quantum mechanical problem of two electrons at zero temperature. I suppose that the two electrons interact via the potential $V(\mathbf{r}_1 - \mathbf{r}_2)$ independent of their spins, and the presence of other electrons, which occupy all the states below the Fermi energy E_F, manifests themselves only through the Pauli exclusion principle. In order to determine the energy levels and the orbital part of the pair wave function $\Phi(\mathbf{r}_1, \mathbf{r}_2)$, one has to solve the Schrodinger equation

$$-\frac{\hbar^2}{2m}(\nabla_1^2 + \nabla_2^2)\Phi(\mathbf{r}_1, \mathbf{r}_2) + V(\mathbf{r}_1 - \mathbf{r}_2)\Phi(\mathbf{r}_1, \mathbf{r}_2) = (\Delta + 2E_F)\Phi(\mathbf{r}_1, \mathbf{r}_2). \tag{2.1}$$

The solution of this equation can be simplified by transforming the problem first to the center-of-mass and relative coordinates

$$\mathbf{R} = \frac{1}{2}(\mathbf{r}_1 + \mathbf{r}_2), \qquad \mathbf{r} = \mathbf{r}_1 - \mathbf{r_2}, \tag{2.2}$$

and by assuming that the pair wave function is separable

$$\Phi(\mathbf{r}_1, \mathbf{r}_2) \rightarrow \Phi(\mathbf{R}, \mathbf{r}) = \Lambda(\mathbf{R})\psi(\mathbf{r}). \tag{2.3}$$

The Schrodinger equation thus becomes

$$\left[-\frac{\hbar^2}{2M}\nabla_{\mathbf{R}}^2 - \frac{\hbar^2}{2m_0}\nabla_{\mathbf{r}}^2 + V(\mathbf{r})\right]\Lambda(\mathbf{R})\psi(\mathbf{r}) = (\Delta + 2E_F)\Lambda(\mathbf{R})\psi(\mathbf{r}), \tag{2.4}$$

where $M = 2m$ is the pair mass and $m_0 = m/2$ is the reduced mass. Furthermore, if the center of mass is assumed to be at rest, i.e., if the constituent electrons have opposite momenta $\mathbf{k}$ and $-\mathbf{k}$, the coordinate $\mathbf{R}$ in the wave function Φ can be omitted, and the equation (2.4) can be simplified to

$$\left[-\frac{\hbar^2}{2m_0}\nabla_{\mathbf{r}}^2 + V(\mathbf{r})\right]\psi(\mathbf{r}) = (\Delta + 2E_F)\psi(\mathbf{r}). \tag{2.5}$$

Here, I introduce the momentum representation of the wave function

$$\psi(\mathbf{r}) = \frac{A}{(2\pi)^3}\int d^3\mathbf{k} e^{i\mathbf{k}\cdot\mathbf{r}} g(\mathbf{k}), \tag{2.6}$$

where A is the volume of space over which $\psi(\mathbf{r})$ is defined (i.e., the volume of the sample). Substituting this momentum representation into Eq. (2.5), one has

$$\int d^3\mathbf{k}\left[\frac{\hbar^2 k^2}{m} - \Delta - 2E_F\right] e^{i\mathbf{k}\cdot\mathbf{r}} g(\mathbf{k}) + \int d^3\mathbf{k} e^{i\mathbf{k}\cdot\mathbf{r}} V(\mathbf{r}) g(\mathbf{k}) = 0. \tag{2.7}$$

The resulting integral equation is then multiplied by $e^{-i\mathbf{k}'\cdot\mathbf{r}}$ and integrated over spatial coordinate, leading to

$$(2\pi)^3\left[\frac{\hbar^2k^2}{m}-\Delta-2E_F\right]g(\mathbf{k})+A\int d^3\mathbf{k}'V(\mathbf{k}-\mathbf{k}')g(\mathbf{k}')=0. \tag{2.8}$$

The interaction potential

$$V(\mathbf{k}-\mathbf{k}')=\frac{(2\pi)^3}{A}\int d^3\mathbf{r}e^{-i(\mathbf{k}-\mathbf{k}')\cdot\mathbf{r}}V(\mathbf{r}), \tag{2.9}$$

which is a function of the momentum difference, and can be expanded in terms of the spherical harmonic $Y_{\ell m_\ell}(\hat{\mathbf{k}})$ with the orbital angular momentum ℓ and its z-component m_ℓ:

$$V(\mathbf{k}-\mathbf{k}')=\sum_{\ell=0}^{\infty}V_\ell(k,k')\sum_{m_\ell=-\ell}^{\ell}b_{\ell m_\ell}Y_{\ell m_\ell}(\hat{\mathbf{k}})Y^*_{\ell m_\ell}(\hat{\mathbf{k}}'). \tag{2.10}$$

Here, $V_\ell(k,k')$ is assumed to be attractive within a thin layer over the Fermi surface of thickness $\epsilon_\ell \ll E_F$,

$$V_\ell(k,k')=\begin{cases}-V_\ell, & \text{for } E_F<\hbar^2k^2/2m,\hbar^2k'^2/2m<E_F+\epsilon_\ell\\ 0, & \text{otherwise.}\end{cases} \tag{2.11}$$

Therefore, the integration over $d^3\mathbf{k}'$ in Eq. (2.8) is performed over a thin shell region on the Fermi surface,

$$A\int d^3\mathbf{k}'\to\rho_0 2\pi^2\int_0^{\epsilon_\ell}d\varepsilon'\int d\Omega', \tag{2.12}$$

where

$$\rho_0=\frac{mk_F}{2\pi^2\hbar^2} \tag{2.13}$$

is the density of states (DOS) at the Fermi level per spin. Thus, the Schrodinger equation (2.8) becomes

$$\left[\frac{\hbar^2k^2}{m}-\Delta-2E_F\right]g(\mathbf{k})-\rho_0\int_0^{\epsilon_\ell}d\varepsilon'\int\frac{d\Omega'}{4\pi}\sum_{\ell=0}^{\infty}V_\ell\sum_{m_\ell=-\ell}^{\ell}b_{\ell m_\ell}Y_{\ell m_\ell}(\hat{\mathbf{k}})Y^*_{\ell m_\ell}(\hat{\mathbf{k}}')g(\mathbf{k}')=0. \tag{2.14}$$

If the interaction is isotropic, as assumed in the original Cooper problem and conventional superconductors, the expansion coefficient $b_{\ell m_\ell}=1$ is a constant. Thus, one can easily verify that each value of the orbital angular momentum ℓ corresponds to a specific eigenstate

$\{g_\ell(\mathbf{k}), \Delta_\ell\}$ determined by Eq. (2.14). In fact, by substituting the pair wave function in the same spherical harmonic basis

$$g(\mathbf{k}) = \sum_{\ell=0}^{\infty} g_\ell(\mathbf{k}) = \sum_{\ell=0}^{\infty} \sum_{m_\ell=-\ell}^{\ell} a_{\ell m_\ell}(k) Y_{\ell m_\ell}(\hat{\mathbf{k}}) \tag{2.15}$$

in equation (2.14), and using the orthonormal property of the spherical harmonics

$$\int \frac{d\Omega\prime}{4\pi} Y^*_{\ell m_\ell}(\hat{\mathbf{k}}') Y_{\ell' m'_\ell}(\hat{\mathbf{k}}') = \delta_{\ell\ell'}\delta_{m_\ell m'_\ell}, \tag{2.16}$$

one obtains

$$\left[\frac{\hbar^2 k^2}{m} - \Delta_\ell - 2E_F\right] g_\ell(\mathbf{k}) - \rho_0 V_\ell \int_0^{\epsilon_\ell} d\varepsilon g_\ell(\mathbf{k}) = 0. \tag{2.17}$$

Therefore,

$$g_\ell(\mathbf{k}) = \frac{\rho_0 V_\ell \int_0^{\epsilon_\ell} d\varepsilon g_\ell(\mathbf{k})}{2\varepsilon - \Delta_\ell}. \tag{2.18}$$

By integrating the left-hand and right-hand sides of the above equation over ε, we get

$$1 = \rho_0 V_\ell \int_0^{\epsilon_\ell} \frac{d\varepsilon}{2\varepsilon - \Delta_\ell} = \frac{\rho_0 V_\ell}{2} \ln \frac{\Delta_\ell - 2\epsilon_\ell}{\Delta_\ell}. \tag{2.19}$$

Thus, one can obtain the result for binding energy

$$\Delta_\ell = \frac{-2\epsilon_\ell}{\exp\left(2/\rho_0 V_\ell\right) - 1} < 0, \tag{2.20}$$

indicating the existence of a bound state whose energy is a function of the interaction strength in a specific orbital angular momentum channel. Notice that if the interaction is anisotropic, the expansion coefficient $b_{\ell m_\ell}$ can be different for various m_ℓ channels given a fixed ℓ. In such a case, one can easily verify that each set of values of $(\ell,\ m_\ell)$ corresponds to a specific solution of $\Delta_{\ell m_\ell}$ determined by Eq. (2.14).

Cooper pairing of two electrons above the Fermi sea in continuum systems discussed above, can be generalized to a similar problem of two electrons in a crystal lattice. In this case, the electron dispersion relation $\epsilon(\mathbf{k})$ is no longer the free electron value $\hbar^2 k^2/2m$, and the electron interaction must acquire the symmetry of the crystal lattice. In this case, the interaction potential $V(\mathbf{k} - \mathbf{k}')$ in Eq. (2.9) can be expanded with respect to a suitable basis in the lattice:

$$V(\mathbf{k} - \mathbf{k}') = \sum_\Gamma V_\Gamma(k, k') \sum_{j=1}^{d_\Gamma} b_j^\Gamma \phi_j^\Gamma(\mathbf{k}) \phi_j^{\Gamma *}(\mathbf{k}'), \tag{2.21}$$

where $V_\Gamma(k,k') = -V_\Gamma < 0$ within a thin layer above the Fermi surface, and is zero everywhere else. Here, $\phi_j^\Gamma(\mathbf{k})$'s are basis functions of an irreducible representation labeled by Γ which belongs to the crystal lattice symmetry group, and d_Γ is the dimension of the span of $\{\phi_j^\Gamma(\mathbf{k})\}$. By expanding the pair wave function in this basis

$$g(\mathbf{k}) = \sum_\Gamma \sum_{j=1}^{d_\Gamma} a_j^\Gamma \phi_j^\Gamma(\mathbf{k}), \tag{2.22}$$

and using the orthonormal property of ϕ's

$$\frac{A}{(2\pi)^3} \int d^3\mathbf{k} \phi_i^\Gamma(\mathbf{k}) \phi_j^{\Gamma *}(\mathbf{k}) = \delta_{ij}, \tag{2.23}$$

one can obtain a similar result of binding energy as in Eq. (2.20), indicating the existence of a bound state of electron pairs in a crystal lattice provided an arbitrarily weak attractive interaction between electrons.

2.2 Spin Structure of Paired States

In the previous section, I discussed the orbital part of the pair wave function $g(\mathbf{k})$. Next, I include the spin component and write the overall pair wave function of a general state as*

$$\Psi_{\alpha\beta}(\mathbf{k}) = g(\mathbf{k}) \chi_{\alpha\beta}, \tag{2.24}$$

where $\chi_{\alpha\beta}$ is the spin wave function of a pair consisting of fermions with spin α and β. Because of Fermi statistics, this pair wave function Ψ must be antisymmetric under particle permutation, i.e., $\Psi_{\alpha\beta}(\mathbf{k}) = -\Psi_{\beta\alpha}(-\mathbf{k})$. Furthermore, in superconductors where Cooper pairs are composed of electrons with spin 1/2, the spin component of a pair wave function can be characterized by its total spin $S = 0$ (singlet) or $S = 1$ (triplet). In principle, the spin wave function can also be a superposition of singlet and triplet states, however this option is not discussed in this thesis since all systems considered here have a definite spatial parity. Therefore, for pairing in the spin singlet channel, the spinor $\chi_{\alpha\beta} = -\chi_{\beta\alpha}$ is antisymmetric and consequently $g(\mathbf{k})$ is even in momentum space such that $g(\mathbf{k}) = g(-\mathbf{k})$; while for pairing in the spin triplet channel, the spinor $\chi_{\alpha\beta} = \chi_{\beta\alpha}$ is symmetric and consequently $g(\mathbf{k})$ is

*By writing the interaction potential in this form, I implicitly assumed that the electron spin orbit coupling in the crystal lattice is weak (zero).

odd in momentum space such that $g(\mathbf{k}) = -g(-\mathbf{k})$. These two cases will be introduced in Sections 2.2.1 and 2.2.2, and their generalization to pseudo-spin space is discussed in Section 2.2.3. For simplicity, I will discuss in this section only Fermi systems in the continuum, as in the original Cooper problem. The analysis of singlet and triplet superconducting states in crystal lattices can be found in other references, such as the wonderful books by Ketterson and Song [145], and by Mineev and Samokhin [146].

2.2.1 Singlet Pairing

The spin wave function of a pair of fermions with spin 1/2 are constructed from one-particle spin wave functions

$$|\uparrow\rangle = \begin{pmatrix} 1 \\ 0 \end{pmatrix} \quad \text{and} \quad |\downarrow\rangle = \begin{pmatrix} 0 \\ 1 \end{pmatrix}, \tag{2.25}$$

which are eigenstates of the one-particle operators $\hat{s}^2$ and $\hat{s}_z$. The spin wave function corresponding to singlet pairing electrons has the form

$$\chi_{\alpha\beta} = |\uparrow\downarrow\rangle - |\downarrow\uparrow\rangle = \begin{pmatrix} 0 & 1 \\ -1 & 0 \end{pmatrix} = i\,(\sigma_y)_{\alpha\beta}\,, \tag{2.26}$$

where σ_y is one of the Pauli matrices. Therefore, the total wave function Eq. (2.24) of a singlet pair becomes

$$\Psi_{\alpha\beta}(\mathbf{k}) = \sum_{\ell} g_\ell(\mathbf{k}) i\,(\sigma_y)_{\alpha\beta} = \sum_{\ell} \sum_{m_\ell=-\ell}^{\ell} a_{\ell m_\ell}(k) Y_{\ell m_\ell}(\hat{\mathbf{k}}) i(\sigma_y)_{\alpha\beta}, \tag{2.27}$$

where the summation of ℓ runs over the values $0,\ 2,\ 4, \cdots$, corresponding to the respective pairing states labeled by letters $s,\ d,\ g, \cdots$, as is traditional in atomic physics. In general, the superconducting states due to Cooper pairing with different orbital angular momenta ℓ and its z-component m_ℓ have different critical temperatures. At a given temperature, the most energetically favorable state among them is realized, so that it is the only state needs to be taken into consideration. In such a case, we label the system by its orbital angular momentum state, e.g., s-, and d-wave superconductors. The complex function $\sum_{m_\ell=-\ell}^{\ell} a_{\ell m_\ell} Y_{\ell m_\ell}(\hat{\mathbf{k}})$ in the equation above is defined as the superconductor *order parameter*. Notice that in this definition, the order parameter may be in general a function

of $\hat{\mathbf{k}}$ (anisotropic), and a function of k.[†] For s-wave ($\ell = 0$) superconductors, only one state characterized by a_{00} is possible, while for d-wave ($\ell = 2$) superconductors, the order parameter depends on a set of five coefficients $\{a_{2,-2}; a_{2,-1}; a_{2,0}; a_{2,1}; a_{2,2}\}$, hence there exist several possible phases distinguished by the configuration of a_{2m_ℓ}'s, such as d_{xy}-phase, $d_{x^2-y^2}$-phase, and linear combinations of them.

2.2.2 Triplet Pairing

In the case of triplet state of a fermion pair ($S = 1$), the wave functions correspond to pairing in three different spin channels, which are symmetric under the particle permutation

$$|\uparrow\uparrow\rangle = \begin{pmatrix} 1 & 0 \\ 0 & 0 \end{pmatrix}, \quad S_z = 1, \tag{2.28a}$$

$$|\uparrow\downarrow\rangle + |\downarrow\uparrow\rangle = \begin{pmatrix} 0 & 1 \\ 1 & 0 \end{pmatrix}, \quad S_z = 0, \tag{2.28b}$$

$$|\downarrow\downarrow\rangle = \begin{pmatrix} 0 & 0 \\ 0 & 1 \end{pmatrix}, \quad S_z = -1. \tag{2.28c}$$

The total wave function of a pair is a linear superposition of the three states

$$\Psi_{\alpha\beta}(\mathbf{k}) = \sum h_1(\mathbf{k})|\uparrow\uparrow\rangle + h_2(\mathbf{k})\left(|\uparrow\downarrow\rangle + |\downarrow\uparrow\rangle\right) + h_3(\mathbf{k})|\downarrow\downarrow\rangle = \begin{pmatrix} h_1(\mathbf{k}) & h_2(\mathbf{k}) \\ h_2(\mathbf{k}) & h_3(\mathbf{k}) \end{pmatrix}, \tag{2.29}$$

where $h_i(\mathbf{k})$ are the amplitudes of states with $S_z = 1,\ 0$, and -1, respectively. The expression above can be written in another form by using symmetric matrices $i\boldsymbol{\sigma}\sigma_y = (i\sigma_x\sigma_y, i\sigma_y\sigma_y, i\sigma_z\sigma_y)$, leading to

$$\begin{aligned} \Psi_{\alpha\beta}(\mathbf{k}) &= i\left[\mathbf{d}(\mathbf{k})\cdot\boldsymbol{\sigma}\right]\sigma_y = i\left[d_x(\mathbf{k})\sigma_x + d_y(\mathbf{k})\sigma_y + d_z(\mathbf{k})\sigma_z\right]\sigma_y \\ &= \begin{pmatrix} -d_x(\mathbf{k}) + id_y(\mathbf{k}) & d_z(\mathbf{k}) \\ d_z(\mathbf{k}) & d_x(\mathbf{k}) + id_y(\mathbf{k}) \end{pmatrix}. \end{aligned} \tag{2.30}$$

The amplitudes $h_i(\mathbf{k})$ and the components of the $\mathbf{d}(\mathbf{k})$ vector are related by

$$h_1 = -d_x + id_y, \qquad h_2 = d_z, \qquad h_3 = d_x + id_y. \tag{2.31}$$

[†]In some references and the following discussions in this thesis, the order parameter can also be defined equivalently by the complex coefficients $a_{\ell m_\ell}$. The present definition is chosen here in order to show explicitly the anisotropy of order parameter.

The d_j components can be expanded in terms of the spherical harmonics

$$d_j(\mathbf{k}) = \sum_{\ell} \sum_{m_\ell=-\ell}^{\ell} \gamma^j_{\ell m_\ell} Y_{\ell m_\ell}(\hat{\mathbf{k}}), \tag{2.32}$$

where the summation of ℓ runs over the values $1,\ 3, \cdots$, corresponding to the p-, f-, $\cdots$ wave superconducting states, respectively.

The $\mathbf{d}(\mathbf{k})$ vector is defined as the superconductor order parameter and from its structure it is clear that the orientation of $\mathbf{d}(\mathbf{k})$ is intimately related to the spin components of the paired electrons. For example, for p-wave symmetry with $\ell = 1$, the order parameter $\mathbf{d}(\mathbf{k})$ is expressed as a set of nine complex functions $\gamma^j_{1m_\ell}$ with $j = x,\ y,\ z$ and $m_\ell = -1,\ 0,\ 1$. Thus, there exist many possible phases of a p-wave triplet superfluid distinguished by the configurations of the vector order parameter $\mathbf{d}(\mathbf{k})$, such as A-phase, B-phase, and polar-phase of ^{3}He [74].

2.2.3 Pseudo-spin Space

Unlike Cooper pairs composed of spin-1/2 electrons in superconductors with weak spin-orbit coupling, Cooper pairs in superfluids are composed of other fermions whose total angular momentum in general can be different from 1/2. For instance, the nuclear spin of ^{40}K atoms is $I = 4$, and the electron spin is $S = 1/2$. Then it can be shown that the lowest two energy states in ^{40}K systems are $|F = 9/2, F_z = -9/2\rangle$ and $|F = 9/2, F_z = -7/2\rangle$, which both have the total angular momentum $F = 9/2$. Thus, the total angular momentum and its z-component of Cooper pairs of ^{40}K atoms can be obtained through the addition of angular momenta, leading to the following possible states:

$$\begin{aligned}
&|F = 9/2, F_z = -9/2\rangle + |F = 9/2, F_z = -9/2\rangle \ \Rightarrow\ |J = 9, J_z = -9\rangle,\\
&|F = 9/2, F_z = -9/2\rangle + |F = 9/2, F_z = -7/2\rangle \ \Rightarrow\ \begin{cases} |J = 9, J_z = -8\rangle \\ |J = 8, J_z = -8\rangle, \end{cases}\\
&|F = 9/2, F_z = -7/2\rangle + |F = 9/2, F_z = -7/2\rangle \ \Rightarrow\ \begin{cases} |J = 9, J_z = -7\rangle \\ |J = 8, J_z = -7\rangle \\ |J = 7, J_z = -7\rangle, \end{cases}
\end{aligned} \tag{2.33}$$

where J and J_z are the pair angular momentum and its z-component, respectively. Therefore, the previous classification of the spin structures of Cooper pairs of spin 1/2 fermions into singlet and triplet states based upon angular momentum is no longer directly applicable.

However, it should be emphasized that the angular momentum and its z-component are not essential for the definition of singlet and triplet states. For instance, consider a Fermi system with fixed parity composed of fermions in two states (or even of two species) labeled by 1 and 2. If the wave function of Cooper pairs is even or odd in coordinate space, then it must be antisymmetric or symmetric under interchanging of the label $1 \leftrightarrow 2$, respectively. The former case corresponds to the antisymmetric combination as $|12\rangle - |21\rangle$, while the latter case corresponds to a mixture of three possible symmetric combinations $|11\rangle$, $|12\rangle + |21\rangle$, and $|22\rangle$. The labels 1 and 2 can be defined as *pseudo-spin* to emphasize the analogy of Cooper pairs of electrons. Thus, the two possible pairing states can be denoted by the singlet and triplet states in pseudo-spin space, respectively. This classification of singlet and triplet states in pseudo-spin space is also used in the literature of superconductors in solids with strong spin-orbit coupling. In such a case, the electron spin becomes a "bad" quantum number, but electron states are still doubly degenerate (because of the Kramers degeneracy due to the time reversal symmetry), which allows the classification in pseudo-spin space [147]. In the following discussion, I may use the name "spin" for both real spin and pseudo-spin, and even use the notation $|\uparrow\rangle$ and $|\downarrow\rangle$ to denote fermions in state 1 and 2, respectively. This notation unifies the general physics of triplet superfluidity in completely different systems.

2.3 Superfluidity as a Many-body Problem

The Cooper's problem introduced in Section 2.1 describes the idea of fermion pairing which helps to explain superconductivity and superfluidity. However, that discussion involves only a system of two interacting fermions, while superconductivity and superfluidity are certainly interacting many-body problems. Therefore, the solution of the Cooper's problem can not be applied directly to understand superconductivity and superfluidity. In fact, its

generalization to many-body systems is not trivial. This section provides a brief derivation of the diagonalization of the many-body Hamiltonian, the order parameter equations, and the Ginzburg–Landau theory.

2.3.1 Hamiltonian and Effective Theory

To describe the instability of the normal state towards a superconducting state, I consider the minimal Hamiltonian of an ensemble of Fermi particles including only the pair attraction between particles with opposite momenta, which is the kind of interaction essential for superconductivity:

$$\mathcal{H} = \sum_{\mathbf{k}} \xi_{\mathbf{k}} c^{\dagger}_{\mathbf{k}\alpha} c_{\mathbf{k}\alpha} + \frac{1}{2} \sum_{\mathbf{k},\mathbf{k}'} V_{\alpha\beta,\gamma\delta}(\mathbf{k},\mathbf{k}') c^{\dagger}_{\mathbf{k}\alpha} c^{\dagger}_{-\mathbf{k}\beta} c_{\mathbf{k}'\gamma} c_{-\mathbf{k}'\delta}, \tag{2.34}$$

where $c^{\dagger}_{\mathbf{k}\alpha}$ and $c_{\mathbf{k}\alpha}$ are creation and annihilation fermionic operators of linear momentum $\mathbf{k}$ and spin (pseudo-spin) α. The first term in the Hamiltonian is the non-interacting contribution where $\xi_{\mathbf{k}} = \epsilon_{\mathbf{k}} - \mu$ is the fermionic dispersion shifted by the chemical potential. The second term is interaction contribution, where $V_{\alpha\beta,\gamma\delta}(\mathbf{k},\mathbf{k}')$ is the interaction potential between fermions. Notice that the summation convention concerning repeated spin (pseudo-spin) indices is used throughout the thesis unless specified.

In the absence of spin-orbit coupling, the attractive potential can be separated as

$$V_{\alpha\beta,\gamma\delta}(\mathbf{k},\mathbf{k}') = V(\mathbf{k},\mathbf{k}')\Lambda_{\alpha\beta,\gamma\delta}. \tag{2.35}$$

In a Fermi system with a spherical Fermi surface, the function $V(\mathbf{k},\mathbf{k}')$ can be expanded in spherical harmonics

$$V(\mathbf{k},\mathbf{k}') = \sum_{\ell=0}^{\infty} V_{\ell}(k,k') \sum_{m_\ell=-\ell}^{\ell} b_{\ell m_\ell} Y_{\ell m_\ell}(\hat{\mathbf{k}}) Y^{*}_{\ell m_\ell}(\hat{\mathbf{k}}'). \tag{2.36}$$

However, in many systems, the expansion of $V(\mathbf{k},\mathbf{k}')$ in terms of spherical harmonics with different ℓ contains only one interaction component V_ℓ which is responsible for the highest critical temperature (see Section 2.2.1). Furthermore, as in the BCS theory, it is assumed that the function $V(\mathbf{k},\mathbf{k}')$ is a negative constant $-V_\ell$ when the two vectors $\mathbf{k}$ and $\mathbf{k}'$ are in a thin layer near the Fermi surface, and is zero otherwise.

The spin dependence of the interaction potential is expressed in terms of the matrices which are antisymmetric under permutation of indices $\alpha\beta$ ($\gamma\delta$) for even ℓ (corresponding to s-, d-, g-$\cdots$ orbital wave symmetries):

$$\Lambda_{\alpha\beta,\gamma\delta} = v_{\alpha\beta} v^{\dagger}_{\gamma\delta}, \tag{2.37}$$

where $v_{\alpha\beta} = (i\sigma_y)_{\alpha\beta}$ and $v^{\dagger}_{\gamma\delta} = (-i\sigma^{\dagger}_y)_{\gamma\delta}$, and symmetric for odd ℓ (corresponding to p-, f-, $\cdots$ orbital wave symmetries):

$$\Lambda_{\alpha\beta,\gamma\delta} = \mathbf{v}_{\alpha\beta} \cdot \mathbf{v}^{\dagger}_{\gamma\delta} \tag{2.38}$$

where $\mathbf{v}_{\alpha\beta} = (i\boldsymbol{\sigma}\sigma_y)_{\alpha\beta}$ and $\mathbf{v}^{\dagger}_{\gamma\delta} = (-i\sigma^{\dagger}_y\boldsymbol{\sigma}^{\dagger})_{\gamma\delta}$.

In Fermi systems subjected to a crystal or optical lattice where the invariance under the point symmetry operation is essential, spherical harmonics in Eq. (2.36) are no longer a suitable basis. Thus, the pair interaction takes a different form

$$V_{\alpha\beta,\gamma\delta}(\mathbf{k},\mathbf{k}') = \sum_{\Gamma} V_{\Gamma}(k,k') \Lambda_{\alpha\beta,\gamma\delta} \sum_{j=1}^{d_\Gamma} b^{\Gamma}_j \phi^{\Gamma}_j(\hat{\mathbf{k}}) \phi^{\Gamma *}_j(\hat{\mathbf{k}}'), \tag{2.39}$$

where $V_\Gamma(k,k') = -V_\Gamma < 0$ within a thin layer above the Fermi surface, and is zero everywhere else. As discussed in Section 2.2.1, usually there exists one interaction V_Γ corresponding to a given irreducible representation Γ which gives the highest critical temperature. The functions $\Lambda_{\alpha\beta,\gamma\delta}$ for even and odd representations are given by equations (2.37) and (2.38), respectively.

The instability of the Fermi system described by the Hamiltonian (2.34) against formation of Cooper pairs can be taken into account by the grand partition function expressed as the trace over fermion states

$$\mathcal{Z} \;=\; \mathrm{Tr} e^{-\beta\mathcal{H}}, \tag{2.40}$$

where $\beta = 1/k_B T$. From now on, natural unit will be used throughout the thesis, where the reduced Planck's constant, the Boltzman's constant, and the speed of light are equal to 1 ($\hbar = k_B = c = 1$). Using the functional integral expression [148], the grand partition function can be represented as

$$\mathcal{Z} = \int_{\mathrm{BC}} \Pi_{\mathbf{k}} \mathcal{D}[c^{\dagger}_{\mathbf{k}\alpha}(\tau), c_{\mathbf{k}\alpha}(\tau)] e^{-\int_0^\beta d\tau \left[\sum_{\mathbf{k}} c^{\dagger}_{\mathbf{k}\alpha}(\tau) \frac{\partial}{\partial\tau} c_{\mathbf{k}\alpha}(\tau) + \mathcal{H}\left(c^{\dagger}_{\mathbf{k}\alpha}(\tau), c_{\mathbf{k}\alpha}(\tau)\right)\right]}, \tag{2.41}$$

where the functional integration is over fermionic fields $c^\dagger$ and c with the anti-periodic boundary condition (BC) $c_{\mathbf{k}\alpha}(\beta) = -c_{\mathbf{k}\alpha}(0)$, and τ is the imaginary time [149].

Notice that the exponent of the integrand Eq. (2.41) has quartic term in the fields $c^\dagger$ and c, due to the presence of the interacting contribution in the Hamiltonian (2.34). Thus the integration can not be evaluated explicitly. One way to solve this problem is to group the non-interacting part of $H(c^\dagger, c)$ together with the other quadratic terms in the exponent and to develop a perturbation series in which the exponential of the interacting part of $H(c^\dagger, c)$ is expanded as a Taylor series. This gives rise to a series of integrals of the products of a Gaussian times polynomials which may be evaluated using Wick's theorem. In this perturbation procedure, each term in the Taylor series can be represented by a Feynman diagram and such diagrams can be constructed from a systematic set of rules even without doing the algebraic expansion. However, this perturbation theory is valid only when the interaction is weak. Here, I will introduce another method through which the exponent in the integrand of Eq. (2.41) containing the quartic terms of fields can be written as an integral over quadratic terms using a transformation introduced by Stratonovich [150] and Hubbard [151]. Since this thesis concentrates on triplet superfluidity, I will only discuss the triplet pairing state.

For a triplet pairing state of a Fermi system in crystal or optical lattices with weak spin–orbit coupling, it is convenient to introduce a vector bosonic field

$$\mathbf{B}_j(\tau) = \frac{1}{2}\sqrt{b_j^\Gamma}\sum_{\mathbf{k}'}\phi_j^{\Gamma *}(\hat{\mathbf{k}}')(\mathbf{v}^\dagger)_{\gamma\delta}c_{\mathbf{k}'\gamma}(\tau)c_{-\mathbf{k}'\delta}(\tau), \tag{2.42a}$$

$$\mathbf{B}_j^\dagger(\tau) = \frac{1}{2}\sqrt{b_j^\Gamma}\sum_{\mathbf{k}}\phi_j^{\Gamma}(\hat{\mathbf{k}})(\mathbf{v})_{\alpha\beta}c_{\mathbf{k}\alpha}^\dagger(\tau)c_{-\mathbf{k}\beta}^\dagger(\tau), \tag{2.42b}$$

where $j = 1, \cdots, d_\Gamma$ runs over all linearly independent basis functions ϕ_j^Γ of an irreducible representation Γ. Then the integrand of Eq. (2.41) corresponding to quartic terms of the exponent can be written as

$$\begin{aligned} Q &= \exp\left[-\frac{1}{2}\int_0^\beta d\tau \sum_{\mathbf{k},\mathbf{k}'} V_{\alpha\beta,\gamma\delta}(\mathbf{k},\mathbf{k}')c_{\mathbf{k}\alpha}^\dagger c_{-\mathbf{k}\beta}^\dagger c_{\mathbf{k}'\gamma}c_{-\mathbf{k}'\delta}\right] \\ &= \exp\left[2V_\Gamma\int_0^\beta d\tau\sum_{j=1}^{d_\Gamma}\mathbf{B}_j^\dagger(\tau)\cdot\mathbf{B}_j(\tau)\right]. \end{aligned} \tag{2.43}$$

However, for a pair of conjugate vector bosonic operators $\mathbf{\Delta}_j$ and $\mathbf{\Delta}_j^\dagger$, the following functional Gaussian integral holds

$$Q = \frac{C}{2V_\Gamma}\int_{\mathrm{BC}} \Pi_j \mathcal{D}[\mathbf{\Delta}_j^\dagger(\tau), \mathbf{\Delta}_j(\tau)] e^{\int_0^\beta d\tau \sum_{j=1}^{d_\Gamma}\left[-\frac{1}{2V_\Gamma}\mathbf{\Delta}_j^\dagger(\tau)\cdot\mathbf{\Delta}_j(\tau)+\mathbf{B}_j^\dagger(\tau)\cdot\mathbf{\Delta}_j(\tau)+\mathbf{\Delta}_j^\dagger(\tau)\cdot\mathbf{B}_j(\tau)\right]}, \tag{2.44}$$

where $\mathbf{\Delta}_j$ and $\mathbf{\Delta}_j^\dagger$ are the auxiliary vector (bosonic) Hubbard–Stratonovich fields, and C is a constant. Here, the functional integral is over bosonic field operators with periodic boundary conditions (BC) $\mathbf{\Delta}_j(\beta) = \mathbf{\Delta}_j(0)$. Substituting this result back into Eq. (2.41) and inverting the order of fermionic (c) and bosonic ($\mathbf{\Delta}_j$) integrations, the grand partition function takes the form

$$\begin{aligned}\mathcal{Z} &= \int_{\mathrm{BC}} \Pi_j \mathcal{D}[\mathbf{\Delta}_j^\dagger(\tau), \mathbf{\Delta}_j(\tau)] \exp\left[-\int_0^\beta d\tau \frac{1}{2V_\Gamma}\sum_{j=1}^{d_\Gamma}\mathbf{\Delta}_j^\dagger(\tau)\cdot\mathbf{\Delta}_j(\tau)\right] \\ &\quad\times \int_{\mathrm{BC}} \Pi_{\mathbf{k}} \mathcal{D}[c_{\mathbf{k}\alpha}^\dagger(\tau), c_{\mathbf{k}\alpha}(\tau)] \exp\left[-\int_0^\beta d\tau \sum_{\mathbf{k}} \mathcal{T}(\mathbf{k},\tau)\right],\end{aligned} \tag{2.45}$$

where

$$\begin{aligned}\mathcal{T}(\mathbf{k},\tau) &= c_{\mathbf{k}\alpha}^\dagger\left(\partial_\tau + \xi_{\mathbf{k}}\right) c_{\mathbf{k}\alpha} - \frac{1}{2}\sum_{j=1}^{d_\Gamma}\sqrt{b_j^\Gamma}\,\phi_j^{\Gamma *}(\hat{\mathbf{k}})\left[\mathbf{\Delta}_j^\dagger\cdot(\mathbf{v}^\dagger)_{\alpha\beta}\right] c_{\mathbf{k}\alpha}c_{-\mathbf{k}\beta}(\tau) \\ &\quad -\frac{1}{2}\sum_{j=1}^{d_\Gamma}\sqrt{b_j^\Gamma}\,\phi_j^\Gamma(\hat{\mathbf{k}})\left[(\mathbf{v})_{\alpha\beta}\cdot\mathbf{\Delta}_j\right] c_{\mathbf{k}\alpha}^\dagger(\tau)c_{-\mathbf{k}\beta}^\dagger(\tau).\end{aligned} \tag{2.46}$$

Here, the prefactor $C/2V_\Gamma$ in Q is dropped out since a multiplicative constant in partition function will not affect thermodynamic properties.

Notice that the integrand $\mathcal{T}(\mathbf{k})$ is only quadratic in fermionic fields, hence the functional integral of c and $c^\dagger$ can be performed by the Gaussian integral formula. Recalling that c and $c^\dagger$ are complex Grassmann variables, we have

$$\frac{\partial}{\partial\tau}\left(c_{\mathbf{k}\alpha}^\dagger c_{\mathbf{k}\alpha}\right) = \left(\partial_\tau c_{\mathbf{k}\alpha}^\dagger\right) c_{\mathbf{k}\alpha} + c_{\mathbf{k}\alpha}^\dagger\left(\partial_\tau c_{\mathbf{k}\alpha}\right) = -c_{\mathbf{k}\alpha}\left(\partial_\tau c_{\mathbf{k}\alpha}^\dagger\right) + c_{\mathbf{k}\alpha}^\dagger\left(\partial_\tau c_{\mathbf{k}\alpha}\right) \tag{2.47}$$

However, the term on the left-hand side vanishes upon integration with respect to τ due to the antiperiodic boundary conditions of fermionic fields c. Thus, we have

$$\int_0^\beta d\tau c_{\mathbf{k}\alpha}^\dagger\partial_\tau c_{\mathbf{k}\alpha} = \int_0^\beta d\tau c_{\mathbf{k}\alpha}\partial_\tau c_{\mathbf{k}\alpha}^\dagger = \int_0^\beta d\tau\left[\frac{1}{2}c_{\mathbf{k}\alpha}^\dagger\partial_\tau c_{\mathbf{k}\alpha} + \frac{1}{2}c_{\mathbf{k}\alpha}\partial_\tau c_{\mathbf{k}\alpha}^\dagger\right]. \tag{2.48}$$

This result, together with the fact that[‡]

$$\sum_{\alpha} c^{\dagger}_{\mathbf{k}\alpha}\xi_{\mathbf{k}}c_{\mathbf{k}\alpha} = \sum_{\alpha}\left[\xi_{\mathbf{k}} - c_{\mathbf{k}\alpha}\xi_{\mathbf{k}}c^{\dagger}_{\mathbf{k}\alpha}\right] = \xi_{\mathbf{k}} + \sum_{\alpha}\left[\frac{1}{2}c^{\dagger}_{\mathbf{k}\alpha}\xi_{\mathbf{k}}c_{\mathbf{k}\alpha} - \frac{1}{2}c_{\mathbf{k}\alpha}\xi_{\mathbf{k}}c^{\dagger}_{\mathbf{k}\alpha}\right], \tag{2.49}$$

can be used to rewrite $-\int_0^\beta d\tau \sum_{\mathbf{k}} \mathcal{T}(\mathbf{k},\tau)$ in a symmetric form $-\int_0^\beta d\tau \sum_{\mathbf{k}} \mathcal{T}'(\mathbf{k},\tau)$, where

$$\begin{aligned}
\mathcal{T}'(\mathbf{k},\tau) &= \xi_{\mathbf{k}} + \frac{1}{2}c^{\dagger}_{\mathbf{k}\alpha}\left(\partial_\tau + \xi_{\mathbf{k}}\right)c_{\mathbf{k}\alpha} + \frac{1}{2}c_{\mathbf{k}\alpha}\left(\partial_\tau - \xi_{\mathbf{k}}\right)c^{\dagger}_{\mathbf{k}\alpha} \\
&\quad -\frac{1}{2}\sum_{j=1}^{d_\Gamma}\sqrt{b_j^\Gamma}\,\phi_j^{\Gamma *}(\hat{\mathbf{k}})\left[\mathbf{\Delta}_j^{\dagger}\cdot(\mathbf{v}^{\dagger})_{\alpha\beta}\right]c_{\mathbf{k}\alpha}c_{-\mathbf{k}\beta} \\
&\quad -\frac{1}{2}\sum_{j=1}^{d_\Gamma}\sqrt{b_j^\Gamma}\,\phi_j^{\Gamma}(\hat{\mathbf{k}})\left[(\mathbf{v})_{\alpha\beta}\cdot\mathbf{\Delta}_j\right]c^{\dagger}_{\mathbf{k}\alpha}c^{\dagger}_{-\mathbf{k}\beta} \\
&= \xi_{\mathbf{k}} + C^{\dagger}\mathcal{G}^{-1}(\mathbf{k},\tau)C.
\end{aligned} \tag{2.50}$$

Here, $C^{\dagger} \equiv (c^{\dagger}_{\mathbf{k}\alpha},\ c_{-\mathbf{k}\beta})$ is a spinor, and the inverse Nambu propagator $\mathcal{G}^{-1}$ is

$$\mathcal{G}^{-1}(\mathbf{k},\tau) = \frac{1}{2}\begin{pmatrix} \left(\partial_\tau + \xi_{\mathbf{k}}\right)\delta_{\alpha\beta} & -\sum_{j=1}^{d_\Gamma}\sqrt{b_j^\Gamma}\,\phi_j^{\Gamma}(\hat{\mathbf{k}})(\mathbf{v})_{\alpha\beta}\cdot\mathbf{\Delta}_j \\ -\sum_{j=1}^{d_\Gamma}\sqrt{b_j^\Gamma}\,\phi_j^{\Gamma *}(\hat{\mathbf{k}})\mathbf{\Delta}_j^{\dagger}\cdot(\mathbf{v}^{\dagger})_{\alpha\beta} & \left(\partial_\tau - \xi_{\mathbf{k}}\right)\delta_{\alpha\beta} \end{pmatrix}. \tag{2.51}$$

Substituting this expression back into Eq. (2.45) and changing the integral variables from fermionic operators c and $c^{\dagger}$ to spinor C and $C^{\dagger}$, the grand partition function takes the form

$$\begin{aligned}
\mathcal{Z} &= \int_{\mathrm{BC}} \mathcal{D}[\mathbf{\Delta}_j^{\dagger}(\tau),\mathbf{\Delta}_j(\tau)]e^{-\int_0^\beta d\tau\left[\frac{1}{2V_\Gamma}\mathbf{\Delta}_j^{\dagger}(\tau)\cdot\mathbf{\Delta}_j(\tau)+\sum_{\mathbf{k}}\xi_{\mathbf{k}}\right]} \\
&\quad \times\left[\int_{\mathrm{BC}}\mathcal{D}[C^{\dagger},C]e^{\int_0^\beta d\tau\sum_{\mathbf{k}}-C^{\dagger}\mathcal{G}^{-1}(\mathbf{k},\tau)C}\right]^{1/2}.
\end{aligned} \tag{2.52}$$

The second fermionic functional integral can be evaluated with the help of the Gaussian integral for Grassmann variables, leading to

$$\begin{aligned}
\mathcal{Z} &= \int_{\mathrm{BC}}\Pi_j\mathcal{D}[\mathbf{\Delta}_j^{\dagger}(\tau),\mathbf{\Delta}_j(\tau)]e^{-\int_0^\beta d\tau\left[\frac{1}{2V_\Gamma}\sum_{j=1}^{d_\Gamma}\mathbf{\Delta}_j^{\dagger}(\tau)\cdot\mathbf{\Delta}_j(\tau)+\sum_{\mathbf{k}}\xi_{\mathbf{k}}\right]}\left(\mathrm{Det}_{\mathbf{k},\tau}\mathcal{G}^{-1}\right)^{1/2} \\
&= \int_{\mathrm{BC}}\Pi_j\mathcal{D}[\mathbf{\Delta}_j^{\dagger}(\tau),\mathbf{\Delta}_j(\tau)]e^{-S_{\mathrm{eff}}[\mathbf{\Delta}_j^{\dagger},\mathbf{\Delta}_j]},
\end{aligned} \tag{2.53}$$

where the effective action is given by[§]

$$S_{\mathrm{eff}}[\mathbf{\Delta}_j^{\dagger},\mathbf{\Delta}_j] = \int_0^\beta d\tau\left[\frac{1}{2V_\Gamma}\sum_{j=1}^{d_\Gamma}\mathbf{\Delta}_j^{\dagger}(\tau)\cdot\mathbf{\Delta}_j(\tau) + \sum_{\mathbf{k}}\xi_{\mathbf{k}}\right] - \frac{1}{2}\mathrm{Tr}_{\mathbf{k},\tau}\left(\ln\mathcal{G}^{-1}(\mathbf{k},\tau)\right). \tag{2.54}$$

[‡]Here, the summation over spin index α is written out explicitly to give the correct prefactor of $\xi_{\mathbf{k}}$.
[§]Here, the relation $\ln(\det A) = \mathrm{tr}(\ln A)$ for a regular matrix A is used.

The subscripts $(\mathbf{k}, \tau)$ of the determinant (Det) and trace (Tr) denote that these operators are the matrix determinant and trace not only over Nambu indices, but also over momentum and imaginary time variables.

Equations (2.53) and (2.54) define the effective theory for the original many-body Hamiltonian (2.34). The effective action is a functional of vector bosonic operators $\mathbf{\Delta}_j$ and $\mathbf{\Delta}_j^\dagger$, which are related to creation and annihilation operators of fermion pairs $\mathbf{B}_j$ and $\mathbf{B}_j^\dagger$ through the Hubbard-Stratonovich transformation. In the next section, I will apply the saddle point approximation[¶] to this effective theory, and derive the saddle-point equations.

2.3.2 Saddle-point Equations

In this section, it will be shown that the BCS gap and number equations are obtained as a saddle-point solution of the more general functional integral formulation. In fact, if $\mathbf{\Delta}_j(\tau) \equiv \mathbf{\Delta}_{j,0}$ is a static solution, then it must render the action stationary, i.e.,

$$\left.\frac{\delta S_{\text{eff}}[\mathbf{\Delta}_j^\dagger, \mathbf{\Delta}_j]}{\delta \mathbf{\Delta}_j^\dagger}\right|_{\mathbf{\Delta}_{j,0}} = 0. \tag{2.55}$$

By substituting the expression for S_{eff}, this saddle-point equation becomes

$$\left.\frac{\delta S_{\text{eff}}[\mathbf{\Delta}_j^\dagger, \mathbf{\Delta}_j]}{\delta \mathbf{\Delta}_j^\dagger}\right|_{\mathbf{\Delta}_{j,0}} = \int_0^\beta d\tau \left\{ \frac{2\mathbf{\Delta}_{j,0}}{V_\Gamma} - \frac{1}{2}\sum_{\mathbf{k}} \text{tr}\left[\frac{\delta}{\delta \mathbf{\Delta}_{j,0}^\dagger} \left(\ln \mathcal{G}_0^{-1}(\mathbf{k}, \tau) \right) \right] \right\} = 0, \tag{2.56}$$

where $\mathcal{G}_0^{-1}(\mathbf{k}, \tau) = \mathcal{G}^{-1}(\mathbf{k}, \tau)|_{\Delta_{j,0}}$. Using the fact that

$$\text{tr}\left(\frac{\partial}{\partial x} \ln A(x) \right) = \text{tr}\left(A^{-1}(x) \frac{\partial}{\partial x} A(x) \right), \tag{2.57}$$

equation (2.56) can be written as

$$\frac{\beta \mathbf{\Delta}_{j,0}}{2V_\Gamma} = \frac{1}{2}\int_0^\beta d\tau \sum_{\mathbf{k}} \text{tr}\left[\mathcal{G}_0(\mathbf{k}, \tau) \frac{\partial \mathcal{G}_0^{-1}(\mathbf{k}, \tau)}{\partial \mathbf{\Delta}_{j,0}^\dagger} \right]. \tag{2.58}$$

The right-hand side of this equation is more conveniently evaluated after Fourier transforming $\mathcal{G}_0(\mathbf{k}, \tau)$ and $\mathcal{G}_0^{-1}(\mathbf{k}, \tau)$ to frequency (ω) variables:

$$\mathcal{G}_0^{-1}(\mathbf{k}, \tau) = \int d\omega e^{-i\omega\tau} \mathcal{G}_0^{-1}(\mathbf{k}, \omega) \tag{2.59a}$$

$$\mathcal{G}_0(\mathbf{k}, \tau) = \int d\omega e^{i\omega\tau} \mathcal{G}_0(\mathbf{k}, \omega). \tag{2.59b}$$

[¶]This approximation is also called mean field or stationary phase approximation.

Using these in Eq. (2.58) and performing the imaginary time integration, one obtains

$$\frac{\beta \mathbf{\Delta}_{j,0}}{2V_\Gamma} = \frac{1}{2}\sum_{\mathbf{k},\omega_n} \mathrm{tr}\left[\mathcal{G}_0(\mathbf{k},\omega_n)\frac{\partial \mathcal{G}_0^{-1}(\mathbf{k},\omega_n)}{\partial \mathbf{\Delta}_{j,0}^\dagger}\right], \tag{2.60}$$

where the frequency integration is reduced to a summation over a set of discrete frequencies ω_n, which is imposed by the antiperiodic boundary conditions for fermionic fields. The set of discrete frequencies is called the fermionic Matsubara frequencies [149]. Here, the $\mathcal{G}_0^{-1}(\mathbf{k},\omega_n)$ and $\mathcal{G}_0(\mathbf{k},\omega_n)$ can be obtained from Eq. (2.51) through the transformation $\partial_\tau \to -i\omega_n$ leading to

$$\mathcal{G}_0^{-1}(\mathbf{k},\omega_n) = \frac{1}{2}\begin{pmatrix} (-i\omega_n + \xi_{\mathbf{k}})\,\delta_{\alpha\beta} & -\sum_{j=1}^{d_\Gamma}\sqrt{b_j^\Gamma}\phi_j^\Gamma(\hat{\mathbf{k}})(\mathbf{v})_{\alpha\beta}\cdot\mathbf{\Delta}_{j,0} \\ -\sum_{j=1}^{d_\Gamma}\sqrt{b_j^\Gamma}\phi_j^{\Gamma *}(\hat{\mathbf{k}})\mathbf{\Delta}_{j,0}^\dagger\cdot(\mathbf{v}^\dagger)_{\alpha\beta} & (-i\omega_n - \xi_{\mathbf{k}})\,\delta_{\alpha\beta} \end{pmatrix} \tag{2.61}$$

and

$$\mathcal{G}_0(\mathbf{k},\omega_n) = \frac{2}{\Lambda}\begin{pmatrix} (-i\omega_n - \xi_{\mathbf{k}})\,\delta_{\alpha\beta} & \sum_{j=1}^{d_\Gamma}\sqrt{b_j^\Gamma}\phi_j^\Gamma(\hat{\mathbf{k}})(\mathbf{v})_{\alpha\beta}\cdot\mathbf{\Delta}_{j,0} \\ \sum_{j=1}^{d_\Gamma}\sqrt{b_j^\Gamma}\phi_j^{\Gamma *}(\hat{\mathbf{k}})\mathbf{\Delta}_{j,0}^\dagger\cdot(\mathbf{v}^\dagger)_{\alpha\beta} & (-i\omega_n + \xi_{\mathbf{k}})\,\delta_{\alpha\beta} \end{pmatrix}, \tag{2.62}$$

where $\Lambda = [(-i\omega_n)^2 - \xi_{\mathbf{k}}^2] - f_{\mathbf{k}}^2$, and $f_{\mathbf{k}}^2 = |\sum_j^{d_\Gamma}\sqrt{b_j^\Gamma}\phi_j^\Gamma(\hat{\mathbf{k}})\mathbf{\Delta}_{j,0}|^2$. It is convenient to absorb the angular dependence $\phi_j^\Gamma(\hat{\mathbf{k}})$ into the bosonic field and define the anisotropic order parameter as $\mathbf{D}_0^\Gamma(\hat{\mathbf{k}}) = \sum_j^{d_\Gamma}\sqrt{b_j^\Gamma}\phi_j^\Gamma(\hat{\mathbf{k}})\mathbf{\Delta}_{j,0}$. Using this notation, $f_{\mathbf{k}}^2 = |\mathbf{D}_0^\Gamma(\hat{\mathbf{k}})|^2$.

This result for inverse Nambu matrix $\mathcal{G}$ is valid when $(D_{0,\mu}^\Gamma)^\dagger(\hat{\mathbf{k}})D_{0,\nu}^\Gamma(\hat{\mathbf{k}})$ are real for all μ and ν components. This condition is equivalent to requiring that the $\mathbf{D}_\Gamma(\hat{\mathbf{k}})$ vector to be represented by a real vector times an overall phase, i.e., $\mathbf{D}_0^\Gamma = e^{i\phi}(D_{0,x}^\Gamma, D_{0,y}^\Gamma, D_{0,z}^\Gamma)$, where $D_{0,\mu}^\Gamma$ are real functions. The superconducting state with an order parameter satisfying this requirement is called the *unitary* state throughout this thesis. This terminology is extensively used in the literature of superfluid ^{3}He, and is well accepted by condensed matter community. In Chapter 4 when I discuss the condensates of ultra-cold Fermi atoms, I will extend the current analysis to some specific *non-unitary* triplet superfluid states. The inverse Nambu matrix for a general non-unitary state, however, is much more complicated and will not be discussed in this thesis.

Substituting the results in Eqs. (2.61) and (2.62) into Eq. (2.60), and noticing that

$$\frac{\partial \mathcal{G}_0^{-1}(\mathbf{k},\omega_n)}{\partial \mathbf{\Delta}_{j,0}^{\dagger}} = \frac{1}{2}\begin{pmatrix} 0 & 0 \\ -\sqrt{b_j^{\Gamma}}\phi_j^{\Gamma *}(\hat{\mathbf{k}})(\mathbf{v}^{\dagger})_{\alpha\beta} & 0 \end{pmatrix}, \tag{2.63}$$

the trace of the right hand side of Eq. (2.60) becomes

$$\begin{aligned} &\frac{-1}{\Lambda}\sum_{\alpha\beta}\sum_{i=1}^{d_\Gamma}\sqrt{b_i^{\Gamma}}\sqrt{b_j^{\Gamma}}\phi_i^{\Gamma}(\hat{\mathbf{k}})\phi_j^{\Gamma *}(\hat{\mathbf{k}})\left[\mathbf{\Delta}_{i,0}\cdot(\mathbf{v})_{\alpha\beta}\right](\mathbf{v}^{\dagger})_{\beta\alpha} \\ &\quad = \frac{-2\sum_{i=1}^{d_\Gamma}\sqrt{b_i^{\Gamma}}\sqrt{b_j^{\Gamma}}\phi_i^{\Gamma}(\hat{\mathbf{k}})\phi_j^{\Gamma *}(\hat{\mathbf{k}})\mathbf{\Delta}_{i,0}}{-\omega_n^2-\xi_{\mathbf{k}}^2-f_{\mathbf{k}}^2} \\ &\quad = \frac{-2\sum_{i=1}^{d_\Gamma}\sqrt{b_i^{\Gamma}}\sqrt{b_j^{\Gamma}}\phi_i^{\Gamma}(\hat{\mathbf{k}})\phi_j^{\Gamma *}(\hat{\mathbf{k}})\mathbf{\Delta}_{i,0}}{(i\omega_n+E_{\mathbf{k}})(i\omega_n-E_{\mathbf{k}})}, \end{aligned} \tag{2.64}$$

where $E_{\mathbf{k}}^2 = \xi_{\mathbf{k}}^2 + f_{\mathbf{k}}^2$. Notice that the numerator of the expression above is independent of ω_n, since the saddle point order parameter $\mathbf{\Delta}_{i,0}$ is time and hence frequency independent. Therefore, the summation over Matsubara frequency ω_n is only in the denominator and can be performed, leading to

$$\begin{aligned} \sum_{\omega_n}\frac{1}{(i\omega_n+E_{\mathbf{k}})(i\omega_n-E_{\mathbf{k}})} &= \frac{1}{2E_{\mathbf{k}}}\sum_{\omega_n}\left[\frac{1}{i\omega_n-E_{\mathbf{k}}}-\frac{1}{i\omega_n+E_{\mathbf{k}}}\right] \\ &= \frac{1}{2E_{\mathbf{k}}}\frac{\beta}{2}\left[\tanh\left(\frac{-\beta E_{\mathbf{k}}}{2}\right)-\tanh\left(\frac{\beta E_{\mathbf{k}}}{2}\right)\right] \\ &= -\frac{\beta}{2E_{\mathbf{k}}}\tanh\left(\frac{\beta E_{\mathbf{k}}}{2}\right). \end{aligned} \tag{2.65}$$

With these results, Eq. (2.60) becomes

$$\frac{\mathbf{\Delta}_{j,0}}{V_\Gamma} = \sum_{\mathbf{k}}\frac{\sqrt{b_j^{\Gamma}}\phi_j^{\Gamma *}(\hat{\mathbf{k}})\sum_{i=1}^{d_\Gamma}\sqrt{b_i^{\Gamma}}\phi_i^{\Gamma}(\hat{\mathbf{k}})\mathbf{\Delta}_{i,0}}{E_{\mathbf{k}}}\tanh\left(\frac{\beta E_{\mathbf{k}}}{2}\right). \tag{2.66}$$

If only one pairing state with a specific b_j^{Γ} and symmetry function $\phi_j^{\Gamma}(\hat{\mathbf{k}})$ is dominant, the equation above can be simplified to the more familiar form

$$1 = V_\Gamma\sum_{\mathbf{k}}\frac{|\phi^{\Gamma}(\hat{\mathbf{k}})|^2}{E_{\mathbf{k}}}\tanh\left(\frac{\beta E_{\mathbf{k}}}{2}\right), \tag{2.67}$$

where the factor b_j^{Γ} is absorbed into the interaction strength V_Γ, and the subscript of ϕ is neglected. Notice that this equation has the same form as the BCS order parameter equation.

Equation (2.67) can be solved together with the number equation to give the saddle point (or mean field) solution for the superconducting order parameter and the chemical potential. From statistical mechanics, the number of particles is related to the grand partition function by

$$N = -\frac{\partial \Omega}{\partial \mu} = \frac{1}{\beta}\frac{\partial \ln \mathcal{Z}}{\partial \mu}. \tag{2.68}$$

Thus, at the saddle point level, the number of particles takes the form

$$N_0 = \frac{1}{\beta}\frac{\partial}{\partial \mu}\left\{-S_{\rm eff}[\mathbf{\Delta}^{\dagger}_{j,0}, \mathbf{\Delta}_{j,0}]\right\} = \frac{1}{\beta}\sum_{\mathbf{k}}\left\{\beta + \frac{1}{2}\sum_{\omega_n}{\rm tr}\left[\mathcal{G}_0\frac{\partial}{\partial \mu}\mathcal{G}_0^{-1}\right]\right\}. \tag{2.69}$$

By using the expression (2.61) and (2.62) for $\mathcal{G}_0^{-1}$ and $\mathcal{G}_0$, and taking the same Matsubara summation as in Eq. (2.65), the saddle point contribution to the number of particles becomes

$$N_0 = \sum_{\mathbf{k}}\left[1 - \frac{\xi_{\mathbf{k}}}{E_{\mathbf{k}}}\tanh\left(\frac{\beta E_{\mathbf{k}}}{2}\right)\right]. \tag{2.70}$$

This equation has the same form as the BCS number equation, which can be solved together with the order parameter equation (2.67) to obtain chemical potential μ and order parameter $\mathbf{\Delta}_0$, for a given temperature and particle density. The solutions of these equations give the saddle point results, which are valid away from critical point. However, when the system moves towards the critical point, one has to take into account of fluctuation effects. In order to do that, one can consider a time dependent fluctuation over the saddle point order parameter $\mathbf{\Delta}_{j,0}$ such that

$$\mathbf{\Delta}_j(\mathbf{k}, \tau) = \mathbf{\Delta}_{j,0} + \boldsymbol{\eta}_j(\mathbf{k}, \tau), \tag{2.71}$$

and then expand the effective action (2.54) up to the quadratic term of $\boldsymbol{\eta}_j$. This expansion is called Gaussian approximation [152]. To address the approach to the critical point, where a second order normal–superfluid transition takes place, one can develop a Ginzburg–Landau (GL) theory. Next, I will use the functional integral formalism to derive the GL equation for triplet superfluidity, and show that each term in the GL functional can be obtained by a corresponding Feynman diagram.

2.3.3 Ginzburg–Landau Theory

To derive the GL theory, I start from the effective action (2.54), and expand $S_{\rm eff}$ in powers of $\mathbf{\Delta}_j(\tau)$. In the following discussion, I assume that only one b_j^Γ and one symmetry function ϕ_j are relevant to the superfluid transition. Thus, I can simplify notation by absorbing b_j^Γ into interaction strength V_Γ, and omitting the subscript j in both ϕ_j and $\mathbf{\Delta}_j$. Using these notations, the effective action becomes

$$S_{\rm eff}[\mathbf{\Delta}^\dagger(\tau),\mathbf{\Delta}(\tau)] = \int_0^\beta d\tau \left[\frac{1}{2V_\Gamma}\mathbf{\Delta}^\dagger(\tau)\cdot\mathbf{\Delta}(\tau) + \sum_{\mathbf{k}}\xi_{\mathbf{k}}\right] - \frac{1}{2}\mathrm{Tr}_{\mathbf{k},\tau}\left(\ln \mathcal{G}^{-1}(\mathbf{k},\tau)\right), \quad (2.72)$$

where the matrix $\mathcal{G}^{-1} = (\mathcal{P}^{-1}+\mathcal{K})/2$ with

$$\mathcal{P}^{-1}(\mathbf{k},\tau) = \begin{pmatrix} (\partial_\tau + \xi_{\mathbf{k}})\,\delta_{\alpha\beta} & 0 \\ 0 & (\partial_\tau - \xi_{\mathbf{k}})\,\delta_{\alpha\beta} \end{pmatrix}, \quad (2.73)$$

and

$$\mathcal{K}(\mathbf{k},\tau) = \begin{pmatrix} 0 & -\phi^\Gamma(\hat{\mathbf{k}})(\mathbf{v})_{\alpha\beta}\cdot\mathbf{\Delta}(\tau) \\ -\phi^{\Gamma *}(\hat{\mathbf{k}})\mathbf{\Delta}^\dagger(\tau)\cdot(\mathbf{v}^\dagger)_{\alpha\beta} & 0 \end{pmatrix}. \quad (2.74)$$

In the region where the order parameter $\mathbf{\Delta}$ is small, the second term in the effective action can be expanded as follows:

$$\begin{aligned}\mathrm{Tr}_{\mathbf{k},\tau}\left[\ln\left(\mathcal{P}^{-1}+\mathcal{K}\right)/2\right] &= \mathrm{Tr}_{\mathbf{k},\tau}\left[\ln\mathcal{P}^{-1} - \ln 2\right] + \mathrm{Tr}_{\mathbf{k},\tau}\ln\left(1+\mathcal{P}\mathcal{K}\right) \\ &= \mathrm{Tr}_{\mathbf{k},\tau}\left[\ln\mathcal{P}^{-1} - \ln 2 + \mathcal{P}\mathcal{K} - \frac{1}{2}\left(\mathcal{P}\mathcal{K}\right)^2 + \frac{1}{3}\left(\mathcal{P}\mathcal{K}\right)^3 - \frac{1}{4}\left(\mathcal{P}\mathcal{K}\right)^4 + \cdots\right], \quad (2.75)\end{aligned}$$

where $\mathcal{P}$ can be easily obtained (since $\mathcal{P}^{-1}$ is diagonal) as

$$\mathcal{P}(\mathbf{k},\tau) = \begin{pmatrix} (\partial_\tau + \xi_{\mathbf{k}})^{-1}\,\delta_{\alpha\beta} & 0 \\ 0 & (\partial_\tau - \xi_{\mathbf{k}})^{-1}\,\delta_{\alpha\beta} \end{pmatrix}. \quad (2.76)$$

Since the expansion is around the critical point with the saddle point solution $\mathbf{\Delta} = 0$, all odd power terms must vanish and the effective action can be written as

$$S_{\rm eff} = S_0 + S_2 + S_4 + \cdots, \quad (2.77)$$

where $S_0 = \sum_{\mathbf{k}}(\beta\xi_{\mathbf{k}} + \ln\sqrt{2}) - (1/2)\mathrm{Tr}_{\mathbf{k},\tau}\ln\mathcal{P}^{-1}$ is a constant.

Assuming a static order parameter $\mathbf{\Delta}(\tau) = \mathbf{\Delta}_0$, the quadratic term S_2 then becomes

$$S_2 = \frac{\beta}{2V_\Gamma}\mathbf{\Delta}_0^\dagger \cdot \mathbf{\Delta}_0 + \frac{1}{4}\sum_{\mathbf{k},\omega_n} \mathrm{tr}\left[\mathcal{P}(\mathbf{k},\omega_n)\mathcal{K}(\mathbf{k},\omega_n)\right]^2 . \tag{2.78}$$

Here, the Fourier transformation from imaginary time to frequency is applied to transform the integral over $d\tau$ into summation over fermionic Matsubara frequencies ω_n. Notice that the matrix $\mathcal{P}(\mathbf{k},\omega_n)$ can be obtained from Eq. (2.76) through the substitution $\partial_\tau \to -i\omega_n$, and $\mathcal{K}(\mathbf{k},\omega_n) = \mathcal{K}(\mathbf{k})$ is frequency independent since $\mathbf{\Delta}$ is time independent. By multiplying the four matrices $(\mathcal{PKPK})$ and taking the trace over the resulting 4×4 matrix, one obtains

$$S_2 = \frac{\beta}{2V_\Gamma}|\mathbf{\Delta}_0|^2 + \sum_{\mathbf{k},\omega_n} \frac{|\phi(\hat{\mathbf{k}})|^2}{(i\omega_n + \xi_\mathbf{k})(i\omega_n - \xi_\mathbf{k})}|\mathbf{\Delta}_0|^2. \tag{2.79}$$

By performing the Matsubara summation as in Eq. (2.65), the quadratic term of the effective action can be written as

$$\begin{aligned} S_2 &= \left[\frac{\beta}{2V_\Gamma} - \sum_\mathbf{k} \frac{\beta}{2\xi_\mathbf{k}} \tanh\left(\frac{\beta\xi_\mathbf{k}}{2}\right)|\phi(\hat{\mathbf{k}})|^2\right]|\mathbf{\Delta}_0|^2 \\ &\equiv a|\mathbf{\Delta}_0|^2. \end{aligned} \tag{2.80}$$

Similarly, the quartic term S_4 is

$$\begin{aligned} S_4 &= \frac{1}{8}\sum_{\mathbf{k},\omega_n} \mathrm{tr}\left[\mathcal{P}(\mathbf{k},\omega_n)\mathcal{K}(\mathbf{k},\omega_n)\right]^4 \\ &= \frac{1}{4}\sum_{\mathbf{k},\omega_n} \frac{1}{(i\omega_n + \xi_\mathbf{k})^2(i\omega_n - \xi_\mathbf{k})^2}|\phi(\hat{\mathbf{k}})|^4 \left(2|\mathbf{\Delta}_0|4 - |\mathbf{\Delta}_0^2|^2\right) \\ &= \frac{1}{4}\sum_\mathbf{k} \left[\frac{\beta}{4\xi_\mathbf{k}^3}\tanh\left(\frac{\beta\xi_\mathbf{k}}{2}\right) - \frac{\beta^2}{8\xi_\mathbf{k}^2}\mathrm{sech}^2\left(\frac{\beta\xi_\mathbf{k}}{2}\right)\right]|\phi(\hat{\mathbf{k}})|^4 \left(2|\mathbf{\Delta}_0|^4 - |\mathbf{\Delta}_0^2|^2\right) \\ &\equiv \frac{b}{2}\left(2|\mathbf{\Delta}_0|^4 - |\mathbf{\Delta}_0^2|^2\right). \end{aligned} \tag{2.81}$$

Here, the multiplication of spin matrices and Matsubara summations are performed using the methods discussed in Appendix A and B, respectively.

It is instructive to notice that S_2 and S_4 can be obtained diagrammatically. For example, the first term of S_2 can be represented diagrammatically as in Fig. 2.1(a). Here, the wavy line represents the bosonic field $\mathbf{\Delta}_0$, and the double line denotes the bare Green's function for $\mathbf{\Delta}_0$, i.e., $G_B = \beta/V_\Gamma$. The second term in S_2 corresponds to the "polarization bubble"

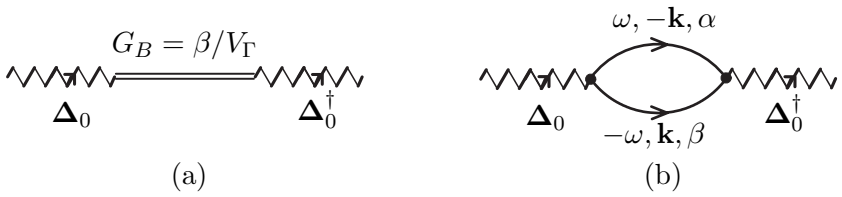

Figure 2.1: Feynman diagrams corresponding to (a) the first, and (b) the second terms of the quadratic effective action S_2, respectively.

as shown in Fig. 2.1(b). In this diagram, the solid line represents the bare fermionic Green's function $G_F(\mathbf{k}, \omega_n) = 1/(i\omega_n + \xi_\mathbf{k})$, and the vertex corresponds to the interaction between fermionic and bosonic fields, which takes the form $\phi^\Gamma(\hat{\mathbf{k}})(\mathbf{v})_{\alpha\beta}$ or $\phi^{\Gamma *}(\hat{\mathbf{k}})(\mathbf{v}^\dagger)_{\alpha\beta}$, depending on whether the vertex is connected to an annihilation or creation field of $\boldsymbol{\Delta}_0$, respectively. In summary, the one-to-one correspondence of the algebraic formalism and the diagrammatic representation is as follows:

1. For each initial bosonic field line connected to a vertex, write a factor $\phi^\Gamma(\hat{\mathbf{k}})\boldsymbol{\Delta}_0 \cdot (\mathbf{v})_{\alpha\beta}$, while for each final bosonic field line connected to a vertex, write the Hermitian conjugate $\phi^{\Gamma *}(-\hat{\mathbf{k}})\boldsymbol{\Delta}_0^\dagger \cdot \left(\mathbf{v}^\dagger\right)_{\alpha\beta}$;

2. For each internal fermionic line, labeled by the momentum $\mathbf{k}$ and frequency ω, write a factor

$$G_F(\omega, \mathbf{k}) = \frac{1}{i\omega + \xi_\mathbf{k}}; \tag{2.82}$$

3. The linear momentum associated with the bosonic line and the two fermionic lines meeting at each vertex satisfy energy–momentum conservation. For each closed loop, carry out the integration $\int d\mathbf{k}$ for each internal momentum $\mathbf{k}$, and carry out the summation $\sum_{\omega_n}$ for each internal frequency ω_n.

4. The spin indices of two fermionic lines meeting at each vertex have to be the same as the spin indices of that vertex, indicating the fermionic spins do not flip. For each spin index α, carry out the summation $\sum_\alpha$. For each closed loop, the summation over spin indices is equivalent to a trace over all spin matrices $\mathbf{v}$.

5. Multiply the expression by the factor $1/N$ for diagram with N external bosonic lines.

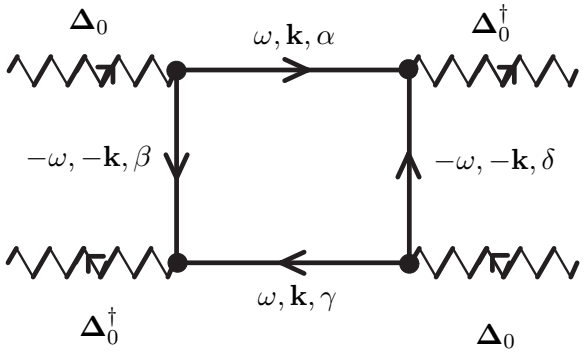

Figure 2.2: Feynman diagrams corresponding to the quartic effective action S_4.

By using these Feynman rules, one can verify that the quartic term S_4 can be obtained from the diagram with four external wavy lines, as shown in Fig. 2.2.

With the GL effective action, either derived using the functional integral method or constructed from Feynman diagrams, one can obtain the GL equation by requiring that $\delta S_{\text{eff}}/\delta \boldsymbol{\Delta}_0^\dagger = 0$, leading to

$$\left[a + \frac{b}{2}\left(2|\boldsymbol{\Delta}_0|^2\boldsymbol{\Delta}_0 - \boldsymbol{\Delta}_0^2\boldsymbol{\Delta}_0^*\right)\right] = 0. \tag{2.83}$$

Notice that the equation above is different from the GL equation for singlet superconductors [145] in two aspects: First, the non-linear terms in Eq. (2.83) are different from those in the singlet superconductivity GL equation. This difference originates from the spin structure of the triplet pairing. Second, the spatial derivative term is absent since I considered in this chapter only the simplified Hamiltonian of Eq. (2.34), where only fermions with opposite momenta can form Cooper pairs. This assumption excludes the possibility of having a non-uniform order parameter since the center-of-mass momentum of the Cooper pair is zero and the pair wave function is completely uniform. However, I will discuss in Chapter 3 and 4 general Hamiltonian which allow for pairing between fermions with arbitrary momenta, derive the spatial and time dependent GL equation for quasi-one-dimensional conductors and p-wave Fermi condensates of ultra-cold atoms. In Chapter 3, I show that the GL coefficients are crucial to determine the phase diagram of the quasi-one-dimensional conductor $(\text{TMTSF})_2\text{PF}_6$. Using parameters suggested by experiments, I propose a coexistence phase

of spin density waves (SDW) and triplet superconductivity (TSC), where both SDW and TSC order parameters are non-uniform. In Chapter 4, I derive the time dependent GL (TDGL) equation for p-wave Fermi condensate, and discuss the polarization effect and time evolution of a harmonically trapped condensate.

CHAPTER III

COEXISTENCE OF SPIN DENSITY WAVES AND TRIPLET SUPERCONDUCTIVITY IN QUASI-ONE-DIMENSIONAL CONDUCTORS

In chapter 2, I presented the background necessary to develop a theory for superconductivity and superfluidity in correlated Fermi systems, emphasizing the possibility of triplet superfluidity as an unconventional pairing state. In this chapter, I will focus on the specific material $(TMTSF)_2PF_6$, which is one of the most well studied quasi-one-dimensional (quasi-1D) organic conductors. The superconducting phase of $(TMTSF)_2PF_6$ seems to be a triplet state, since its upper critical field exceeds the Pauli paramagnetic limit, and the Knight shift difference is absent. In addition, the interplay between magnetic and superconducting orders seems to be very important. Thus, here I will discuss in detail the coexistence or competition of spin density waves (SDW) and triplet superconductivity (TSC) in $(TMTSF)_2PF_6$, and mention other aspects only briefly.

The interplay between spin density waves and triplet superconductivity in $(TMTSF)_2PF_6$ is an important problem because most experiments that reveal exotic behavior of the superconducting phase were performed in the pressure versus temperature phase diagram close to the SDW phase. Therefore, the effects of SDW order on the superconducting state of quasi-1D systems must be addressed. In addition, the competition or coexistence of magnetic order and superconductivity is itself a very important problem in condensed matter physics. There is a broad class of systems that present magnetic order and superconductivity in close vicinity. One of the most important systems are the copper oxides, where singlet superconductivity (SSC) is found next to antiferromagnetism (AFM) [153]. Another interesting system is strontium ruthenate Sr_2RuO_4, where the proximity to ferromagnetism

(FM) has been argued as being important to the existence of possible triplet superconductivity in these materials [154]. Furthermore the ferromagnetic superconductors $ZrZn_2$ and UGe_2 have stimulated a debate on the coexistence of ferromagnetism and triplet or singlet superconductivity [155, 156]. However, unlike any of these previous examples, the TSC and SDW orders in quasi-1D systems would avoid coexistence at first glance, since the two orders are competing to correlate electrons in the triplet and singlet spin sectors, respectively. For instance, the presence of SDW order would disrupt TSC in a more dramatic way than it would SSC, while the FM order would disrupt SSC more than TSC. Therefore, it is easier to find in nature examples of coexistence of SSC and SDW or TSC and FM, while the conditions to find the coexistence of TSC and SDW are much more stringent.

The main results described in this chapter are as follows. First, I will derive microscopically the pressure versus temperature phase diagram indicating the TSC, the SDW and the coexistence of TSC and SDW (TSC/SDW) phases, and show that the TSC and SDW order parameters are both non-uniform in the coexistence region. Second, I propose that external magnetic fields cause a canting transition of the SDW order parameter, which alter the nature of the TSC state in the coexistence region since SDW and TSC are coupled. In addition, to the normal phase, I find new phases in the magnetic field versus temperature phase diagram near the critical pressure.

3.1 Background

The discovery of the first organic superconductor bistetramethyltetraselenafulvalene hexafluorophosphate [$(TMTSF)_2PF_6$] by Jerome *et al.* [19] in 1980 stimulated a dramatic search for superconductivity in other quasi-1D Bechgaard salts family. This search has lead to discoveries of other very interesting physical effects, among these phenomena it is worth highlighting the existence of metallic, spin density wave and superconducting phases. These phases can exist in the same material depending on temperature, pressure, magnetic field, and anion ordering. A schematic pressure versus temperature phase diagram for $(TMTSF)_2X$ and $(TMTTF)_2X$ is shown in Fig. 3.1 [157], where X represents different anions. In addition, the discovery of magnetic field induced spin density waves (FISDW) [158]

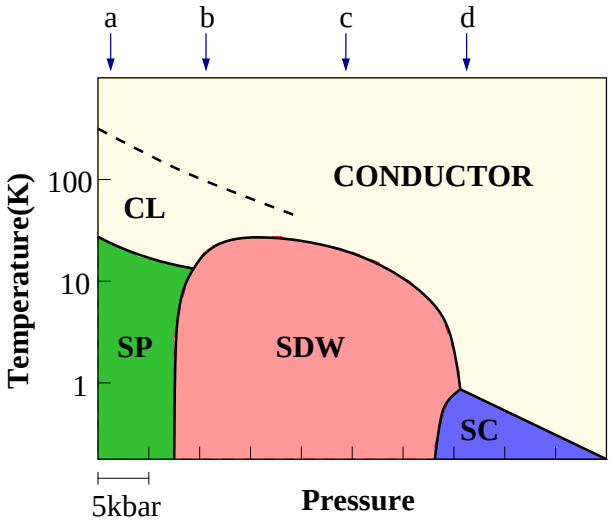

Figure 3.1: Generalized phase diagram for $(TMTSF)_2X$ and $(TMTTF)_2X$ compounds adapted from Ref. [157]. The notation CL, SP, SDW and SC refers to charge-localized, spin-Peierls, spin density wave, and superconducting states, respectively. The lower-case letters designate compounds and indicate their location at ambient pressure in the generalized diagram. (a) $(TMTTF)_2PF_6$, (b) $(TMTTF)_2Br$, (c) $(TMTSF)_2PF_6$, (d) $(TMTSF)_2ClO_4$.

in these systems stimulated an incredible surge of theoretical and experimental interest in the 1980's, as can be verified in the book by Saito and Kagoshima [159]. Among the recent aspects related to these phenomena it is important to single out the quantum Hall effect and the new angle-dependent magneto-resistance oscillations [34, 160, 45, 161, 162]. More recently there has been some experimental and theoretical efforts in trying to decipher the nature of the metallic state in a magnetic field [163, 164]. The origin of many of these features lies in the extremely anisotropic nature of the electronic structure in these materials resulting from their weakly coupled chain-like crystalline structure.

3.1.1 Crystal Structure and Electronic Dispersion

The $(TMTSF)_2X$ family is iso-structural, where all members are triclinic crystals with very similar lattice parameters. As can be seen is Fig. 3.2, nearly planar TMTSF molecules form chains along the so-called **a** (x) axis, and form sheets in the **a**-**b**$'$ (xy) plane [165]. These sheets are separated by anions along the $\mathbf{c}^*$ (z) axis. Selenium (Se) orbitals play an important role on the electronic properties of these materials [selenium corresponds to S in the chemical formula $(TMTSF)_2X$]. Although Se–Se spacings along the **a** (x)

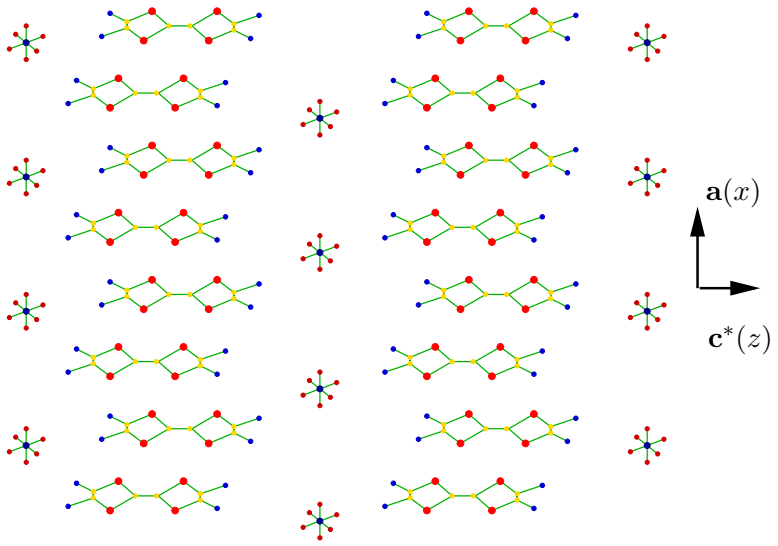

Figure 3.2: View of the crystal structure of $(TMTSF)_2PF_6$ showing the **a** and $\mathbf{c}^*$ axes.

axis and along the $\mathbf{b}'$ (y) axis are comparable, the overlap of π orbitals is strongest along the chains (**a** direction). As a consequence, the electronic spectrum is quasi-1D and the electron transfer energies are estimated [166] to be of the order of 6000, 600, 24 K along special directions x, y and z. Throughout this chapter, I use interchangeably $x \leftrightarrow \mathbf{a}$, $y \leftrightarrow \mathbf{b}'$ and $z \leftrightarrow \mathbf{c}^*$, unless specified. I may also use the anion formulae PF_6 and ClO_4 as a shorthand notation to represent the corresponding Bechgaard salts $(TMTSF)_2PF_6$ and $(TMTSF)_2ClO_4$, respectively.

A simple approximation for these systems is to take the dispersion relation [167]

$$\epsilon_{\mathbf{k}} = -t_x \cos(k_x a) - t_y \cos(k_y b) - t_z \cos(k_z c), \tag{3.1}$$

with $t_x \gg t_y \gg t_z > 0$, where the a, b, and c are the lattice constants and t_x, t_y and t_z are the transfer integrals along the x, y and z directions, respectively. Even though this dispersion relation should be considered as a simplification, it contains some of the essential characteristics of the quasi-1D band structure near the Fermi energy. The use of this dispersion relation implicity assumes an orthorhombic crystal structure for Bechgaard salts. However, these systems are really triclinic with lattice parameters at room temperature $a = 3.648$Å, $b = 7.711$Å, $c = 13.522$Å, with angles $\alpha = 83.39°$, $\beta = 86.27°$, and $\gamma = 71.01°$, as seen in Fig. 3.3 [168, 169]. This means that all the discussions presented here in connection

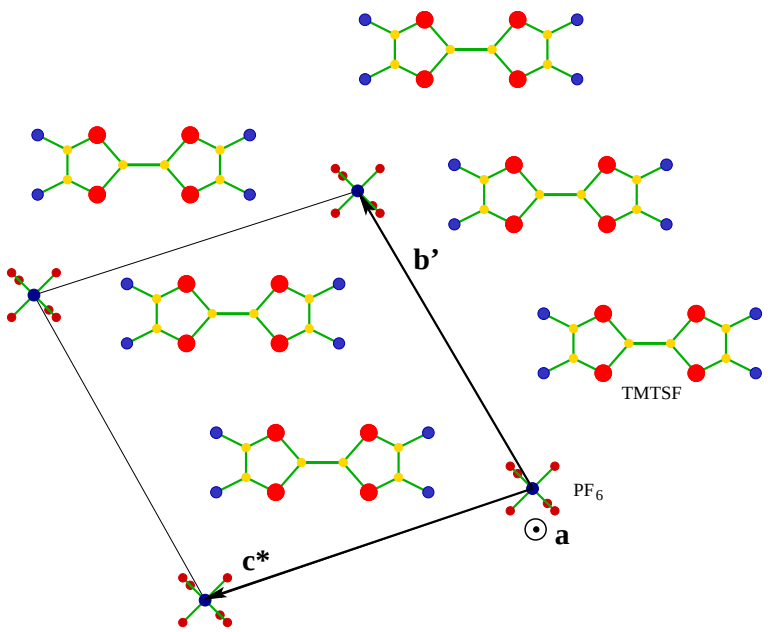

Figure 3.3: View of the crystal structure of $(TMTSF)_2PF_6$ showing the principal directions **a**, **b**′ and **c***. Adapted from Ref. [168].

with triclinic Bechgaard salts should be viewed only as qualitative at best.

As a consequence of this anisotropy, the Fermi surface of quasi-1D systems is open and has two separate sheets (see Fig. 3.4), such that the electronic motion then can be classified as *right* going (with sheet index $\alpha = +$) or *left* going (with sheet index $\alpha = -$). With the limiting condition that $t_x \gg \max(t_y, t_z)$, the dispersion relation above can be linearized

$$\epsilon_{\mathbf{k},\alpha} = v_F(\alpha k_x - k_F) - t_y \cos(k_y b) - t_z \cos(k_z c), \tag{3.2}$$

where the approximations $v_x \approx v_F$ and $t_x \approx E_F$ were used with v_F and E_F being Fermi velocity and Fermi energy, respectively. This strong anisotropy of the dispersion relation above leads to very interesting effects, especially in a magnetic field.

3.1.2 Upper Critical Fields of $(TMTSF)_2PF_6$

Typically the application of an external magnetic field is detrimental to superconductivity due to the following reasons. First, the coupling of the magnetic field with the electron charge forces electronic orbits to bend, and as a result it becomes more difficult for two electrons to form a Cooper pair. Therefore, the suppression of the formation of these

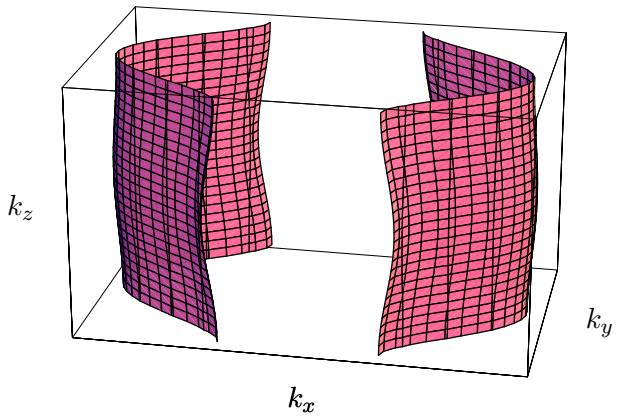

Figure 3.4: The Fermi surface of quasi-1D systems with transfer integrals $t_x \gg t_y \gg t_z > 0$ is open.

bound states immediately undermines superconductivity. This phenomenon is called orbital frustration, and affects both singlet and triplet superconductors. Second, the coupling of the magnetic field to spins also tends to break Cooper pairs because of the Zeeman energy cost. The Zeeman splitting affects directly singlet superconductors which have magnetic quantum numbers ($S = 0$, $m_S = 0$), since electrons with spin up and with spin down are separated in energy. In the case of triplet superconductors, a magnetic field also has a direct effect on states with magnetic quantum numbers ($S = 1$, $m_S = 0$), but not on states with both spins aligned, i.e. ($S = 1$, $m_S = \pm 1$).

Therefore, in order to make the quantum level structure work in favor of superconductivity at high magnetic fields (beyond the semiclassical orbital upper critical fields and beyond the Pauli paramagnetic limit), one must envision a mechanism that eliminates or compensates for (i) the orbital frustration, and (ii) the Zeeman splitting introduced by the magnetic field. For three-dimensional isotropic systems, such a mechanism was proposed by Tesanovic *et al.* [170] and later by Norman, MacDonald and Akera [171], building up and expanding on earlier works [172, 173]. The survival of superconductivity up to very high magnetic fields involved reaching the extreme quantum limit, where only a single Landau level is occupied. Then Cooper pairing can occur between electronic states in the same Landau level, thus beating the detrimental orbital frustration. In this case, superconductivity

is only limited by the Pauli pair breaking effect and impurity scattering. The magnetic fields required to reach this extreme quantum limit for ordinary metals is very high, being typically in the range of thousands of tesla. The reason for such high fields is that ordinary metals are high density materials with large Fermi energies. However, it is very difficult to reach fields of the order of thousands of tesla with current technology.

The advantage of quasi-1D systems is that the extreme quantum limit can be reached for magnetic fields beginning in the range from 5 to 30 T [166]. This is possible for magnetic fields applied along the y axis, because of the extreme anisotropic electronic structure of these systems ($t_x \gg t_y \gg t_z$). When $\omega_c \equiv v_F|e|H_y c \gg t_z$ the electronic wave functions are confined along the z axis, hence they represent a highly degenerate single quantum Landau level at the Fermi energy [38, 166]. In such a case, pairing within the same quantum level is possible, and here it means pairing in the xy plane. Therefore, the quasi-1D, but nevertheless 3D anisotropic superconductors become essentially 2D anisotropic superconductors [34, 36]. This effect is called magnetic field induced dimensional crossover (MFIDC). On the other hand, at high magnetic fields, the confinement of the electronic motion along the z axis, also tends to confine the formation and motion of Cooper pairs mostly in the xy planes (pairing in the lowest quantum Landau level). This produces an effective coherence length $\xi_z^{\rm eff}$ which is smaller than the inter-planar lattice spacing c. As a result, there exists a novel MFIDC from a strongly 3D but highly anisotropic Abrikosov vortex lattice to a nearly 2D highly anisotropic Josephson vortex lattice [36]. Beyond the crossover regime, the magnetic field along the y axis can not break Cooper pairs, thus the orbital frustration disappears, and hence the Pauli paramagnetic pair breaking effect determines the final shape of the upper critical field. This MFIDC mechanism then leads to the survival of superconductivity in high magnetic fields for singlet superconductors and to a reentrant behavior for triplet superconductors. This high field behavior is most likely to occur in a triplet superconductor with equal spin pairing [38, 166] similar to the A-phase [74] of liquid ^{3}He, in order to take advantage of the external field. Motivated by this theoretical prediction, Lee *et al.* [41] carefully designed a more delicate experiment to measure the upper critical field of $(TMTSF)_2PF_6$, and observe some anomalous results which favor triplet

pairing states.

Surprisingly, prior to 1997, experimental investigations of the upper critical field of $(TMTSF)_2PF_6$ and its anisotropy [174, 175, 21, 176] had not been undertaken in the temperature and field regimes where anomalous effects were theoretically predicted, i.e., $T \ll T_c$ and $(H/T_c) \gg (dH_{c_2}/dT)_{T_c}$. This regime started to be explored only after the initial experimental work of Naughton's and Chaikin's groups [41], where the upper critical field of $(TMTSF)_2PF_6$ was studied at pressure $P \approx 6.0$ kbar. This pressure is large enough to suppress the nearby spin density wave phase and allow the existence of a metallic state at high temperatures and of a superconducting state at low temperatures [55]. (The insulator–superconductor transition pressure P_c, is about 5.9 kbar in their calibrated pressure scale.) In these experiments, Lee *et al.* [41] extracted the critical temperature $T_c(H)$ as a function of magnetic field from resistance measurements for magnetic fields precisely aligned with the three principal directions $\mathbf{a}$, $\mathbf{b}'$ and $\mathbf{c}^*$, and obtained the H–T phase diagram as shown in Fig. 3.5.

Notice that the phase diagram is consistent with previous low field studies [174, 175, 177, 21, 178, 27] of $(TMTSF)_2ClO_4$, and the upper critical fields obey the relation $H_{c_2}^a > H_{c_2}^{b'} > H_{c_2}^{c^*}$ for temperatures close to $T_c(0) = 1.13$ K. However, there are two unusual features embedded in the phase diagram of Fig. 3.5. The first one is that the upper critical fields for $\mathbf{H} \parallel \mathbf{a}$ and for $\mathbf{H} \parallel \mathbf{b}'$ do not seem to saturate at low temperatures. Furthermore, the upper critical field along these directions exceeds the Pauli paramagnetic limit for this compound by a factor of 2, at least. This paramagnetic limit is given by $H_P(T = 0) = 1.84T_c(H = 0)$ for an isotropic s-wave system in the absence of spin-orbit coupling [29, 30], or by $H_P(T = 0) = 1.58T_c(H = 0)$ for an anisotropic s-wave singlet pairing [33]. In the case of $(TMTSF)_2PF_6$ these estimates correspond to 2.1 T and 1.8 T, respectively. Thus, at low temperatures, $H_{c_2}^{b'} > 2H_P$.

The second unusual feature is the anisotropy inversion that occurs above the characteristic field $H^* \approx 1.6$ T, where $H_{c_2}^{b'}$ becomes larger than $H_{c_2}^a$. The fact that this anisotropy inversion was not seen prior to their work, is attributed to the strong sensitivity of H_{c_2} to sample alignment with respect to the external magnetic field. For instance, a tilt of

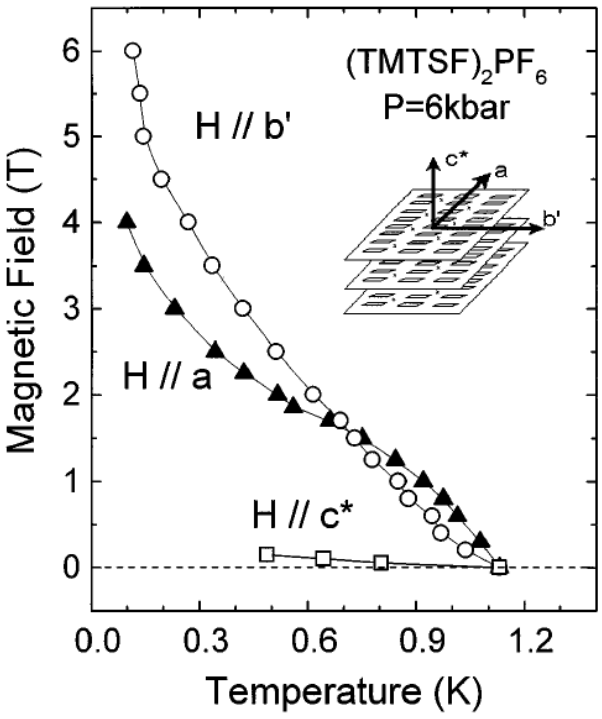

Figure 3.5: The magnetic field versus temperature (H–T) phase diagram for $(TMTSF)_2PF_6$ for magnetic fields aligned along the three principal axis $\mathbf{a}$, $\mathbf{b}'$, and $\mathbf{c}^*$. Adapted from Ref. [41].

0.1° away from $\mathbf{b}'$ towards $\mathbf{c}^*$ is sufficient to bring $H_{c_2}^{b'}$ below $H_{c_2}^{a}$ at low temperatures. Another possible reason is that early upper critical field measurements in Bechgaard salts were performed on $(TMTSF)_2ClO_4$ (at $P = 0$), or on $(TMTSF)_2PF_6$ and $(TMTSF)_2AsF_6$ at higher pressures. However, the pressure used in this experiment is very close to the critical value for the suppression of the insulating SDW phase, and yields a maximized critical temperature T_c.

The unusual upper curvature and exceeding of Pauli limit for $H_{c_2}(T)$ can be related to interpretations from existing theories of layered superconductors. In a theory by Ovchinikov and Kresin [179], it was shown that a upward curvature in $H_{c_2}(T)$ results at low temperatures, because the pair breaking ability of magnetic impurities is reduced as $T \to 0$. However magnetic scattering is essentially negligible in $(TMTSF)_2PF_6$ since the PF_6 ion is non-magnetic. Strong upward curvature was also discussed by Kotliar and Varma [180] in the context of cuprate superconductors for magnetic fields normal to the layers. They suggested that the proximity to a quantum critical point is responsible for the upward curvature in $H_{c_2}(T)$ at low temperatures. They found that $H_{c_2}(T) \approx 1 - t^\alpha$, with $t = T/T_c$ and $\alpha = 2/5$ would fit a small portion of the experimental data close to $T = 0$ for cuprate superconductors. Although the above expression agrees reasonably well with the measured $H_{c_2}^{b'}(T)$ over the entire temperature range $0.1 < t < 1$, this theory is only applicable to fields perpendicular to the layers, and thus cannot explain the $(TMTSF)_2PF_6$ data. One theory which remains consistent with the upward curvature and the exceeding of Pauli paramagnetic limit of $H_{c_2}(T)$ is the triplet superconductivity scenario proposed by Lebed [34], Burlachkov, Gorkov and Lebed [35], and by Dupuis, Montambaux, and Sá de Melo [36]. However, since the agreement between theoretical and experimental results is only qualitative, further work is necessary in order to explore the symmetry of the superconducting state. In the absence of phase sensitive experiments like those performed in high-T_c superconductors [59, 60, 61], Knight shift experiments are the next natural candidate to get information about the spin structure of the superconducting state.

3.1.3 ^{77}Se Knight Shift and NMR Measurements in $(TMSTF)_2PF_6$

The Knight shift is a very important technique to measure electron spin susceptibility. It is defined as the shift of NMR resonant frequency due to interaction between nuclear and electron spins. In the presence of a magnetic field **H**, nuclear spins in a material precess with the frequency $\omega \propto H$. At this frequency a nuclear magnetic resonance can be detected, i.e., there is a resonant absorption of energy from a radio-frequency magnetic field $\mathbf{H}_{\rm rf}$ with polarization perpendicular to the constant magnetic field **H**. Due to the finite probability of an electron to be located at the nucleus site R_n, there is an interaction between the nuclear magnetic moments and those of the conducting electrons, $\mathcal{H}_{\rm int} \propto \mathbf{m}_{\rm el}\delta(r - R_n)$. The average value of $\mathbf{m}_{\rm el}$ in this external field is given by $\langle \mathbf{m}_{\rm el} \rangle \propto \chi H$, where χ is the electronic paramagnetic susceptibility. Thus, the nuclear spin energy levels due to this interaction shift the NMR frequency by $\delta\omega \equiv K_s \propto \chi H$, which defines the Knight shift K_s.

In a superconductor with singlet pairing, Cooper pairs do not contribute to the spin paramagnetic susceptibility since $m_s = 0$, and the entire spin magnetic moment is determined by the contribution from elementary excitations. Therefore, the electronic spin susceptibility for a singlet superconductor is

$$\chi = \frac{\partial M}{\partial H} = \chi_n Y(T), \tag{3.3}$$

where χ_n is the normal state spin susceptibility and the function $Y(T)$ is the Yosida function, which determines the fraction of normal electrons in a superconductor. In the singlet case, $Y(T)$ vanishes at $T \to 0$, which means the Knight shift K_s will be strongly suppressed at low temperatures below the superconducting transition. On the contrary, in an equal spin triplet pairing superconductor, the Knight shift will remain unchanged upon cooling into the superconducting state, and will not vanish as $T \to 0$. Detailed discussions can be found in Leggett's review [74] for ^{3}He, and in Ref. [54] for triplet superconductors.

Prior to the experiment on ^{77}Se atoms by Lee *et al.* [65, 51], there exists an extensive NMR literature on both ambient pressure spin density wave [181] and pressurized metallic [182, 183] phases of $(TMTSF)_2PF_6$. Most of the previous works included studies of local magnetic environments of either protons in methyl groups or ^{13}C spin-labeled on various

inequivalent sites. However, band structure calculations and EPR studies suggest that the largest spin densities associated with the conduction band are closely linked to molecular orbitals connected to Se atoms [184]. Since the Knight shift is proportional to the magnitude square of the electron wave function at the ionic nucleus, ^{77}Se is a natural choice for NMR studies. Under this consideration, Lee *et al.* [65, 51] performed NMR measurements on ^{77}Se of $(TMTSF)_2PF_6$ in the superconducting state. To ensure that the pressurized sample is superconducting while acquiring the NMR data, they conducted simultaneous transport measurements in parallel (synchronization) to the application of radio-frequency pulses. From the measured spectra, Lee *et al.* [65, 51] concluded that there is no change in the Knight shifts of ^{77}Se when $\mathbf{H} \parallel \mathbf{a}$ or $\mathbf{H} \parallel \mathbf{b}'$.

The absorption spectra is shown in Fig. 3.6 (from Ref. [51]). The lower set of spectra is collected as free induction decays (FIDs), and the upper as spin echoes. These spectra were recorded at temperatures above and below T_c, for a magnetic field aligned parallel to the layers to within 0.1° and parallel to the $\mathbf{b}'$ axis to within $\approx 5°$. Notice that there is no change in the absorption peak (marked by the vertical solid line in Fig. 3.6), to within the experimental error bars ($\delta K_s = \pm 20$ ppm). The lack of any observable difference between the spectra as the temperature is varied indicates that the system is not a singlet superconductor.

The vertical shaded region in Fig. 3.6 corresponds to the estimated range where the center of the spectrum would have been if the spin susceptibility had vanished. This expected Knight shift window is extrapolated from the NMR frequency shift K in the normal state as a function of spin susceptibility χ for $\mathbf{H} \parallel \mathbf{b}'$. The vertical lines that bound the shaded region in Fig. 3.6 mark the corresponding first moment at 340–480 ppm above the measured value. At the measuring field of $H = 2.38$ T, this corresponds to about 6–9 kHz, with an estimated uncertainty of about 1 kHz. Lee *et al.* [65] also discovered that ^{77}Se spectroscopy with the field aligned along the **a** axis was more sensitive. Thus, they worked at much lower fields $H = 1.43$ T for $\mathbf{H} \parallel \mathbf{a}$ and observed similar results.

In order to guarantee the validity of the ^{77}Se NMR data, Lee *et al.* [51] performed transport measurements simultaneously to confirm the superconducting state. Furthermore,

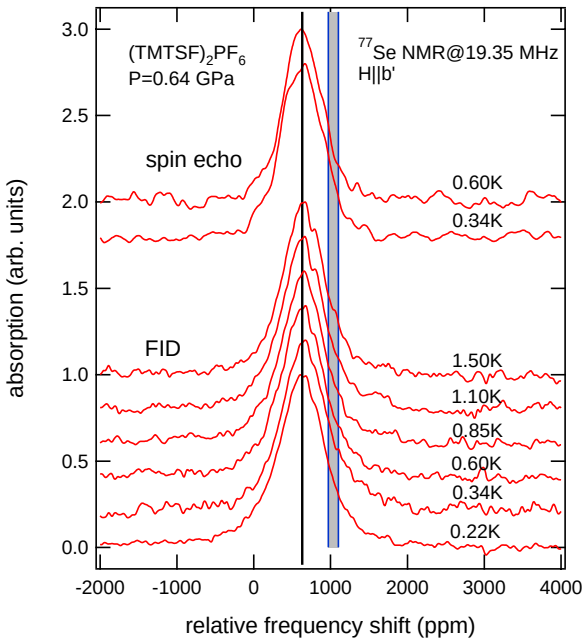

Figure 3.6: NMR ^{77}Se absorption spectra collected at temperatures below and above T_c for a magnetic field $H = 2.38$ T applied along the $\mathbf{b}'$ axis. The solid line indicates the measured first moment, and the shaded region indicates the expected first moment for a singlet ground state. Adapted from Ref. [51].

to obtain an independent bulk measurement of the superconducting transition, Lee *et al.* [51] also recorded the spin-lattice relaxation rates $1/T_1$ for ^{77}Se at $H = 2.38$ T, and for the methyl group protons ^{1}H at $H = 232$ mT and 12.8 mT. From their data (not shown here), a signature for superconductivity can be observed from the ^{77}Se relaxation rates, which shows no change in spin susceptibility between the normal and superconducting states. This evidence is consistent with the Knight shifts results discussed above, and strongly suggests triplet superconductivity in $(TMTSF)_2PF_6$.

3.1.4 Triplet Superconducting State in $(TMTSF)_2PF_6$

In addition to the spin structure, the orbital symmetry of the superconducting order parameter is another important property that needs to be characterized. The previous discussion on singlet versus triplet states is helpful to refine the number of possible choices, since the wave function is antisymmetric due to Pauli principle. However, even if we clarify the spin symmetry, either singlet or triplet, there are still several candidates for the orbital symmetry.

One way to investigate all possible symmetries systematically is through a group theoretical analysis, within the assumption that the normal state of quasi-1D superconductors does not break the full lattice symmetry. This group theoretical analysis was performed for the orthorhombic group by Duncan, Vaccarella and Sá de Melo [53] and extended by Duncan, Cherng and Sá de Melo [54]. In principle, superconductors with different orbital symmetries show distinct thermodynamic properties since the quasiparticle excitation spectra are different. However, a direct comparison between experimental and theoretical values of thermodynamic quantities is still lacking for superconducting $(TMTSF)_2PF_6$. This is mainly due to difficulties in fine tuning the pressure near the critical value required for the appearance of superconductivity.

On the other hand, thermodynamic measurements are more easily performed in the sister compound $(TMTSF)_2ClO_4$, which is superconducting at ambient pressure. For example, Belin and Behnia [42] measured the thermal conductivity of $(TMTSF)_2ClO_4$ and concluded that the electronic contribution to heat transport decreases rapidly below the critical temperature for superconductivity, thus indicating the absence of low energy electronic excitations, i.e., a fully gapped quasi-particle spectrum. Under the assumption that the superconducting order parameters have the same symmetry for $(TMTSF)_2ClO_4$ and $(TMTSF)_2PF_6$, the combined studies of upper critical field and Knight shift for PF_6, and thermal conductivity for ClO_4 are very suggestive of a fully gapped triplet state. According to the group analysis [53, 54], the triplet state with p_x-wave symmetry is a good candidate, where the quasi-particle excitation spectrum has no zeros due to the open Fermi surface in these quasi-1D systems. In this thesis, I will focus on this unitary triplet superconducting state with p_x-wave symmetry in $(TMTSF)_2PF_6$. However, further work is necessary to confirm this suggestion. For example, if experimental difficulties can be surmounted, it would be very useful to perform NMR experiments in $(TMTSF)_2ClO_4$, and thermal conductivity experiments in $(TMTSF)_2PF_6$. These two experiments combined can provide information about the spin and orbital nature of the order parameter for each of the compounds.

3.2 *Experiments Suggesting Coexistence of Spin Density Waves and Superconductivity in* $(TMTSF)_2PF_6$

In the previous section, I introduced the background of the superconducting state in quasi-1D organic conductors, and concluded that the existing experiments highly suggest a triplet superconducting phase in $(TMTSF)_2PF_6$. It is important to emphasize that all experiments that reveal exotic behavior of superconducting $(TMTSF)_2PF_6$ were performed in the phase diagram close to the insulating antiferromagnetic state, which is characterized by a spin density wave (SDW). Therefore, the effects of SDW on superconducting states of these quasi-1D systems should be addressed.

In $(TMTSF)_2PF_6$, experiments that explore physical properties in the vicinity of the SDW–Superconductivity (SC) phase boundaries in the P–T diagram are technically difficult because it is not easy to fine tune the pressure near the critical pressure P_c. However, some earlier measurements indicated the presence of an inhomogeneous state in the vicinity of P_c [66, 67]. Specifically, Azevedo *et al.*[66] found that the quenching of the SDW state was a slow function of pressure from measurements of the Knight shift in ^{77}Se. This was interpreted as an indication of the coexistence of the SDW and metallic states. Lee *et al.* [67] assumed the presence of macroscopic domains of superconducting and insulating SDW states to explain an unusual upper curvature of $H_{c2}^{c^*}(T)$. Recently, transport measurements by Vuletić *et al.* [68] and Kornilov *et al.* [69], as well as a simultaneous NMR and electrical transport measurements by Lee *et al.* [70] in $(TMTSF)_2PF_6$ all suggest an "inhomogeneous" coexistence region of SDW and Metal(SC) orders.

For instance, Vuletić *et al.* [68] performed resistivity measurements and suggested an inhomogeneous SDW–Metal (SDW–SC) phase due to a strong hysteretic behavior of resistivity between $T_{\rm SC}$ and $T_{\rm SDW}$ at a fixed pressure within $8.6 < P < 9.43$ kbar, as shown in Fig. 3.7. This pressure range is lower than but close to the SDW–SC critical pressure P_c, which is 9.43 kbar in their pressure gauge. Here $T_{\rm SC}$ and $T_{\rm SDW}$ are transition temperatures of superconducting and SDW phases, respectively. Notice that in the phase diagram Fig. 3.7, there is a 0.8 kbar wide pressure region which exhibits features of coexisting SDW/Metal and SDW/SC orders, such as hysteretic behavior of resistance as a function of temperature.

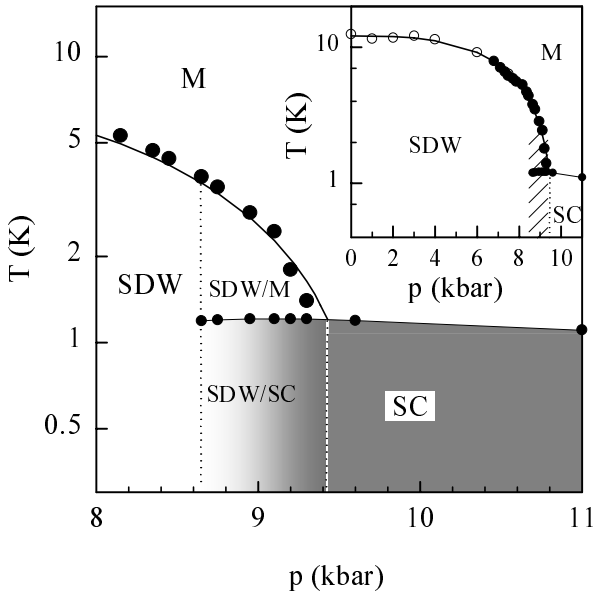

Figure 3.7: P–T phase diagram of $(TMTSF)_2PF_6$. SDW/M denotes the region where metallic and SDW phases coexist inhomogeneously, below T_{SDW} line (large dots). Below $T_{SC} = 1.20 \pm 0.01$ K line (small dots), this coexistence switches into a coexistence of SC and SDW phases, due to Metal–Superconductivity phase transition. A gradient in shading (SDW/SC region) below T_{SC} denotes the increase of SC volume. The solid curve separating the M and SDW phases is a fit to the data using the empirical formula $T_{SDW}(P) = T_1 - [(T_1 - T_{SC})(P/P_c)^3]$. Adapted from Ref. [68].

A similar hysteretic behavior was also observed in magneto-resistance measurements performed by Kornilov *et al.* [69] on $(TMTSF)_2PF_6$. Unlike Vuletić *et al.* [68], Kornilov *et al.* [69] used an alternative approach to cross the phase boundary by varying the magnetic field at fixed values of pressure and temperature. This technique has two advantages: (i) crossing phase boundaries may be achieved almost continuously, and (ii) different phases can be determined by various magneto-resistance characteristics. Using this method, Kornilov *et al.* also observed the hysteretic behavior in magneto-resistance, as the pressure and temperature is properly chosen such that the sweep of magnetic field from 0 to 16 T can drive the system through the SDW-Metal transition. Extending this result to the SDW–SC boundary, it is possible to have a transition from the SDW to SC state involving an inhomogeneous mixed state with coexisting SDW and SC phases. Motivated by this suggestion, Lee *et al.* [70] performed simultaneous NMR and transport measurements on

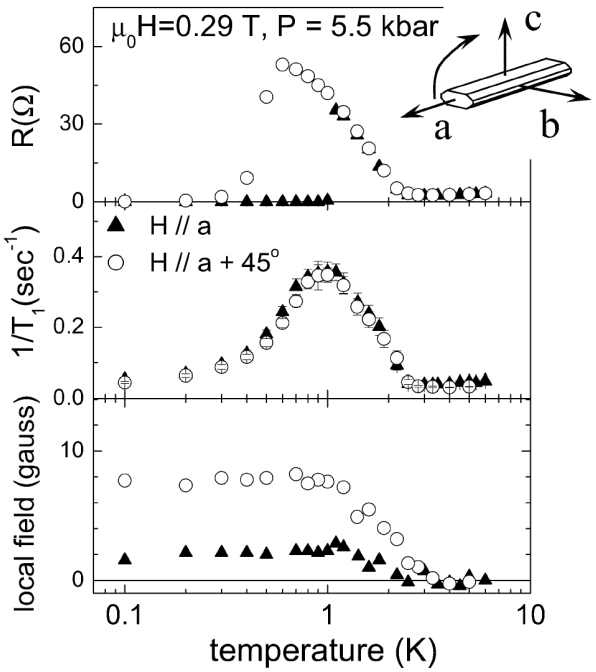

Figure 3.8: Simultaneous resistivity and proton NMR measurements. Shown here are the temperature dependence of interlayer resistance (top panel), proton spin-lattice relaxation rate (middle panel), and local field variations at the proton site (bottom panel). The data with triangles were obtained with a magnetic field aligned along the **a** axis and circles with a 45 degree tilt toward the $\mathbf{c}^*$ axis. Adapted from Ref. [70].

$(TMTSF)_2PF_6$, and directly showed the presence of SDW order in the superconducting state.

The main results of Lee *et al.* are shown in Fig. 3.8 [70], under a pressure of 5.5 kbar and in a magnetic field of 0.29 T. Data with triangles (circles) are obtained with field along the **a** axis (tilted 45 degrees towards the $\mathbf{c}^*$ axis). The top panel shows the results from interlayer ($\mathbf{c}^*$ axis) electrical transport, in which the resistance is enhanced below 3 K due to the SDW transition, followed by a superconducting transition near 1 K. The middle panel of Fig. 3.8 shows the simultaneously measured proton spin-lattice relaxation time ($1/T_1$). In the metallic state above 3 K, a single exponential curve describes fairly well the recovery of the magnetic moments. However, below 3 K, the recovery deviates significantly from an exponential, as local variations of the spectral density develop. The bottom panel shows the temperature dependence of the local magnetic field at the proton site, which is

essentially a measure of the full width of the NMR absorption spectra. It is important to note that the proton NMR results are dominated by the SDW signal, which is largely unaffected by the emergence of the superconducting state. Lee *et al.* [70] hence argued that the SDW and SC regions are macroscopically separated, and each SDW and SC domain is larger than its respective correlation length. By performing an angular magneto-resistance oscillation (AMRO) study, they also concluded that there are multiply connected SDW and SC domains, which are larger than several microns in linear dimension, and thus comparable to the mean free path of the uniform metallic phase.

Through different methods and approaches, the experiments by Vuletić *et al.* [68], Kornilov *et al.* [69] and Lee *et al.* [70] suggest a similar scenario of coexisting SDW/SC and SDW/Metal states on the P–T diagram. These authors concluded that the coexistence region consists of macroscopically segregated regions of SDW and M(SC), where there may be little or no effect of one ordered phase on another, due to their spatial separation. In order to explain this coexistence region, Vuletić *et al.* [68] proposed a free energy that included contributions from the ordered phases and elastic energy. Moreover, Podolsky *et al.* [71, 185] found similar coexistence for non-unitary TSC order within a modified SO(4) theoretical treatment, as do Zhang and Sá de Melo [72] within a variational free energy approach which includes negative interface energies. However, these previous theories are not directly applicable to three-dimensional but highly anisotropic superconductors like the Bechgaard salts, where the SO(4) symmetry is absent, and negative interface energies are not necessary conditions for the coexistence. Next, I will discuss the coexistence of SDW and TSC in $(TMTSF)_2PF_6$, starting from the highly anisotropic but nevertheless three-dimensional Hamiltonian.

3.3 The Microscopic Hamiltonian

As discussed in Section 3.1.1, the compound $(TMTSF)_2PF_6$ can be described approximately by an orthorhombic lattice with dispersion relation (3.1)

$$\epsilon_{\mathbf{k}} = -t_x \cos(k_x a) - t_y \cos(k_y b) - t_z \cos(k_z c),$$

where transfer integrals t_x, t_y, and t_z satisfy the relations $t_x \gg t_y \gg t_z > 0$ representing the quasi-one-dimensionality. The minimal Hamiltonian which can describe the instability towards triplet superconducting and SDW state can be written as $\mathcal{H} = \mathcal{H}_0 + \mathcal{H}_{\rm int}$, where the non-interacting part is

$$\mathcal{H}_0 = \sum_{\mathbf{k},\alpha} (\epsilon_{\mathbf{k}} - \mu) c^\dagger_{\mathbf{k},\alpha} c_{\mathbf{k},\alpha}, \tag{3.4}$$

with μ is the chemical potential and $\xi_{\mathbf{k}} = \epsilon_{\mathbf{k}} - \mu$ is the dispersion shifted by the chemical potential, which may include a Hartree shift. The interacting term is

$$\begin{aligned} \mathcal{H}_{\rm int} &= \frac{1}{2} \sum_{\mathbf{k}\mathbf{k}'\mathbf{p}} \sum_{\alpha\beta\gamma\delta} V_{\alpha\beta\gamma\delta}(\mathbf{k},\mathbf{k}') c^\dagger_{\mathbf{k}+\mathbf{p}/2,\alpha} c^\dagger_{-\mathbf{k}+\mathbf{p}/2,\beta} c_{\mathbf{k}'+\mathbf{p}/2,\gamma} c_{-\mathbf{k}'+\mathbf{p}/2,\delta} \\ &\quad + \frac{1}{2} \sum_{\mathbf{k}\mathbf{k}'\mathbf{q}} \sum_{\alpha\beta\gamma\delta} J_{\alpha\beta\gamma\delta}(\mathbf{q}) c^\dagger_{\mathbf{k}-\mathbf{q}/2,\alpha} c_{\mathbf{k}+\mathbf{q}/2,\beta} c^\dagger_{\mathbf{k}'-\mathbf{q}/2,\gamma} c_{\mathbf{k}'+\mathbf{q}/2,\delta}, \end{aligned} \tag{3.5}$$

where the first and second terms describe interactions that favor triplet superconductivity and antiferromagnetism, respectively. These interactions allow for the possibility of competition or coexistence of TSC and SDW instabilities at low temperatures. Here, $c^\dagger_{\mathbf{k},\alpha}$ and $c_{\mathbf{k},\alpha}$ represent creation and annihilation operators with spin α and linear momentum $\mathbf{k}$, respectively.

As shown in Eqs. (2.38) and (2.39), the TSC channel interaction $V_{\alpha\beta\gamma\delta}(\mathbf{k},\mathbf{k}')$ in the weak spin-orbit coupling limit can be represented by

$$V_{\alpha\beta\gamma\delta}(\mathbf{k},\mathbf{k}') = V_\Gamma(k,k') \phi^\Gamma(\hat{\mathbf{k}}) \phi^{\Gamma *}(\hat{\mathbf{k}}') \mathbf{v}_{\alpha\beta} \cdot \left(\mathbf{v}^\dagger\right)_{\gamma\delta}, \tag{3.6}$$

where $\phi^\Gamma(\hat{\mathbf{k}})$ represents the symmetry function for an irreducible representation Γ of the orthorhombic $D_{2\rm h}$ group [53, 54], which gives the highest transition temperature. Assuming that the interaction strength is separable such that $V_\Gamma(k,k') = -V_\Gamma \lambda(k)\lambda(k')$, the first term in $\mathcal{H}_{\rm int}$ can be written as

$$\mathcal{H}^{\rm TSC}_{\rm int} = \frac{1}{2} \sum_{\mathbf{k}\mathbf{k}'\mathbf{p}} \sum_{\alpha\beta\gamma\delta} V_\Gamma \mathbf{d}^\dagger_{\alpha\beta}(\mathbf{k},\mathbf{p}) \cdot \mathbf{d}_{\gamma\delta}(\mathbf{k}',\mathbf{p}), \tag{3.7}$$

where the vector operator $\mathbf{d}$ is defined as follows:

$$\mathbf{d}_{\alpha\beta}(\mathbf{k},\mathbf{p}) \equiv \phi^\Gamma(\mathbf{k}) c^\dagger_{\mathbf{k}+\mathbf{p}/2,\alpha} (\mathbf{v})_{\alpha\beta} c^\dagger_{-\mathbf{k}+\mathbf{p}/2,\beta}, \tag{3.8a}$$

$$\mathbf{d}^\dagger_{\gamma\delta}(\mathbf{k}',\mathbf{p}) \equiv \phi^{\Gamma *}(\mathbf{k}') c_{\mathbf{k}'+\mathbf{p}/2,\gamma} \left(\mathbf{v}^\dagger\right)_{\gamma\delta} c_{-\mathbf{k}'+\mathbf{p}/2,\delta}. \tag{3.8b}$$

Here, the symmetry functions are redefined by $\phi^{\Gamma}(\mathbf{k}) = \lambda(k)\phi^{\Gamma}(\hat{\mathbf{k}})$.

Notice that this TSC channel interaction is a generalization of the interaction Hamiltonian Eq. (2.34) discussed in Section 2.3.1, where the momentum summation over $\mathbf{p}$ is absent. By adding the degree of freedom $\mathbf{p}$ in the generalized Hamiltonian above, pairing processes between two fermions with arbitrary momenta are allowed, while in Section 2.3.1 only paring between fermions with opposite momenta were considered.

The second term in Eq. (3.5) describes the interaction which leads the spin density wave instability. This interaction potential $J_{\alpha\beta\gamma\delta}(\mathbf{q}) \equiv J(\mathbf{q})\boldsymbol{\sigma}_{\alpha\beta} \cdot \boldsymbol{\sigma}_{\gamma\delta}$ represents the exchange energy which arises from antisymmetrized wave functions. In order to see that, I consider here two electrons interacting with each other and a fixed positive point charge Ze. The two-electron Hamiltonian is

$$\mathcal{H}_2 = \mathcal{H}_0(\mathbf{r}_1) + \mathcal{H}_0(\mathbf{r}_2) + \frac{e^2}{|\mathbf{r}_1 - \mathbf{r}_2|}, \tag{3.9}$$

where $\mathcal{H}_0(\mathbf{r}) = p^2/(2m) - Ze^2/|\mathbf{R} - \mathbf{r}|$ is the single electron Hamiltonian. Here, I implicitly assume that the spin-orbit coupling is negligible by writing $\mathcal{H}_0(\mathbf{r})$ as a function independent of the electron spin $\mathbf{s}$. Furthermore, I assume that the electron-electron interaction is smaller than the ground state energy of $\mathcal{H}_0$, so that it may be treated by perturbation theory. The fact that the Hamiltonian *without* the electron-electron interaction is separable suggests the usage of product wave functions as the basis for computing the matrix elements of the interaction. Thus, if electron 1 is in an orbital state n with spin up and electron 2 is in an orbital state m, also with spin up, we may try $\psi_n(\mathbf{r}_1)\eta_1(\mathbf{s}_1)\psi_m(\mathbf{r}_2)\eta_1(\mathbf{s}_2)$, where $\psi_n(\mathbf{r})$ is the orbital function and η_1 is the spin-up spinor. However, the Pauli exclusion principle requires that the wave functions be antisymmetric with respect to particle interchanges. This condition may be satisfied by writing the wave function as a normalized *Slater determinant*. If the single-electron wave functions are orthogonal, the appropriate determinantal wave function is

$$\frac{1}{\sqrt{2}} \begin{vmatrix} \psi_n(\mathbf{r}_1)\eta_1(\mathbf{s}_1) & \psi_n(\mathbf{r}_2)\eta_1(\mathbf{s}_2) \\ \psi_m(\mathbf{r}_1)\eta_1(\mathbf{s}_1) & \psi_m(\mathbf{r}_2)\eta_1(\mathbf{s}_2) \end{vmatrix}. \tag{3.10}$$

Since there are an infinite number of orbital states, one can construct an infinite number of such Slater determinants. The general wave function is a linear combination of such

determinants. However, if the electron-electron interaction is small, one may neglect this admixture of other orbital states, and assume that electron 1 has a low-lying non-degenerate orbital state ψ_a with energy E_a and electron 2 has a similar low-lying non-degenerate orbital state ψ_b with energy E_b. If both spin functions are up, the determinantal wave function becomes,

$$\Psi_1 = \frac{1}{\sqrt{2}} \begin{vmatrix} \psi_a(\mathbf{r}_1)\eta_1(\mathbf{s}_1) & \psi_a(\mathbf{r}_2)\eta_1(\mathbf{s}_2) \\ \psi_b(\mathbf{r}_1)\eta_1(\mathbf{s}_1) & \psi_b(\mathbf{r}_2)\eta_1(\mathbf{s}_2) \end{vmatrix}. \tag{3.11}$$

If the spin function associated with orbital a is down, then

$$\Psi_2 = \frac{1}{\sqrt{2}} \begin{vmatrix} \psi_a(\mathbf{r}_1)\eta_{-1}(\mathbf{s}_1) & \psi_a(\mathbf{r}_2)\eta_{-1}(\mathbf{s}_2) \\ \psi_b(\mathbf{r}_1)\eta_1(\mathbf{s}_1) & \psi_b(\mathbf{r}_2)\eta_1(\mathbf{s}_2) \end{vmatrix}, \tag{3.12}$$

where η_{-1} is the spin-down spinor. There are two additional possible spin configurations which lead to wave functions Ψ_3 and Ψ_4. These four functions form a complete orthonormal set and therefore constitute an appropriate basis with which to evaluate the matrix elements of $\mathcal{H}_2$. The result is

$$\mathcal{H}_2 = \begin{pmatrix} E_a + E_b + K_{ab} - J_{ab} & 0 & 0 & 0 \\ 0 & E_a + E_b + K_{ab} & -J_{ab} & 0 \\ 0 & -J_{ab} & E_a + E_b + K_{ab} & 0 \\ 0 & 0 & 0 & E_a + E_b + K_{ab} - J_{ab} \end{pmatrix}, \tag{3.13}$$

where

$$K_{ab} = \int\int d\mathbf{r}_1 d\mathbf{r}_2 \frac{e^2}{|\mathbf{r}_1 - \mathbf{r}_2|} |\psi_a(\mathbf{r}_1)|^2 |\psi_b(\mathbf{r}_2)|^2 \tag{3.14}$$

and

$$J_{ab} = \int\int d\mathbf{r}_1 d\mathbf{r}_2 \psi_a^*(\mathbf{r}_1)\psi_b^*(\mathbf{r}_1) \frac{e^2}{|\mathbf{r}_1 - \mathbf{r}_2|} \psi_b(\mathbf{r}_1)\psi_a(\mathbf{r}_2). \tag{3.15}$$

Diagonalizing this matrix gives a singlet state with energy

$$E_s = E_a + E_b + K_{ab} + J_{ab} \tag{3.16}$$

and triplet states with energy

$$E_t = E_a + E_b + K_{ab} - J_{ab}, \tag{3.17}$$

which are three-fold degenerate. Since J_{ab} is the self-energy of the charge distribution $e\psi_a^*(\mathbf{r})\psi_b(\mathbf{r})$, it is positive definite. Therefore the triplet always has a lower energy than the singlet. This is just the origin of *Hund's rule*, which says that the ground state of an atom has *maximum multiplicity*.

The eigenvalues (3.16) and (3.17) can be obtained with a basis consisting only of products of spin functions if an exchange interaction were added to the Hamiltonian. To obtain the form of this effective interaction term one may notice that just as any 2×2 matrix can be expressed as a linear combination of Pauli matrices plus the unit matrix, any 4×4 matrix can be written as a quadratic function of direct products of Pauli matrices[186]. For example, if

$$\sigma_{1x} = \begin{pmatrix} 0 & 1 \\ 1 & 0 \end{pmatrix} \quad \text{and} \quad \sigma_{2x} = \begin{pmatrix} 0 & 1 \\ 1 & 0 \end{pmatrix},$$

then

$$\sigma_{1x} \otimes \sigma_{2x} = \begin{pmatrix} 0 & 0 & 0 & 1 \\ 0 & 0 & 1 & 0 \\ 0 & 1 & 0 & 0 \\ 1 & 0 & 0 & 0 \end{pmatrix}. \tag{3.18}$$

Therefore, by defining the dot product $\boldsymbol{\sigma}_1 \cdot \boldsymbol{\sigma}_2 \equiv \sum_{i=x,y,z} \sigma_{1i} \otimes \sigma_{2i}$, we obtain

$$\boldsymbol{\sigma}_1 \cdot \boldsymbol{\sigma}_2 = \begin{pmatrix} 1 & 0 & 0 & 0 \\ 0 & -1 & 2 & 0 \\ 0 & 2 & -1 & 0 \\ 0 & 0 & 0 & 1 \end{pmatrix}. \tag{3.19}$$

Therefore, the Hamiltonian which will produce in a spinor basis the same eigenvalues as Eq. (3.9) evaluated in a fully antisymmetrized basis is

$$\mathcal{H}_2 = \frac{1}{4}(E_s + E_t) - \frac{1}{4}(E_s - E_t)\boldsymbol{\sigma}_1 \cdot \boldsymbol{\sigma}_2 = \text{const.} - \frac{J}{4}\boldsymbol{\sigma}_1 \cdot \boldsymbol{\sigma}_2. \tag{3.20}$$

Thus the exchange interaction may be expressed as a spin–spin interaction. As discussed above, the exchange parameter $J = E_s - E_t$ is positive definite for this two-electron problem, hence favors electrons in the triplet state. Thus, we say that the interaction is ferromagnetic.

However, in general cases of many electron systems, the sign of J can be negative and we say that the interaction is antiferromagnetic.

In obtaining the exchange interaction Eq. (3.20) two important assumptions were made. First, only a certain subset of non-degenerate orbital states were considered. However, the Coulomb interaction may couple different orbital states. Second, it was assumed that the orbital functions were orthogonal, since the electronic wave functions have a common origin (the position of the ion) in the two-electron problem discussed above. However, if one considers electrons centered at different sites the problem becomes very complex, leading to an apparent divergence in the integrals (3.14) and (3.15). This "nonorthogonality catastrophe" is a purely mathematical difficulty, and it can be shown [187] that even for large systems the energies and eigenstates are given by the exchange interaction with exchange constants having the same values as for the two-electron system.

One approach to the problem of exchange among many electrons is to give up the well-defined but nonorthogonal functions $\psi_n(\mathbf{r})$ and work with functions which are orthogonal. As an example, one can consider the Wannier functions $W_{n\alpha}(\mathbf{r}-\mathbf{R}_i)$ resembling the n-th atomic orbital with spin α near the i-th lattice site, which falls off throughout the crystal in such a way that it is orthogonal to similar functions centered at other sites. Using this set of functions as a basis, it can be shown [188] that the Coulomb interaction between the valence electrons on different ions can be expressed as an effective interaction between the individual electron spins,

$$\mathcal{H}_{\text{int}}^{\text{SDW}} = \frac{1}{2}\sum_{i\neq j} J_{ij}\mathbf{S}_i \cdot \mathbf{S}_j, \tag{3.21}$$

where $\mathbf{S}_i$ is the spin of electron at the ith site. This exchange interaction is often larger in comparison to other interactions which may lead to SDW instabilities, such as the magnetic dipole-dipole interaction, hence it can be considered alone to describe the main magnetic interaction features.

For the quasi-1D organic conductor $(TMTSF)_2PF_6$, the coefficient J_{ij} must be positive in order to describe the antiferromagnetic state at low temperatures. By noticing that the spin operator $\mathbf{S}_i$ can be written in the second quantization form as $c_{i,\alpha}^{\dagger}\boldsymbol{\sigma}_{\alpha\beta}c_{i,\beta}$, and by

Fourier transforming into the momentum space, one obtains

$$\mathcal{H}_{\rm int}^{\rm SDW} = \frac{1}{2}\sum_{\mathbf{k}\mathbf{k}'\mathbf{q}}\sum_{\alpha\beta\gamma\delta} J(\mathbf{q})\boldsymbol{\sigma}_{\alpha\beta}\cdot\boldsymbol{\sigma}_{\gamma\delta}c^{\dagger}_{\mathbf{k}-\mathbf{q}/2,\alpha}c_{\mathbf{k}+\mathbf{q}/2,\beta}c^{\dagger}_{\mathbf{k}'-\mathbf{q}/2,\gamma}c_{\mathbf{k}'+\mathbf{q}/2,\delta}, \tag{3.22}$$

which gives the second term of the Eq. (3.25). Here, I have assumed that the interaction coefficient J_{ij} in Eq. (3.21) is homogeneous. By defining the momentum space operators

$$\begin{aligned}\mathbf{s}^{\dagger}_{\alpha\beta}(\mathbf{k},\mathbf{q}) &\equiv c^{\dagger}_{\mathbf{k}-\mathbf{q}/2,\alpha}\boldsymbol{\sigma}_{\alpha\beta}c_{\mathbf{k}+\mathbf{q}/2,\beta},\\ \mathbf{s}_{\gamma\delta}(\mathbf{k},\mathbf{q}) &\equiv c^{\dagger}_{\mathbf{k}+\mathbf{q}/2,\gamma}\boldsymbol{\sigma}_{\gamma\delta}c_{\mathbf{k}-\mathbf{q}/2,\delta},\end{aligned} \tag{3.23}$$

the SDW channel interaction can be written as

$$\mathcal{H}_{\rm int}^{\rm SDW} = \frac{1}{2}\sum_{\mathbf{k}\mathbf{k}'\mathbf{q}}\sum_{\alpha\beta\gamma\delta} J(\mathbf{q})\mathbf{s}^{\dagger}_{\alpha\beta}(\mathbf{k},\mathbf{q})\cdot\mathbf{s}_{\gamma\delta}(\mathbf{k},-\mathbf{q}). \tag{3.24}$$

By adding the two parts of the interaction potential Eqs. (3.7) and (3.24), the interaction Hamiltonian (3.5) can be written as

$$\begin{aligned}\mathcal{H}\text{int} &= \mathcal{H}_{\rm int}^{\rm TSC} + \mathcal{H}_{\rm int}^{\rm SDW}\\ &= \frac{1}{2}\sum_{\mathbf{k}\mathbf{k}'\mathbf{p}}\sum_{\alpha\beta\gamma\delta} V_{\Gamma}(k,k')\mathbf{d}^{\dagger}_{\alpha\beta}(\mathbf{k},\mathbf{p})\cdot\mathbf{d}_{\gamma\delta}(\mathbf{k}',\mathbf{p})\\ &\quad +\frac{1}{2}\sum_{\mathbf{k}\mathbf{k}'\mathbf{q}}\sum_{\alpha\beta\gamma\delta} J(\mathbf{q})\mathbf{s}^{\dagger}_{\alpha\beta}(\mathbf{k},\mathbf{q})\cdot\mathbf{s}_{\gamma\delta}(\mathbf{k},-\mathbf{q}).\end{aligned} \tag{3.25}$$

Next, I will develop an effective field theory for this many-body Hamiltonian, and derive the Ginzburg–Landau (GL) functional around the critical point. I will show that the coefficients of quartic terms in the GL functional are crucial to determine the phase diagram around the critical point.

3.4 Ginzburg–Landau Theory

By using the functional integral formalism discussed in Chapter 2, the grand partition function of this Hamiltonian can be written as

$$\mathcal{Z} = \int_{\rm BC}\mathcal{D}[\mathbf{D}^{\dagger}(\mathbf{p}),\mathbf{D}(\mathbf{p})]\mathcal{D}[\mathbf{N}^{\dagger}(\mathbf{q}),\mathbf{N}(\mathbf{q})]e^{-S_{\rm eff}[\mathbf{D}^{\dagger},\mathbf{D},\mathbf{N}^{\dagger},\mathbf{N}]}. \tag{3.26}$$

The effective action $S_{\rm eff}$ can be expanded in a power series of fields $\mathbf{D}$ and $\mathbf{N}$ around the critical point where both $\mathbf{D}$ and $\mathbf{N}$ are small, hence defining the GL functional for two

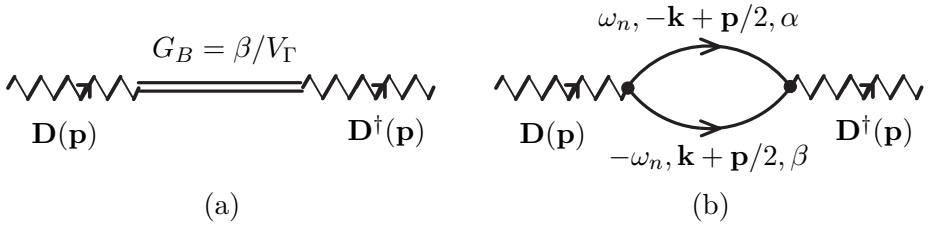

Figure 3.9: Feynman diagrams corresponding to the TSC quadratic terms of the effective action S_{eff}. Here, the wavy lines represent the TSC field $\mathbf{D}$, the double line represent the TSC bare bosonic field propagator β/V_Γ, and the single lines represent bare Green's function of electrons.

different orders. Each term of the effective action can be obtained by integrating out the fermions using the Gaussian integration formula, or by directly drawing the corresponding Feynman diagrams.

The quadratic terms of the expansion correspond to Feynman diagrams which contain two external legs of bosonic fields $\mathbf{D}$ and $\mathbf{N}$. The diagrams with two external $\mathbf{D}$ fields given in Fig. 3.9 are similar to the diagrams in Fig. 2.1 discussed in Chapter 2. However, notice that the present diagrams are more general than the ones in Fig. 2.1 since the bosonic field $\mathbf{D}(\mathbf{p})$ is momentum dependent, indicating that the superconducting order parameter can be inhomogeneous in the present theory.

Using the Feynman rules listed in Chapter 2, the quadratic contribution of the TSC order parameter to the effective action can be written as

$$S_2^{\text{TSC}} = \sum_{\mathbf{p}} A(\mathbf{p}) \mathbf{D}^\dagger(\mathbf{p}) \cdot \mathbf{D}(\mathbf{p}). \tag{3.27}$$

The coefficient $A(\mathbf{p})$ takes the form

$$A(\mathbf{p}) = \frac{\beta}{2V_\Gamma} + \sum_{\mathbf{k},\omega_n} \frac{|\phi^\Gamma(\mathbf{k})|^2}{(i\omega_n + \xi_{-\mathbf{k}+\mathbf{p}/2})(i\omega_n - \xi_{\mathbf{k}+\mathbf{p}/2})}. \tag{3.28}$$

The Matsubara summation $\sum_{\omega_n}$ can be performed using the method discussed in Appendix B, leading to

$$A(\mathbf{p}) = \frac{\beta}{2V_\Gamma} - \sum_{\mathbf{k}} \frac{\beta|\phi^\Gamma(\mathbf{k})|^2}{2(\xi_{\mathbf{k}+\mathbf{q}/2} + \xi_{-\mathbf{k}+\mathbf{q}/2})} \left[\tanh\left(\frac{\beta\xi_{\mathbf{k}+\mathbf{q}/2}}{2}\right) + \tanh\left(\frac{\beta\xi_{-\mathbf{k}+\mathbf{q}/2}}{2}\right)\right]. \tag{3.29}$$

In the spirit of the GL theory, we are interested in slowly varying order parameters,

hence one can expand Eq. (3.29) into powers of $\mathbf{p}$ around $\mathbf{p} = 0$:

$$A(\mathbf{p}) = A(0) + \sum_{\mu,\nu=x,y,z} a_{\mu\nu} p_\mu p_\nu + \cdots , \tag{3.30}$$

where the coefficients are

$$A(0) = \frac{\beta}{2V_\Gamma} - \sum_{\mathbf{k}} \frac{\beta |\phi^\Gamma(\mathbf{k})|^2}{2\xi_{\mathbf{k}}} \tanh\left(\frac{\beta\xi_{\mathbf{k}}}{2}\right), \tag{3.31}$$

and

$$a_{\mu\nu} = \sum_{\mathbf{k}} \left\{ \left[\frac{\beta}{16\xi_{\mathbf{k}}^2} X(\mathbf{k}) - \frac{\beta^2}{32\xi_{\mathbf{k}}} Y(\mathbf{k}) \right] \frac{\partial^2 \xi_{\mathbf{k}}}{\partial k_\mu \partial k_\nu} + \frac{\beta^3}{32\xi_{\mathbf{k}}} \frac{\partial \xi_{\mathbf{k}}}{\partial k_\mu} \frac{\partial \xi_{\mathbf{k}}}{\partial k_\nu} X(\mathbf{k}) Y(\mathbf{k}) \right\} \left|\phi^\Gamma(\mathbf{k})\right|^2 . \tag{3.32}$$

Here, $X(\mathbf{k}) \equiv \tanh(\beta\xi_{\mathbf{k}}/2)$ and $Y(\mathbf{k}) \equiv \mathrm{sech}^2(\beta\xi_{\mathbf{k}}/2)$. In order to derive the equation above, the property that the dispersion relation (3.1) is an even function with respect to $\mathbf{k}$ is used, i.e., $\xi_{-\mathbf{k}+\mathbf{p}/2} = \xi_{\mathbf{k}-\mathbf{p}/2}$. Notice that $\partial\xi_{\mathbf{k}}/\partial k_\mu = t_\mu a_\mu \sin(k_\mu a_\mu)$ where a_μ is the lattice spacing along the μ direction and that the second derivative $\partial^2\xi_{\mathbf{k}}/\partial k_\mu \partial k_\nu = 0$ for $\mu \neq \nu$.* Furthermore, consider $\partial\xi_{\mathbf{k}}/\partial k_\mu$ is an odd function with respect to k_μ, and the functions $X(\mathbf{k})$ and $Y(\mathbf{k})$ are only functions of $\xi_{\mathbf{k}}$, hence are both even functions as well as $|\phi^\Gamma(\mathbf{k})|^2$, the last term in Eq. (3.32) must vanish after summation over $\mathbf{k}$ for $\mu \neq \nu$. As a consequence, the coefficient $a_{\mu\nu} = a_{\mu\mu}\delta_{\mu\nu}$ is diagonal and

$$A(\mathbf{p}) = A(0) + \sum_{\mu=x,y,z} a_{\mu\mu} p_\mu^2 + \cdots . \tag{3.33}$$

As I will discuss later, the coefficient $a_{\mu\mu}$ is related to the coherence length of the superconducting order parameter along the μ direction. At the saddle point level, the TSC contribution to the effective action is dominated by the zero center-of-mass momentum component $\mathbf{D}_0 \equiv \mathbf{D}(\mathbf{p} = 0)$. Thus, the TSC quadratic term can be approximated by

$$S_2^{\mathrm{TSC}} \approx A(0)|\mathbf{D}_0|^2. \tag{3.34}$$

In addition to the TSC term, the SDW also contributes to the effective action in the quadratic order. Unlike the TSC diagrams of Fig. 3.9, the Feynman diagrams corresponding to the the SDW contribution are shown in Fig. 3.10. In order to obtain the algebraic

*Here, μ is a direction index ($\mu = x, y, z$), but not the chemical potential.

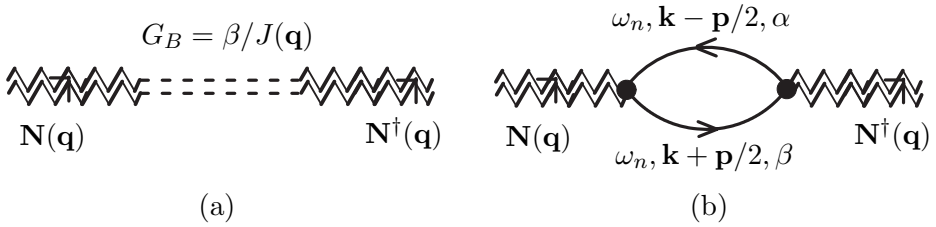

Figure 3.10: Feynman diagrams corresponding to the SDW quadratic terms of the effective action S_{eff}. Here, the double wavy lines represent the SDW field $\mathbf{N}$, the double dashed lines represent the SDW bare bosonic field propagator $\beta/J(\mathbf{q})$, and the single lines represent bare Green's function of electrons.

representation of the SDW contribution to the effective action, it is necessary to add the additional Feynman rules listed as follows:

6. For each initial SDW bosonic field line connected to a vertex, write a factor $\mathbf{N}(\mathbf{q})\cdot\boldsymbol{\sigma}_{\alpha\beta}$, while for each final SDW bosonic field line connected to a vertex, write the Hermitian conjugate $\mathbf{N}^\dagger(\mathbf{q})\cdot(\boldsymbol{\sigma})_{\alpha\beta}$;

7. The linear momentum associated with the SDW bosonic line and the two fermionic lines meeting at each vertex satisfy energy–momentum conservation. For each closed loop, carry out the integration $\int d\mathbf{k}$ for each internal momentum $\mathbf{k}$ and carry out the summation $\sum_{\omega_n}$ for each internal frequency ω_n.

Therefore, the quadratic contribution of SDW order parameter to the effective action can be written as

$$S_2^{\text{SDW}} = \sum_{\mathbf{q}} B(\mathbf{q})\mathbf{N}(-\mathbf{q})\cdot\mathbf{N}(\mathbf{q}), \tag{3.35}$$

where

$$B(\mathbf{q}) = \frac{\beta}{2J(\mathbf{q})} + \sum_{\mathbf{k},\omega_n} \frac{1}{(i\omega_n + \xi_{\mathbf{k}-\mathbf{q}/2})(i\omega_n + \xi_{\mathbf{k}+\mathbf{q}/2})}. \tag{3.36}$$

By performing the Matsubara summation, the coefficient takes the form

$$B(\mathbf{q}) = \frac{\beta}{2J(\mathbf{q})} - \sum_{\mathbf{k}} \frac{\beta}{2(\xi_{\mathbf{k}+\mathbf{q}/2} - \xi_{\mathbf{k}-\mathbf{q}/2})} \left[\tanh\left(\frac{\beta\xi_{\mathbf{k}+\mathbf{q}/2}}{2}\right) - \tanh\left(\frac{\beta\xi_{\mathbf{k}-\mathbf{q}/2}}{2}\right)\right]. \tag{3.37}$$

The saddle point solution for the modulation of the spin density wave in $(TMTSF)_2PF_6$ is directly related to the nesting vector of the quasi-1D Fermi surfaces. In a completely one-dimensional electron system, the SDW phase is present with the modulation wave vector

$\mathbf{Q}_0 = 2\mathbf{k}_F$ due to optimal nesting [189]. Here, $\mathbf{k}_F$ is the Fermi vector. For quasi-1D systems with electronic dispersion

$$\epsilon(\mathbf{k}) = -t_x \cos(k_x a) - t_y \cos(k_y b) - t_z \cos(k_z c) \tag{3.38}$$

with $t_x \gg t_y \gg t_z > 0$, the Fermi surface is open in the k_y and k_z directions and is given by

$$\begin{aligned} k_x \;\approx\; \pm\Bigg[& k_F + \left(\frac{t_y}{t_x a \sin(k_F a)}\right)\cos(k_y b) + \left(\frac{t_z}{t_x a \sin(k_F a)}\right)\cos(k_z c) \\ & - \frac{t_y^2 \cos(k_F a)}{4 t_x^2 a \sin^3(k_F a)}\cos(2k_y b) - \frac{t_z^2 \cos(k_F a)}{4 t_x^2 a \sin^3(k_F a)}\cos(2k_z c)\Bigg], \end{aligned} \tag{3.39}$$

where $k_F = \pi/(2a)$ is the one-dimensional Fermi wave vector for half-filling systems. If one neglects the second harmonic terms in the equation above, the Fermi surface is sinusoidal like the continuous curves of Fig. 3.11. Then, the left part of the Fermi surface with $k_x \approx -k_F$ completely nests with the right part with $k_x \approx k_F$ when the former is moved by

$$\mathbf{Q}_i = \left(2k_F, \pm\frac{\pi}{b}, \pm\frac{\pi}{c}\right). \tag{3.40}$$

The wave vectors $\mathbf{Q}_i$ are called *optimal* or *perfect* nesting vectors and lead to a divergence of the spin susceptibility when $B(\mathbf{Q}_i)$ changes sign, thus producing SDW ordering with the same wave vector.

Therefore, the SDW order parameter $\mathbf{N}(\mathbf{q})$ is dominated by the Fourier components $\mathbf{N}(\mathbf{Q}_i)$ with $\mathbf{Q}_i = (\pm Q_a, \pm Q_b, \pm Q_c)$. In such a case, the coefficients $B(\mathbf{Q}_i)$ are identical for all $\mathbf{Q}_i$'s, since both the lattice dispersion and the antiferromagnetic interaction $J(\mathbf{q})$ are invariant under reflections and inversions compatible with the $D_{2\mathrm{h}}$ group. As a result, the spin density modulation $\mathbf{N}(\mathbf{r})$ has the same magnitude for all wave vectors $\mathbf{Q}_i$. Given that $\mathbf{N}(\mathbf{r})$ is real, and that we have periodic boundary conditions over the sample, one can choose a specific reference frame such that $\mathbf{N}(\mathbf{r})$ is an even function along all different $\mathbf{Q}_i$ directions. This choice of reference frame has the advantage to make all $\mathbf{N}(\mathbf{Q}_i)$ real and identical. Thus, we can define $\mathbf{N}_0 \equiv \mathbf{N}(\mathbf{Q}_i)$ for all $\mathbf{Q}_i$, and the SDW quadratic term is dominated by

$$S_2^{\mathrm{SDW}} \approx \frac{n}{2} B(\mathbf{Q}_1) |\mathbf{N}_0|^2, \tag{3.41}$$

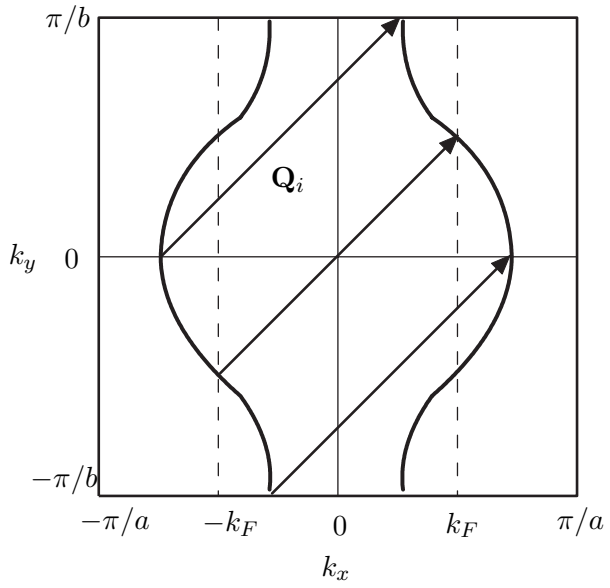

Figure 3.11: The left part of quasi-one-dimensional Fermi surfaces perfectly nests with the right part when the former is shifted by the nesting vector $\mathbf{Q}_i$.

where n is the number of distinct nesting vectors, and $\mathbf{Q}_1 = (Q_a, Q_b, Q_c)$ is chosen for definiteness.

Notice that the two order parameters $\mathbf{D}(\mathbf{p})$ and $\mathbf{N}(\mathbf{q})$ do not couple to quadratic order, because TSC and SDW are instabilities in the particle-particle and particle-hole channels, respectively. This conclusion can be reached using the language of Feynman diagram. Under the Feynman rules defined before, a TSC field line entering (leaving) a vertex is connected to two outgoing (incoming) electron lines, but a SDW field line is connected to one incoming and one outcoming electron lines. Therefore, it is topologically forbidden to draw a diagram with only one external TSC field line and one external SDW field line, since conservation laws are not obeyed.

In addition, notice that the effective action is independent of the directions of TSC and SDW order parameter vectors, which means that the theory is completely isotropic so far. However, it is well known that the SDW order parameter $\mathbf{N}$ is weakly anisotropic for $(TMTSF)_2PF_6$, having an easy axis along the crystallographic $\mathbf{b}'$ axis [190]. This small anisotropy due to spin-orbit coupling is ignored here since it is not crucial for the phase diagram of TSC and SDW orders at zero magnetic field. This anisotropy will be taken into

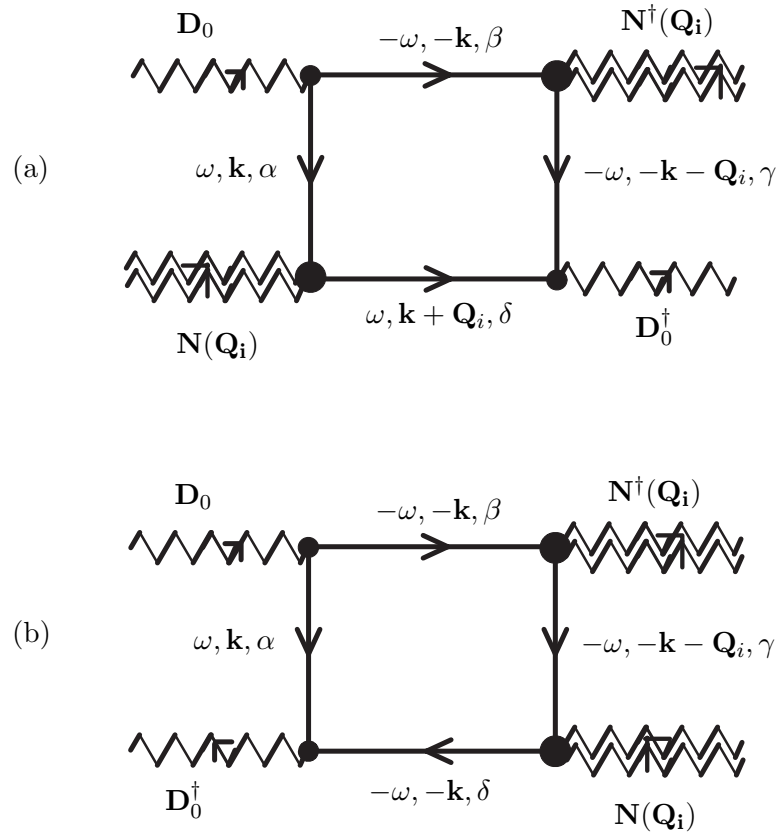

Figure 3.12: Feynman diagrams corresponding to the TSC and SDW coupling term S_4^{C} in Eq. (3.42).

account later when discussing the effects of a magnetic field in Section 3.6.

Although the order parameters for TSC and SDW do not couple to quadratic order, the coupling between $\mathbf{D}$ and $\mathbf{N}$ in fourth order is given by

$$S_4^{\mathrm{C}} = (C_1 + C_2/2)|\mathbf{D}_0|^2|\mathbf{N}_0|^2 - C_2|\mathbf{D}_0 \cdot \mathbf{N}_0|^2, \tag{3.42}$$

where coefficients C_1 and C_2 can be obtained from the corresponding diagrams shown in Fig. 3.12. Using the Feynman rules discussed above, the diagram Fig. 3.12(a) gives

$$\begin{aligned} S_{4,a}^{\mathrm{C}} &= -\frac{1}{2}\cdot\frac{1}{2}\sum_{\mathbf{Q}_i}\sum_{\mathbf{k},\omega_n} \frac{\phi^\Gamma(-\mathbf{k})\phi^{\Gamma *}(\mathbf{k}+\hat{\mathbf{Q}}_i)}{(i\omega_n + \xi_{\mathbf{k}})(-i\omega_n + \xi_{-\mathbf{k}})(i\omega_n + \xi_{\mathbf{k}+\mathbf{Q}_i})(-i\omega_n + \xi_{-\mathbf{k}-\mathbf{Q}_i})} \\ &\quad \times \left(2|\mathbf{D}_0 \cdot \mathbf{N}_0|^2 - |\mathbf{D}_0|^2|\mathbf{N}_0|^2\right), \end{aligned} \tag{3.43}$$

where the coupling structure of the two vector order parameters is given by the trace of the spin matrices. Here, an additional prefactor of 1/2 appears in $S_{4,a}^{\mathrm{C}}$ and in $S_{4,b}^{\mathrm{C}}$, since

the summation over $\mathbf{Q}_i$ double counts the same Feynman diagram with $\mathbf{Q}_i$ and $-\mathbf{Q}_i$. After performing the Matsubara summation, we obtain

$$S_{4,a}^{\mathrm{C}} = C_2 \left(\frac{1}{2} |\mathbf{D}_0|^2 |\mathbf{N}_0|^2 - |\mathbf{D}_0 \cdot \mathbf{N}_0|^2 \right), \tag{3.44}$$

where

$$C_2 = \frac{\beta}{2} \sum_{\mathbf{Q}_i} \sum_{\mathbf{k}} \frac{\phi^{\Gamma}(-\mathbf{k}) \phi^{\Gamma *}(\mathbf{k}+\mathbf{Q}_i)}{(\xi_{\mathbf{k}+\mathbf{Q}_i} - \xi_{\mathbf{k}})^2} \left[\frac{X(\mathbf{k}+\mathbf{Q}_i) + X(\mathbf{k})}{\xi_{\mathbf{k}+\mathbf{Q}_i} + \xi_{\mathbf{k}}} - \frac{X(\mathbf{k}+\mathbf{Q}_i)}{2\xi_{\mathbf{k}+\mathbf{Q}_i}} - \frac{X(\mathbf{k})}{2\xi_{\mathbf{k}}} \right]. \tag{3.45}$$

Similarly, the diagram in Fig. 3.12(b) gives

$$\begin{aligned} S_{4,b}^{\mathrm{C}} &= C_1 |\mathbf{D}_0|^2 |\mathbf{N}_0|^2 \\ &= -\frac{1}{4} \sum_{\mathbf{Q}_i} \sum_{\mathbf{k}, \omega_n} \frac{|\phi^{\Gamma}(\mathbf{k})|^2 |\mathbf{D}_0|^2 |\mathbf{N}_0|^2}{(i\omega_n + \xi_{\mathbf{k}})(-i\omega_n + \xi_{-\mathbf{k}})^2 (-i\omega_n + \xi_{-\mathbf{k}-\mathbf{Q}_i})}, \end{aligned} \tag{3.46}$$

where the coefficient C_1 is

$$\begin{aligned} C_1 = & -\frac{\beta}{4} \sum_{\mathbf{Q}_i} \sum_{\mathbf{k}} \frac{|\phi^{\Gamma}(\mathbf{k})|^2}{\xi_{\mathbf{k}} (\xi_{\mathbf{k}+\mathbf{Q}_i} - \xi_{\mathbf{k}})} \left[\frac{X(\mathbf{k})}{\xi_{\mathbf{k}}} - \frac{\beta Y(\mathbf{k})}{2} \right. \\ & \left. + \frac{X(\mathbf{k}+\mathbf{Q}_i) - X(\mathbf{k})}{\xi_{\mathbf{k}+\mathbf{Q}_i} - \xi_{\mathbf{k}}} - \frac{X(\mathbf{k}+\mathbf{Q}_i) + X(\mathbf{k})}{\xi_{\mathbf{k}+\mathbf{Q}_i} + \xi_{\mathbf{k}}} \right] \end{aligned} \tag{3.47}$$

after performing the Matsubara summation.

The second term on Eq. (3.42) can be parameterized as $C_2 \cos^2(\theta) |\mathbf{D}_0|^2 |\mathbf{N}_0|^2$, where

$$\cos^2 \theta \equiv \frac{|\mathbf{D}_0 \cdot \mathbf{N}_0|^2}{|\mathbf{D}_0|^2 |\mathbf{N}_0|^2} \leq 1 \tag{3.48}$$

is independent of $|\mathbf{D}_0|$ and $|\mathbf{N}_0|$. Since I consider only unitary states for TSC, its global phase can be eliminated in S_4^{C}, and θ can be regarded as the angle between $\mathbf{D}_0$ and $\mathbf{N}_0$. The coefficient C_2 for $(\mathrm{TMTSF})_2\mathrm{PF}_6$ is positive, indicating that $\mathbf{D}_0$ and $\mathbf{N}_0$ are not free to rotate independently, but tend to be aligned ($\theta = 0$) or anti-aligned ($\theta = \pi$).

Additional fourth order terms are

$$S_4^{\mathrm{TSC}} = D_1 |\mathbf{D}_0|^4; \tag{3.49a}$$

$$S_4^{\mathrm{SDW}} = D_2 |\mathbf{N}_0|^4 \tag{3.49b}$$

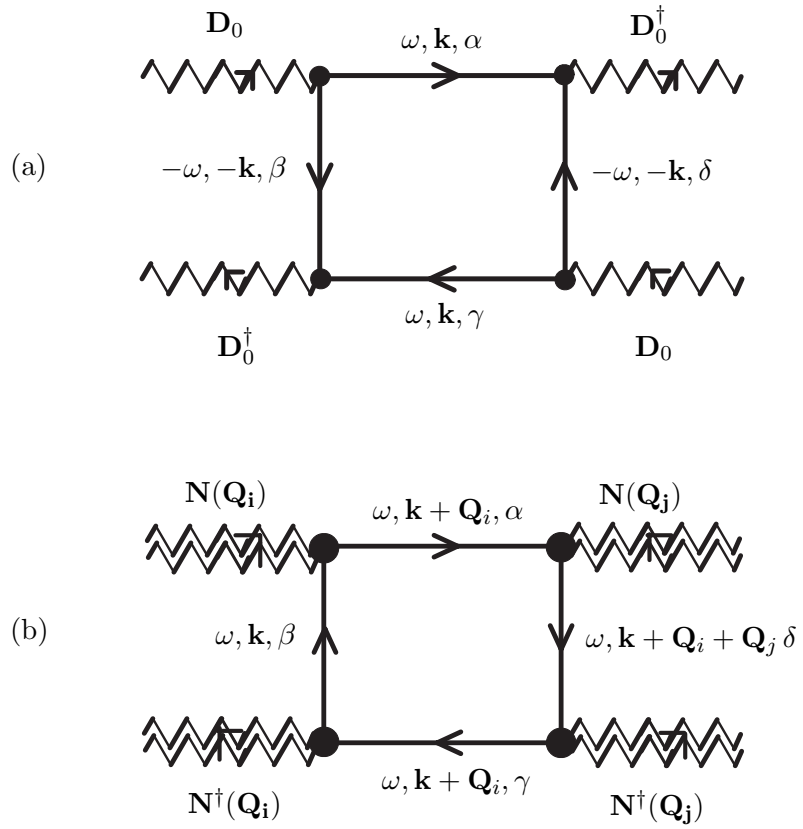

Figure 3.13: Feynman diagram corresponding to (a) the TSC term S_4^{TSC} and (b) the SDW term S_4^{SDW} in Eq. (3.49).

where coefficients D_1 and D_2 can be obtained from the diagrams in Fig. 3.13. The diagram in Fig. 3.13(a) gives

$$\begin{aligned} S_4^{\rm TSC} &= D_1\left(2|\mathbf{D}_0|^4 - |\mathbf{D}_0^2|^2\right) = D_1|\mathbf{D}_0|^4 \\ &= \frac{1}{2}\sum_{\mathbf{k},\omega_n}\frac{|\phi^\Gamma(\hat{\mathbf{k}})|^4|\mathbf{D}_0|^4}{(i\omega_n+\xi_{\mathbf{k}})^2(-i\omega_n+\xi_{-\mathbf{k}})^2}, \end{aligned} \tag{3.50}$$

where the coefficient D_1 is

$$D_1 = \frac{\beta}{2}\sum_{\mathbf{k}}\frac{|\phi^\Gamma(\hat{\mathbf{k}})|^4}{4\xi_{\mathbf{k}}^2}\left[\frac{X(\mathbf{k})}{\xi_{\mathbf{k}}} - \frac{\beta Y(\mathbf{k})}{2}\right]. \tag{3.51}$$

The diagram in Fig. 3.13(b) gives

$$\begin{aligned} S_4^{\rm SDW} &= D_2\left(2|\mathbf{N}_0|^4 - |\mathbf{N}_0^2|^2\right) = D_2|\mathbf{N}_0|^4 \\ &= \frac{1}{4}\cdot\frac{1}{2}\sum_{\mathbf{Q}_i,\mathbf{Q}_j}\sum_{\mathbf{k},\omega_n}\frac{|\mathbf{N}_0|^4}{(i\omega_n+\xi_{\mathbf{k}})(i\omega_n+\xi_{\mathbf{k}+\mathbf{Q}_i})^2(i\omega_n+\xi_{\mathbf{k}+\mathbf{Q}_i+\mathbf{Q}_j})}, \end{aligned} \tag{3.52}$$

where an additional factor of 1/4 appears since the summations over $\mathbf{Q}_i$ and $\mathbf{Q}_j$ count each identical diagram four times. The coefficient D_2 is

$$\begin{aligned} D_2 &= \frac{\beta}{16}\sum_{\mathbf{Q}_i,\mathbf{Q}_j}\sum_{\mathbf{k}}\frac{1}{(\xi_{\mathbf{k}+\mathbf{Q}_i}-\xi_{\mathbf{k}})(\xi_{\mathbf{k}+\mathbf{Q}_i}-\xi_{\mathbf{k}+\mathbf{Q}_i+\mathbf{Q}_j})}\left[\frac{X(\mathbf{k}+\mathbf{Q}_i+\mathbf{Q}_j)-X(\mathbf{k}+\mathbf{Q}_i)}{\xi_{\mathbf{k}+\mathbf{Q}_i+\mathbf{Q}_j}-\xi_{\mathbf{k}+\mathbf{Q}_i}}\right. \\ &\left. + \frac{X(\mathbf{k}+\mathbf{Q}_i)-X(\mathbf{k})}{\xi_{\mathbf{k}+\mathbf{Q}_i}-\xi_{\mathbf{k}}} - \frac{X(\mathbf{k}+\mathbf{Q}_i+\mathbf{Q}_j)-X(\mathbf{k})}{\xi_{\mathbf{k}+\mathbf{Q}_i+\mathbf{Q}_j}-\xi_{\mathbf{k}}} - \frac{\beta Y(\mathbf{k}+\mathbf{Q}_i)}{2}\right]. \end{aligned} \tag{3.53}$$

As a consequence, the saddle point effective action is

$$S_{\rm eff} = S_0 + S_2^{\rm TSC} + S_2^{\rm SDW} + S_4, \tag{3.54}$$

where S_0 is the normal state contribution, and

$$S_4 = D_1|\mathbf{D}_0|^4 + D_2|\mathbf{N}_0|^4 + C(\theta)|\mathbf{D}_0|^2|\mathbf{N}_0|^2 \tag{3.55}$$

with $C(\theta) = C_1 + C_2/2 - C_2\cos^2\theta$. Notice that this effective action depends only on the magnitudes of TSC and SDW order parameters, and the relative orientation between the two vectors. Furthermore, after minimizing the action Eq. (3.54) with respect to θ, the action is only a function of $|\mathbf{D}_0|$ and $|\mathbf{N}_0|$, leading to phase diagrams with either bicritical or tetracritical points, to be discussed next.

3.5 Phase Diagram

Minimization of the action Eq. (3.54) with respect to the relative angle θ between TSC and SDW order parameter vectors leads to

$$S_{\text{eff}} = S_0 + A(0)|\mathbf{D}_0|^2 + \frac{n}{2}B(\mathbf{Q}_1)|\mathbf{N}_0|^2 + D_1|\mathbf{D}_0|^4 + D_2|\mathbf{N}_0|^4 + C(0)|\mathbf{D}_0|^2|\mathbf{N}_0|^2, \quad (3.56)$$

where $C(0) = C_1 - C_2/2$. Notice that this action is only a function of the two scalar parameters $|\mathbf{D}_0|$ and $|\mathbf{N}_0|$. Thus, the present problem involving two *vector* order parameters can be mapped into a system of two *scalar* order parameters ϕ_1 and ϕ_2 with the effective action

$$S_{\phi_1-\phi_2} = \frac{r}{2}\left(\phi_1^2 + \phi_2^2\right) - \frac{g}{2}\left(\phi_1^2 - \phi_2^2\right) + u_1\phi_1^4 + u_2\phi_2^4 + 2u_{12}\phi_1^2\phi_2^2 \quad (3.57)$$

through the mapping

$$\begin{gathered} |\mathbf{D}_0| \to \phi_1, \quad |\mathbf{N}_0| \to \phi_2; \\ A(0) \to (r-g)/2, \quad nB(\mathbf{Q}_1)/2 \to (r+g)/2; \\ D_1 \to u_1, \quad D_2 \to u_2, \text{ and } C(0) \to 2u_{12}. \end{gathered} \quad (3.58)$$

If $g = 0$ and $u_1 = u_2 = u_{12}$, the so-called "ϕ_1–ϕ_2" model with action (3.57) reduces to the xy-model with a two-component vector order parameter $\boldsymbol{\phi} = (\phi_1, \phi_2)$ and isotropic interactions. When $g > 0$, however, one obtains an ordered phase with $\phi_1 \neq 0$ and $\phi_2 = 0$. When $g < 0$, the converse occurs with $\phi_1 = 0$ and $\phi_2 \neq 0$. The details of the phase diagram for Eq. (3.57) depend on the relative magnitudes of the fourth-order terms. When $u_1u_2 < u_{12}^2$, there is a first-order line along $g_1 = 0$, $r < 0$ separating the phase with $\phi_1 \neq 0$ and $\phi_2 = 0$ from the phase with $\phi_1 = 0$ and $\phi_2 \neq 0$, as shown in Fig. 3.14(a). Two distinct second-order lines meet at the point $r = 0$, $g = 0$, and this point is called a *bicritical* point [191]. When $u_1u_2 > u_{12}^2$, there is an intermediate phase, with both ϕ_1 and ϕ_2 nonzero, separated by a second-order line from the phases with $\phi_1 = 0$ and $\phi_2 = 0$, as shown in Fig. 3.14(b). In this case, four second-order lines meet at the point $r = 0$, $g = 0$, which is now a *tetracritical* point [191].

In the case of quasi-1D systems with competing TSC and SDW orders, the phase diagram that emerges from the action (3.56) leads to either bicritical or tetracritical points as

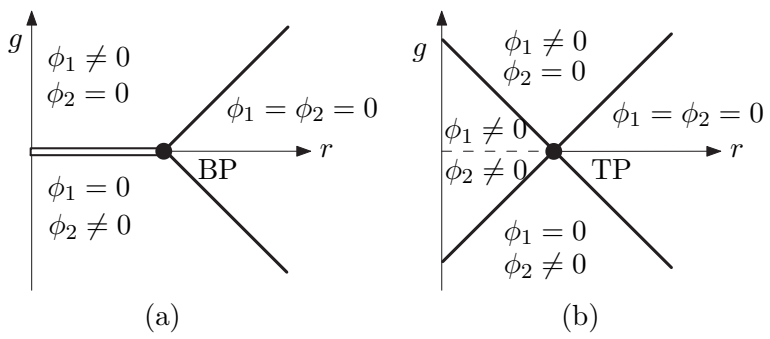

Figure 3.14: Phase diagrams from the ϕ_1–ϕ_2 model described by Eq. (3.57) showing (a) a bicritical point (BP) when $u_1 u_2 < u_{12}^2$ and (b) a tetracritical point (TP) when $u_1 u_2 > u_{12}^2$.

illustrated in Fig. 3.15. When $R = C^2(0)/(4D_1D_2) > 1$ the critical point (P_c, T_c) is bicritical and there is a first order transition line at $(n/2)B(\mathbf{Q}_1) = A(0)$ when both $B(\mathbf{Q}_1) < 0$ and $A(0) < 0$, as seen in Fig. 3.15(a). However when $R < 1$, (P_c, T_c) is tetracritical and a coexistence region of TSC and SDW occurs when both $B(\mathbf{Q}_1) < 0$ and $A(0) < 0$, as shown in Fig. 3.15(b). The pressure versus temperature phase diagrams in Fig. 3.15 are obtained by assigning the standard linear temperature and pressure dependence on the GL coefficients around the critical point,

$$A(0) = \alpha_{\rm TSC}[T - T_{\rm TSC}(P)], \text{ with } T_{\rm TSC}(P) = T_c + \beta_{\rm TSC}(P - P_c); \quad (3.59a)$$

$$B(\mathbf{Q}_1) = \alpha_{\rm SDW}[T - T_{\rm SDW}(P)], \text{ with } T_{\rm SDW} = T_c + \beta_{\rm SDW}(P_c - P). \quad (3.59b)$$

Here, the GL prefactors $\alpha_{\rm TSC}$ and $\alpha_{\rm SDW}$, and the pressure coefficients $\beta_{\rm TSC}$ and $\beta_{\rm SDW}$ are all positive.

The ratio $R \approx 0.12$ for the Bechgaard salt $(\mathrm{TMTSF})_2\mathrm{PF}_6$ around (P_c, T_c), when the interaction strengths V, J are chosen to give the same $T_c = 1.2$ K at quarter filling for parameters $t_x = 5800$ K, $t_y = 1226$ K, $t_z = 58$ K, used in combination with $\phi^{\Gamma}(\mathbf{k}) = \sin(k_x a)$ (p_x-symmetry for TSC) and the nesting vectors $\mathbf{Q} = (\pm\pi/2a, \pm\pi/2b, 0)$ ($n = 4$), as suggested by experiments [165, 192, 193]. Therefore, the analysis above shows that $(\mathrm{TMTSF})_2\mathrm{PF}_6$ has a TSC/SDW coexistence region as suggested by experiments [68, 69, 70].

To investigate the TSC/SDW coexistence region the effective action (3.54) is Fourier

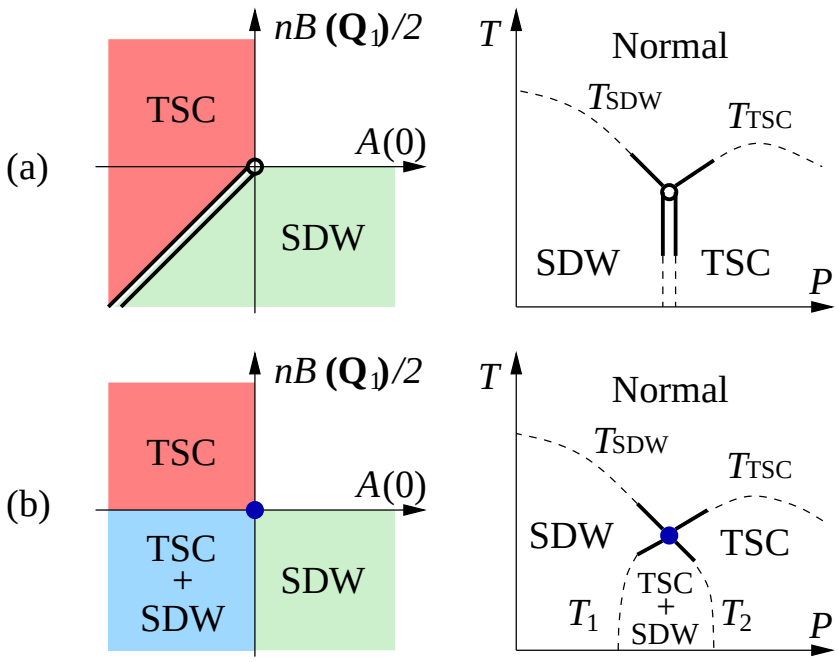

Figure 3.15: Schematic phase diagrams indicating (a) first order transition line with no coexistence phase, and (b) two second order lines with coexistence region between TSC and SDW phases. Adapted from Ref. [73].

transformed into real space to give the GL free energy density

$$\mathcal{F} = \mathcal{F}_n + \mathcal{F}_{\rm TSC} + \mathcal{F}_{\rm SDW} + \mathcal{F}_{\rm C}, \tag{3.60}$$

where $\mathcal{F}_n$ is the normal state contribution, and $\mathcal{F}_{\rm C} = C(\theta)|\mathbf{N}(\mathbf{r})|^2|\mathbf{D}(\mathbf{r})|^2$ is the coupling term of the two order parameters. The TSC and SDW contributions are

$$\mathcal{F}_{\rm TSC} = A(0)|\mathbf{D}(\mathbf{r})|^2 + D_1|\mathbf{D}(\mathbf{r})|^4 + \sum_\mu \gamma^\mu_{\rm TSC} \frac{\partial \mathbf{D}(\mathbf{r})^\dagger}{\partial r_\mu} \cdot \frac{\partial \mathbf{D}(\mathbf{r})}{\partial r_\mu}, \tag{3.61}$$

$$\mathcal{F}_{\rm SDW} = \int d\mathbf{r}' \left[B(\mathbf{r},\mathbf{r}')\mathbf{N}(\mathbf{r})\cdot\mathbf{N}(\mathbf{r}')\right] + \frac{D_2}{n^2}|\mathbf{N}(\mathbf{r})|^4, \tag{3.62}$$

where $\gamma^\mu_{\rm TSC}$ is equal to $a_{\mu\mu}$ defined in Eq. (3.32), and the integration kernel $B(\mathbf{r},\mathbf{r}')$ is the Fourier transform of $B(\mathbf{q})$ in Eq. (3.37). For the Bechgaard salt parameters, the prefactor $C(0)$ of the coupling term $\mathcal{F}_{\rm C}$ is positive, hence represents a local repulsive interaction between the TSC and SDW order parameters. As a consequence, the TSC order parameter is non-uniform in the TSC/SDW coexistence region, and has a modulation induced by the SDW order parameter. Since $R \ll 1$ for $(\mathrm{TMTSF})_2\mathrm{PF}_6$, the coupling term $\mathcal{F}_{\rm C}$ is small in

comparison with the other fourth order terms, and a perturbative solution is possible for $|\mathbf{D}(\mathbf{r})|$ and $|\mathbf{N}(\mathbf{r})|$.

At assumed zero TSC/SDW coupling $\mathcal{F}_{\rm C} = 0$, the saddle point modulation for the SDW order parameter is $\mathbf{N}(\mathbf{r}) = n\mathbf{N}_0 \cos(\mathbf{Q}_1 \cdot \mathbf{r})$, with $|\mathbf{N}_0| = [-nB(\mathbf{Q}_1)/3D_2]^{1/2}$, while the saddle point magnitude for the TSC order parameter is $|\mathbf{D}(\mathbf{r})| = |\mathbf{D}_0| = [-A(0)/2D_1]^{1/2}$. Including the coupling $\mathcal{F}_{\rm C}$ the new solution for the magnitude of TSC order parameter is

$$\begin{aligned} |\mathbf{D}(\mathbf{r})| - |\mathbf{D}_0| &= -\frac{|N_0|^2}{|D_0|}\left(\frac{6D_2R}{D_1}\right)^{1/2}\left[\frac{\cos(2Q_a x)}{4+8\xi_x^2Q_a^2} + \frac{\cos(2Q_b y)}{4+8\xi_y^2Q_b^2}\right. \\ &\quad \left. + \frac{\cos(2Q_a x)\cos(2Q_b y)}{4+8\xi_x^2Q_a^2+8\xi_y^2Q_b^2} + \frac{1}{4}\right], \end{aligned} \tag{3.63}$$

which shows explicitly $2Q_a$ and $2Q_b$ modulations along the $\mathbf{a}$ and $\mathbf{b}'$ axes, respectively. Here, $\xi_\mu = [|\gamma^\mu_{\rm TSC}/A(0)|]^{1/2}$ represents the TSC coherence length along the μ direction. Notice that the modulation in $|\mathbf{D}(\mathbf{r})|$ disappears as the SDW order goes away $|\mathbf{N}_0| \to 0$. The qualitative behavior of $|\mathbf{D}(\mathbf{r})|$ is shown in Fig. 3.16(a). Since the wave vector of spin density modulation is unaffected to first order, the solution for the magnitude of SDW order parameter to the first order correction is

$$|\mathbf{N}(\mathbf{r})| = \sum_{\mathbf{Q}_i}\left[1 - \left(\frac{D_1R}{6D_2}\right)^{1/2}\frac{|\mathbf{D}_0|^2}{4|\mathbf{N}_0|^2}\right]|\mathbf{N}_0|\cos(\mathbf{Q}_i \cdot \mathbf{r}), \tag{3.64}$$

which is shown in Fig. 3.16(b). Notice that the maxima of $|\mathbf{D}(\mathbf{r})|$ coincide with the minima of $|\mathbf{N}(\mathbf{r})|$ indicating that the two orders try to be locally excluded. Since the TSC and SDW modulations are out of phase, experiments that are sensitive to the spatial distribution of the spin density or Cooper pair charge density may reveal the coexistence of these inhomogeneous phases. In addition, since the TSC and SDW order parameters respond differently to a magnetic field, it is instructive to investigate the effects of a magnetic field on the TSC/SDW coexistence region, which is discussed next.

3.6 Magnetic Field Effect

A uniform magnetic field $\mathbf{H}$ couples with electrons in both the charge and the spin channels. The coupling to the charge channel can be described by the Peierl's substitution $\mathbf{k} \to \mathbf{k} - |e|\mathbf{A}$

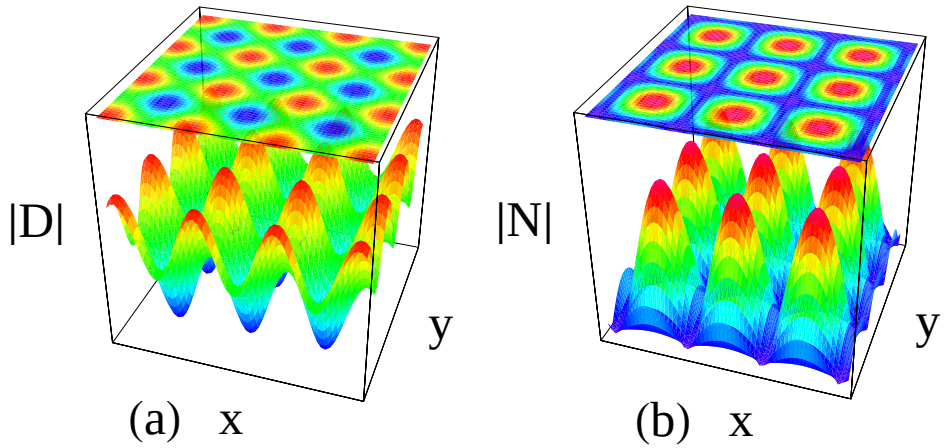

Figure 3.16: Magnitude of (a) TSC and (b) SDW order parameters in the x-y plane, within the coexistence region. Adapted from Ref. [73].

in the dispersion relation Eq. (3.1) to give

$$\epsilon_{\mathbf{k}-e\mathbf{A}} = -t_x \cos\left[(k_x - eA_x)a\right] - t_y \cos\left[(k_y - eA_y)b\right] - t_z \cos\left[(k_z - eA_z)c\right], \tag{3.65}$$

where $-e < 0$ is the electron charge, and $\mathbf{A}$ is the vector potential such that $\mathbf{H} = \nabla \times \mathbf{A}$. The magnetic field couples with the electron spin via the paramagnetic term

$$\mathcal{H}_{\mathrm{P}} = -\mu_0 \mathbf{H} \cdot \sum_{\mathbf{k},\alpha\beta} c^{\dagger}_{\mathbf{k}\alpha} \boldsymbol{\sigma}_{\alpha\beta} c_{\mathbf{k}\beta}, \tag{3.66}$$

where μ_0 is the effective magnetic moment of electrons.

Upon integrating out the fermions, the corresponding effective action in the presence of a magnetic field becomes

$$S_{\mathrm{eff}}(\mathbf{H}) = S_0(\mathbf{H}) + S_2^{\mathrm{TSC}}(\mathbf{H}) + S_2^{\mathrm{SDW}}(\mathbf{H}) + S_4(\mathbf{H}), \tag{3.67}$$

where

$$S_0(\mathbf{H}) = S_0 + \frac{|\mathbf{H}|^2}{8\pi} - \frac{1}{2}\chi_n |\mathbf{H}|^2 \tag{3.68}$$

with χ_n is the uniform electronic spin susceptibility of the normal state. The quadratic terms $S_2^{\mathrm{TSC}}(\mathbf{H})$ and $S_2^{\mathrm{SDW}}(\mathbf{H})$ are obtained from S_2^{TSC} and S_2^{SDW} by the Peierls substitution, respectively. The quartic term $S_4(\mathbf{H})$ is

$$S_4(\mathbf{H}) = S_4^0(\mathbf{H}) + \delta S_4^{\mathrm{TSC}}(\mathbf{H}) + \delta S_4^{\mathrm{SDW}}(\mathbf{H}), \tag{3.69}$$

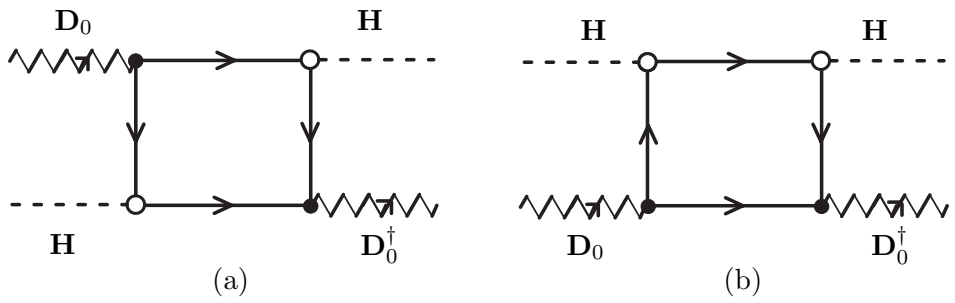

Figure 3.17: Feynman diagrams corresponding to the interacting term $\delta S_4^{\rm TSC}$ between a magnetic field and the TSC order parameter in Eq. (3.69). Here, dashed lines represent external magnetic field.

where $S_4^0(\mathbf{H})$ is obtained from S_4 in Eq. (3.55) by Peierls substitution, and $\delta S_4^{\rm TSC}(\mathbf{H})$ and $\delta S_4^{\rm SDW}(\mathbf{H})$ represent the magnetic field interaction with the TSC and SDW orders, respectively.

In order to calculate $\delta S_4^{\rm TSC}(\mathbf{H})$ and $\delta S_4^{\rm SDW}(\mathbf{H})$, one can also use the diagrammatic technique. For example, the TSC and magnetic field coupling term can be obtained from the diagrams shown in Fig. 3.17, via the following Feynman rules for the magnetic field lines:

8. For each initial magnetic field line connected to a vertex, write a factor $-\mu_0\mathbf{H}\cdot\boldsymbol{\sigma}_{\alpha\beta}$, while for each final magnetic field line connected to a vertex, write the Hermitian conjugate $-\mu_0\mathbf{H}\cdot(\boldsymbol{\sigma}^\dagger)_{\alpha\beta}$;

Using these new Feynman rules and others discussed previously, the $\delta S_4^{\rm TSC}(\mathbf{H})$ can be written as

$$\delta S_4^{\rm TSC}(\mathbf{H}) = (E_1 + E_2/2)|\mathbf{H}|^2|\mathbf{D}_0|^2 - E_2|\mathbf{H}\cdot\mathbf{D}_0|^2, \tag{3.70}$$

where

$$E_1 = -\frac{1}{2}\sum_{\mathbf{k},\omega_n}\frac{\mu_0^2|\phi^\Gamma(\hat{\mathbf{k}})|^2}{(i\omega_n+\xi_{\mathbf{k}})^3(-i\omega_n+\xi_{-\mathbf{k}})}, \tag{3.71a}$$

$$E_2 = -\sum_{\mathbf{k},\omega_n}\frac{\mu_0^2|\phi^\Gamma(\hat{\mathbf{k}})|^2}{(i\omega_n+\xi_{\mathbf{k}})^2(-i\omega_n+\xi_{-\mathbf{k}})^2} \tag{3.71b}$$

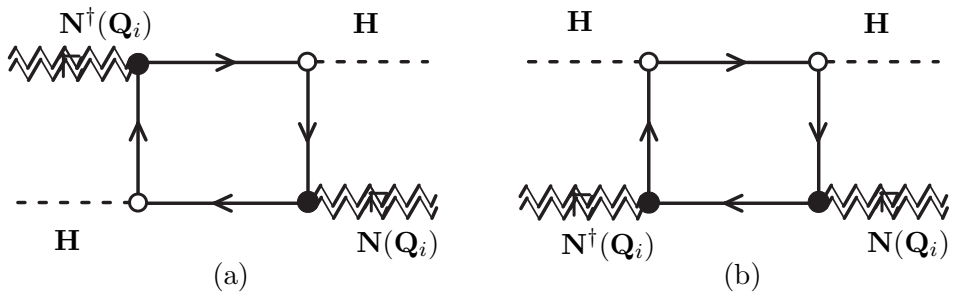

Figure 3.18: Feynman diagrams corresponding to the interacting term $\delta S_4^{\rm SDW}$ between a magnetic field and the SDW order parameter in Eq. (3.69). Here, dashed lines represent external magnetic field.

are obtained from Figs. 3.17(a) and (b), respectively. By performing the Matsubara summations, we have the following results for the coefficients

$$E_1 = -\frac{\beta}{2}\sum_{\mathbf{k}} \frac{\mu_0^2|\phi^\Gamma(\hat{\mathbf{k}})|^2}{8\xi_{\mathbf{k}}}\left[\frac{X(\mathbf{k})}{\xi_{\mathbf{k}}^2} - \frac{\beta Y(\mathbf{k})}{2\xi_{\mathbf{k}}} - \frac{\beta^2 X(\mathbf{k})Y(\mathbf{k})}{2}\right]; \tag{3.72a}$$

$$E_2 = -\beta\sum_{\mathbf{k}} \frac{\mu_0^2|\phi^\Gamma(\hat{\mathbf{k}})|^2}{4\xi_{\mathbf{k}}^2}\left[\frac{X(\mathbf{k})}{\xi_{\mathbf{k}}} - \frac{\beta Y(\mathbf{k})}{2}\right]. \tag{3.72b}$$

Similarly, the SDW and magnetic field coupling term can be obtained from the diagrams shown in Fig. 3.18, leading to

$$\delta S_4^{\rm SDW}(\mathbf{H}) = (F_1 + F_2/2)|\mathbf{H}|^2|\mathbf{N}_0|^2 - F_2|\mathbf{H}\cdot\mathbf{N}_0|^2, \tag{3.73}$$

with coefficients

$$F_1 = \frac{1}{4}\sum_{\mathbf{Q}_i}\sum_{\mathbf{k},\omega_n} \frac{\mu_0^2}{(i\omega_n + \xi_{\mathbf{k}})^3(i\omega_n + \xi_{\mathbf{k}+\mathbf{Q}_i})}; \tag{3.74a}$$

$$F_2 = -\frac{1}{2}\sum_{\mathbf{Q}_i}\sum_{\mathbf{k},\omega_n} \frac{\mu_0^2}{(i\omega_n + \xi_{\mathbf{k}})^2(i\omega_n + \xi_{\mathbf{k}+\mathbf{Q}_i})^2}. \tag{3.74b}$$

By performing the Matsubara summations,

$$F_1 = \frac{\beta}{4}\sum_{\mathbf{Q}_i}\sum_{\mathbf{k}} \frac{\mu_0^2}{\xi_{\mathbf{k}} - \xi_{\mathbf{k}+\mathbf{Q}_i}}\left[\frac{X(\mathbf{k}+\mathbf{Q}_i) - X(\mathbf{k})}{2(\xi_{\mathbf{k}+\mathbf{Q}_i} - \xi_{\mathbf{k}})^2} + \frac{\beta Y(\mathbf{k})}{4(\xi_{\mathbf{k}} - \xi_{\mathbf{k}+\mathbf{Q}_i})} + \frac{\beta^2 X(\mathbf{k})Y(\mathbf{k})}{8}\right]; \tag{3.75a}$$

$$F_2 = -\frac{\beta}{2}\sum_{\mathbf{Q}_i}\sum_{\mathbf{k}} \frac{\mu_0^2}{(\xi_{\mathbf{k}+\mathbf{Q}_i} - \xi_{\mathbf{k}})^2}\left[\frac{X(\mathbf{k}+\mathbf{Q}_i) - X(\mathbf{k})}{\xi_{\mathbf{k}+\mathbf{Q}_i} - \xi_{\mathbf{k}}} - \frac{\beta Y(\mathbf{k})}{4} - \frac{\beta Y(\mathbf{k}+\mathbf{Q}_i)}{4}\right]. \tag{3.75b}$$

A numerical calculation using the same parameters used in Section 3.5 for the Bechgaard salt $(TMTSF)_2PF_6$ shows that the coefficients $E_2 < 0$ and $F_2 < 0$, indicating that the TSC and SDW order parameters **D** and **N** prefer to be perpendicular to the magnetic field **H**. These conditions, when combined with $C_2 > 0$ in Eq. (3.42), indicate that **D** and **N** prefer to be parallel to each other, but perpendicular to **H**. However, the relative orientation of these vectors in magnetic fields is affected by small spin anisotropies which were already observed in $(TMTSF)_2PF_6$, where the easy axis for **N** is the $\mathbf{b}'$ direction [190]. Such an anisotropy effect can be described by adding a quadratic term $-u_N N_{b'}^2$ with $u_N > 0$, which favors $\mathbf{N} \parallel \mathbf{b}'$. Similarly, the **D** vector also has an anisotropic effect caused by the spin-orbit coupling, thus can be described by adding a quadratic term $-u_D D_i^2$, where i is the easy axis for TSC which is not experimentally known thus far. However, this anisotropy of TSC order parameter is expected to be small due to the weak spin-orbit coupling effect in Bechgaard salts [55, 63]. The quartic TSC and SDW terms may also become weakly anisotropic when these effects are taken into account.

However, a sufficiently large $\mathbf{H} \parallel \mathbf{b}'$ can overcome spin anisotropy effects, and drive the **N** vector to flop into the **a**-$\mathbf{c}^*$ plane. This canting (flop) transition of the SDW vector was reported [190] in $(TMTSF)_2PF_6$ for $H \approx 1$ T at zero pressure and $T = 8$ K. If such a spin-flop transition persists near the TSC/SDW critical point (P_c, T_c), then the flop transition of the **N** vector forces the **D** vector to flop as well, since the pinning effect of TSC order parameter caused by spin-orbit coupling is weak. This flop transition of TSC order parameter can dramatically change the magnetic field versus temperature phase diagram, and has potentially serious consequences to the superconducting state.

For $P < P_c$, if a flop transition occurs for $H_F < H_1(0)$ [see Fig. 3.19(a)], then **N** flops both in the pure SDW and in the TSC/SDW coexistence phases, in which case it forces **D** vector to flop as well. If the flop transition occurs for $H_{\rm SDW}(0) < H_F < H_1(0)$ [see Fig. 3.19(b)] then only the pure SDW phase is affected. The situation is qualitatively different for $P > P_c$. In the zero (weak) spin-orbit coupling limit the **D** vector is free to rotate in a magnetic field and tends to be perpendicular to **H**. Thus, for $\mathbf{H} \parallel \mathbf{b}'$ and $|\mathbf{H}| > H_2(T)$, the **D** vector lies in the **a**-$\mathbf{c}^*$ plane since there is no SDW order. However, at

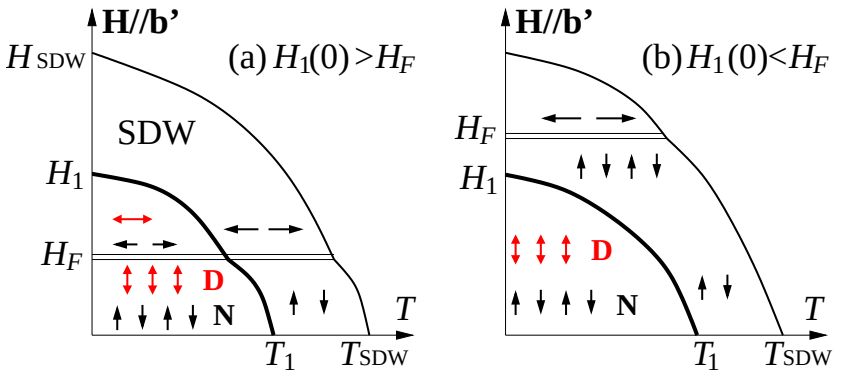

Figure 3.19: Schematic H-T phase diagrams showing the TSC/SDW coexistence region (thick solid line) and canting transition (double line) for (a) $H_F(0) < H_1(0)$ and (b) $H_F(0) > H_1(0)$, where $H_F(0)$ and $H_1(0)$ are the zero temperature SDW flopping field and the TSC/SDW coexistence transition field, respectively. In this figure, pressure P is assumed to be smaller than the critical pressure P_c. Adapted from Ref. [73].

lower temperatures and small magnetic fields when TSC and SDW orders coexist, the spin anisotropy field forces **N** to be along $\mathbf{b}'$ and **N** forces **D** to flop from the $\mathbf{a}$-$\mathbf{c}^*$ plane to $\mathbf{b}'$ direction. This canting transition occurs at $H_F < H_2(T)$ (see Fig. 3.20).

This canting transition of the superconducting order parameter can only be present in systems with *triplet* superconductivity. In the case of coexistence of SDW and singlet superconductivity (SSC), there would be no vector coupling between SDW and SSC, and thus the canting transition of the SDW has no effect on the SSC order parameter.

3.7 Summary

In summary, I discussed in this chapter the interplay between triplet superconductivity and spin density wave orders in quasi-one-dimensional organic conductor $(TMTSF)_2PF_6$. Starting from a microscopic Hamiltonian which allowed both TSC and SDW instabilities at low temperatures, I derived the effective action for TSC and SDW order parameters. The phase diagram that emerged from this effective field theory showed that the TSC and SDW order parameters can coexist. A detailed calculation using microscopic parameters compatible with experiments confirmed the possibility of a TSC/SDW coexistence region in the pressure versus temperature phase diagram of $(TMTSF)_2PF_6$. Within the coexistence region, the TSC order parameter is nonuniform and its modulation is induced by the SDW

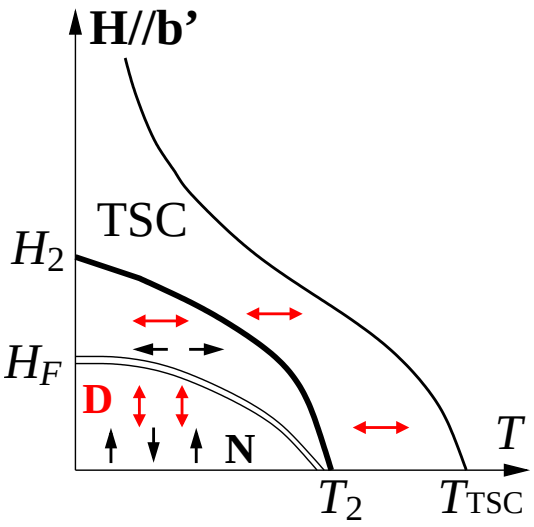

Figure 3.20: Schematic H-T phase diagram showing the TSC/SDW coexistence region (thick solid line) and canting transition (double line) for $P > P_c$. Adapted from Ref. [73].

order parameter. The modulations of TSC and SDW order parameters are out of phase since these orders tend to avoid each other because of their effective repulsive interaction. It should be emphasized that the effective action in Eq. (3.54) is not SO(4) invariant. In fact, theories based on SO(4) symmetry [71] cannot be applied to these highly anisotropic three-dimensional systems, since they are strictly valid only in the one-dimensional limit.

Furthermore, I discussed qualitatively magnetic field effects on the coexistence region. I proposed that a magnetic field pointing along the $\mathbf{b}'$ direction can induce a canting transition of the SDW order parameter, and consequently flop the TSC order parameter. This canting transition of TSC order parameter can dramatically alter the properties of the superconducting phase and the phase diagram of the coexistence region. For instance, new phases in the magnetic field versus temperature phase diagram were found both below and above the critical pressure. This anomalous magnetic field effect on the superconducting phase is directly related to the vector nature of the TSC order parameter, and its coupling to the SDW order. This phenomena is absent in singlet superconductors (SSC), when SDW and SSC coexist.

The vector nature of the order parameter for triplet superconductivity is a crucial distinction from the singlet case, and can cause other interesting properties such as polarization

effect in a triplet superconductor–insulator–triplet superconductor Josephson junction [63]. If spin-orbit coupling is weak in both superconductors, the Josephson current should depend on the relative orientation of the two vector order parameters in addition to their relative U(1) phase. This expectation is related to the Malus' law of polarization in optics, although the physics is completely different. For triplet superfluidity in trapped Fermi gases, the vector nature of order parameter also affects the matter-wave interference between two condensates, and leads to a similar polarization effect. In the next chapter, I will discuss the matter-wave interference between two triplet Fermi condensates, as well as the time evolution of a single cloud.

CHAPTER IV

TIME EVOLUTION AND MATTER-WAVE INTERFERENCE IN P-WAVE FERMI CONDENSATES

In addition to the quasi-one-dimensional conductors discussed in Chapter 3, ultra-cold Fermi gases are another kind of system which may produce triplet superfluidity. It is encouraging that many groups have reported some progress towards the formation of p-wave Fermi condensates in harmonically trapped clouds [117, 131, 132, 133] and in optical lattices [134], where p-wave Feshbach resonances have been observed. Unfortunately, for Feshbach resonances currently tried in harmonically trapped clouds atom losses have been significant, and the realization of stable p-wave condensates has not been achieved yet. However, other unexplored Feshbach resonances in harmonically trapped clouds may show less dramatic two-body dipolar or three-body losses as observed in optical lattices [134].

In this chapter, I will discuss the time dynamics and matter-wave interference of p-wave Fermi condensates on the Bose–Einstein condensation side of the Feshbach resonances. The dynamics of a harmonically trapped cloud is an important issue since much information on Bose and Fermi condensates can be obtained experimentally from images of the expanded atomic cloud [92]. This includes in particular the temperature of the gas (which is extracted from the tail of the thermal component), the release energy, and the aspect ratio of the velocity distribution. From the theoretical point of view, the free expansion of a harmonically trapped cloud, following the switching off of the trap, has been studied for both Bose [194, 195, 196, 197, 198] and s-wave Fermi [199] condensates. For triplet p-wave Fermi condensates, I will show that the free expansion of a harmonically trapped cloud can be anisotropic, reflecting the spatial anisotropy of the underlying interaction between fermions and the orbital nature of the vector order parameter.

Matter-wave interference is a very powerful tool to study quantum phase coherence between atomic Bose condensates [200, 201, 202], and spatial quantum noise of bosons

in optical lattices [203]. Similar techniques can also be applied to study Fermi condensates [78, 80, 104, 81, 124, 82], where superfluidity can be tuned from the weakly interacting (the so-called BCS) regime to the strongly interacting (the so-called BEC) regime. These experiments may reveal that the time dynamics in the BCS regime is overdamped (large Cooper pairs can decay into two atoms), while in the BEC regime it is essentially undamped (tightly bound molecules are stable) [140, 204]. Matter-wave interference experiments of s-wave Fermi condensates may be readily performed, since stable condensates already exist. For s-wave Fermi condensates in the BEC regime quantum interference effects are expected to be similar to those of atomic Bose condensates, and the interference pattern should depend essentially on the phase difference of the order parameters between two interfering clouds. For p-wave Fermi condensates, however, I will show that the interference pattern can also have a strong dependence on the relative angle between the two vector order parameters, thus producing a polarization effect. Therefore, both properties (anisotropic expansion and polarization dependent matter-wave interference) are key features of p-wave Fermi condensates, which are absent in their s-wave counterparts.

4.1 Background

The first experimental realizations of Bose–Einstein condensation of diatomic molecules in ultra-cold Fermi gases in 2003 stimulated investigations of superfluidity in atomic systems [78, 79, 80]. These Fermi condensates are not only another type of sample, but are also systems which allow tuning of the effective inter-atomic interaction. Unlike the pairing mechanism in superconductors, the attractive potential in atomic systems is provided by the van der Waals interaction between two atoms, and can be tuned by a magnetic field. The sensitive magnetic-field dependence of the potential occurs through a scattering resonance known as the Feshbach resonance [205, 206, 207, 208].

4.1.1 Feshbach Resonance

Calculating the interaction between two ground state alkali atoms is a nontrivial problem in atomic physics. The study of this problem shows that the s-wave interatomic potential is repulsive for very small r and has a long weak attractive tail that goes as $-C_6/r^6$ as

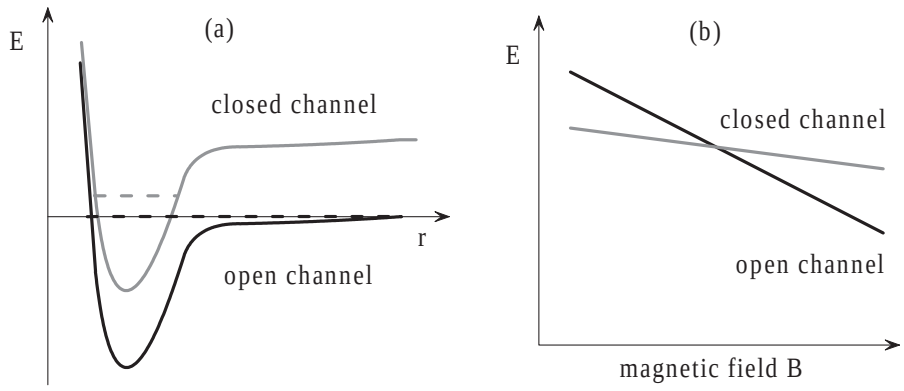

Figure 4.1: (a) Feshbach resonance is present when a bound state in the closed channel is nearly degenerate with the threshold energy of the open channel. (b) The bound state of the closed channel responds differently to a magnetic field from the open-channel threshold. This can lead to a crossing of the two levels, and provide a technique to tune the FR. Adapted from Ref. [209].

$r \to \infty$, while the p-wave interatomic potential has the similar behavior but is anisotropic. The interatomic potentials are deep enough to contain a large number of bound states. A Feshbach resonance (FR) occurs when one of these bound states coincides with the collision energy (usually called the threshold) of two free atoms in a different scattering channel. For simplicity, I discuss in this section only the s-wave FR in Fermi systems of identical fermions.

A schematic depiction of FR is shown in Fig. 4.1(a) [209]. The interatomic potential of the two free atoms (black line) is often referred to as the open channel, while the potential containing the bound state (gray line) is referred to as the closed channel. When the closed and open channels describe atoms in different magnetic sublevels, they respond to a magnetic field in a difference manner and can be shifted with respect to each other through the Zeeman effect (as shown in Fig. 4.1(b)b [209]).

Typically the effect of the coupling between the closed and open channels is small, but at a FR when the open-channel threshold is nearly degenerate with a bound state in the closed-channel, the effect of the coupling can be significantly enhanced. This coupling changes the effective interatomic potential from the single-channel form to the so-called multichannel potential [210]. A new bound state is present in this multichannel potential

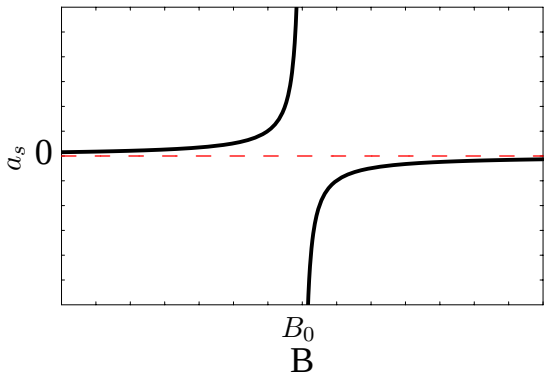

Figure 4.2: Qualitative behavior of the s-wave scattering length a_s around a FR at magnetic field B_0.

at a value near the magnetic field position of the crossing of the closed-channel bound state and open-channel threshold. This new bound state is usually called a "dressed molecule", in comparison with the "bare molecule" referring the bound state in the closed-channel away from FR*. The wavefunction of these molecules is generally a linear superposition of open-channel and closed-channel wavefunctions. However, I will consider only the broad resonance limit where the open-channel component dominates. This approximation seems to be valid for many s-wave and p-wave FRs currently studied.

As the magnetic field is tuned, this multichannel bound state moves through the threshold, and the scattering length between atoms in the open channel diverges. The scattering length near a FR varies with the magnetic field, B, according to the following relation [209]

$$a(B) = a_{bg}\left(1 - \frac{w}{B - B_0}\right), \tag{4.1}$$

where a_{bg} is the background (nonresonant) scattering length for atoms scattering in the open channel, B_0 is the magnetic field position at which the bound state of the closed channel goes through the threshold of the open channel, and w is the magnetic field width of the FR, defined as the distance in magnetic field between B_0 and the magnetic field at which $a = 0$. The behavior of Eq. (4.1), in particular the divergence of a, is shown in Fig. 4.2.

In addition to the scattering length a, the binding energy of the dressed molecule E_b

*In this chapter, the term "molecule" is always used to denote the dressed molecule.

is also a function of magnetic field. To calculate E_b exactly one would need to carry out a multichannel calculation using realistic potentials of specific atoms. The main goal is to solve the coupled Schrodinger equations for the two-channel system [211]

$$\mathcal{H} = \begin{pmatrix} -\nabla^2/m + V_{oc}(\mathbf{r}) & W(\mathbf{r}) \\ W(\mathbf{r}) & -\nabla^2/m + V_{cc}(\mathbf{r}) \end{pmatrix}, \tag{4.2}$$

where V_{oc} is the uncoupled open-channel potential, V_{cc} is the uncoupled closed-channel potential, the potential W describes the coupling between the open and closed channels, and m is the mass of fermions. These interactions can be related to the scattering parameter a and the binding energy of the bound state in the closed channel by the continuum energy wavefunctions, or equivalently, by the T-matrix [212]. The two-channel states are of the general form $|o\rangle\phi_{oc}(\mathbf{r}) + |c\rangle\phi_{cc}(\mathbf{r})$, where $|o\rangle$ and $|c\rangle$ denote the internal states of an atom pair in the open channel and the closed channel strongly coupled to it, respectively. The two components of the energy states are solutions of the coupled Schrodinger equations

$$\left[-\frac{\nabla^2}{m} + V_{oc}(\mathbf{r})\right]\phi_{oc}(\mathbf{r}) + W(\mathbf{r})\phi_{cc}(\mathbf{r}) = E\phi_{oc}(\mathbf{r}), \tag{4.3a}$$

$$W(\mathbf{r})\phi_{oc}(\mathbf{r}) + \left[-\frac{\nabla^2}{m} + V_{oc}(\mathbf{r})\right]\phi_{cc}(\mathbf{r}) = E\phi_{cc}(\mathbf{r}). \tag{4.3b}$$

This problem can be solved using a technique discussed by K. Góral *et al.* [211]. This technique uses only a set of five experimentally measurable parameters to produce the important physics of a FR. The main approximation is the "pole approximation" [211], which holds when the kinetic energies in the collision are small in comparison to the typical spacing between bound states in the closed channel, i.e., the open channel is strongly coupled to only one bound state in the closed channel. Under this assumption, the binding energy of the new multi-channel bound state can be obtained by solving the coupled equations (4.3). In the small region of magnetic field strengths on the low-field side of the FR (the scattering length $a \gg r_0$ with r_0 is the effective range of the van der Waals potential), the binding energy E_b has the universal form [211]

$$E_b(B) = -\frac{1}{ma^2}. \tag{4.4}$$

The behavior of E_b as a function of B is shown in Fig. 4.3, in comparison with the binding energy in the closed channel E_{-1} (dotted line), and the open channel threshold E_0 (dashed

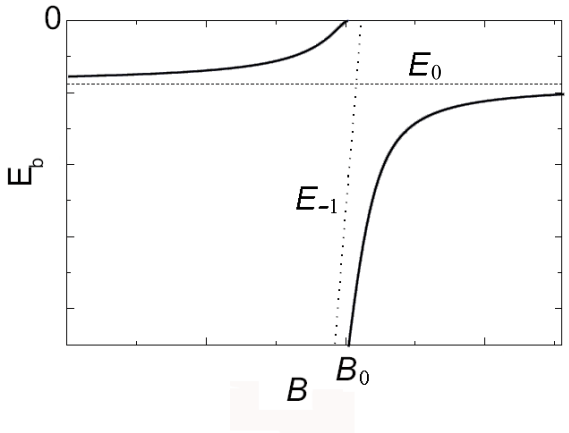

Figure 4.3: The magnetic field dependence of the binding energy E_b of the bound state of the two-channel Hamiltonian (solid line). The binding energy (E_{-1}) of the bound state in the closed channel (dotted line) and the threshold E_0 of the open channel (dashed line) for the single-channel Hamiltonian are shown for comparison. Notice that the new bound state with energy E_b emerges on the low-field side of the FR to avoid the two single-channel levels crossing. Adapted from Ref. [209].

line). Notice that when sweeping the magnetic field, the states E_{-1} and E_0 cross at the FR, and the new bound state E_b emerges due to the avoided crossing of the two levels.

In conclusion, I have discussed how a Feshbach resonance can be used to add an additional bound state to a given interatomic potential, leading to a divergence in the zero-energy scattering cross section for atoms colliding through the open channel. The binding energy of the new bound state and the effective interaction strength between two atoms depend sensitively on the magnetic field. The scattering length a_s is negative for $B > B_0$ (where there are no Feshbach molecules). The region is called the BCS side because there are no two-atom bound state, but there are very "large" many-body Cooper pairs at low temperatures [204]. The scattering length a_s is positive for $B < B_0$ (where there are Feshbach molecules). This region is called the BEC side because the two-atom bound states correspond to very "small" many-body Cooper pairs at low temperatures and low densities [204]. In this chapter, I will discuss only the BEC side of p-wave FRs in a Fermi system

4.1.2 Experimental Observations of p-wave Feshbach Resonances

In the previous section, I discussed s-wave collisions between atoms and the corresponding Feshbach resonances. For Fermi systems, s-wave collisions occur between fermions in different states or different species, because the Pauli exclusion principle forbids s-wave collision between identical fermions. In contrast, p-wave collisions in Fermi systems with identical fermions are allowed. Unfortunately, they are suppressed by centrifugal effects as described in the Wigner threshold law [213, 214], which demands that the elastic scattering cross section decreases with temperature as $\sigma \propto T^2$. This characteristic behavior ordinarily suppresses p-wave interactions at ultra-cold temperatures. However, p-wave collisions can become dominant in the presence of a p-wave Feshbach resonance, which was first measured by Regal *et al.* [117] for ^{40}K.

In their experiment, Regal *et al.* [117] performed a collision measurement in an ultra-cold Fermi system of ^{40}K atoms in the lowest lying state $|9/2, -9/2\rangle$. The scattering cross sections for p-wave collisions has a peak that rises over 3 orders of magnitude about the small background cross section. This peak in the cross section thus suggests a divergence of the scattering parameter[†] a_p at the p-wave FR. In addition, Regal *et al.* also observed sensitive dependence of observables on temperature. This dependence arises from a centrifugal barrier through which the wave function must tunnel to access the resonant state.

Further experiments were performed by the same [131] and other experimental groups [132, 133, 134] in Fermi gases of potassium [131, 134] and lithium [132, 133], and showed two features of p-wave FRs. The first feature is the splitting of FRs in "spin" (hyperfine state) space, such that three resonances are observed at different magnetic fields in a mixture of two "spin" states $|1\rangle$ and $|2\rangle$. Therefore, it is possible in principle to tune p-wave interactions between fermions in different "spin" states independently. For example, p-wave FRs for $|1\rangle + |1\rangle$, $|1\rangle + |2\rangle$, and $|2\rangle + |2\rangle$ located respectively at 159.14 G, 185.09 G, and 214.95 G are observed in ^{6}Li system [133], as shown in Fig. 4.4. The atomic numbers in these plots were obtained from absorption images taken after quickly switching off the magnetic field

[†]The scattering parameter for p-wave collision has dimension of L^3, hence should be called "scattering volume" instead of scattering length in the s-wave case.

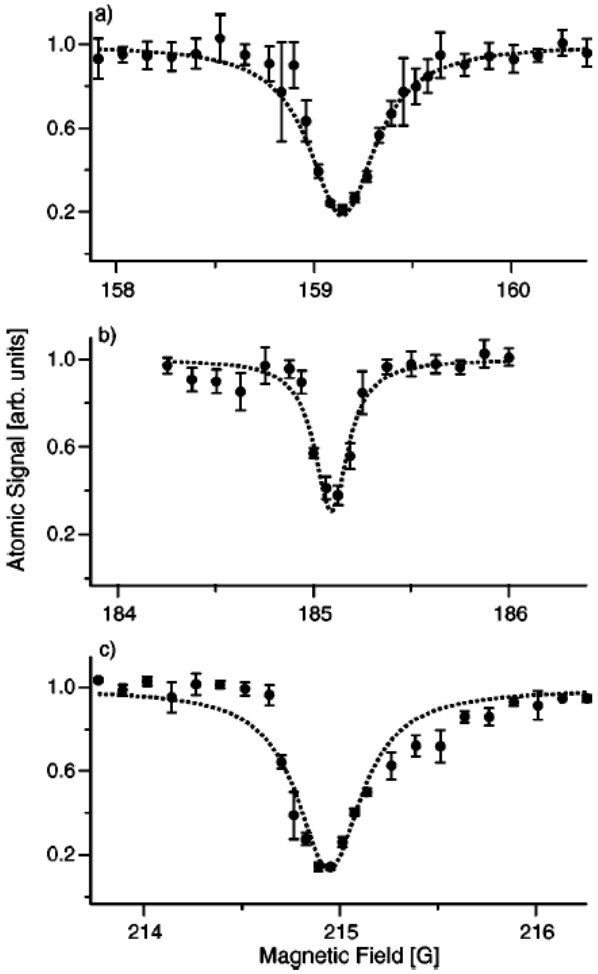

Figure 4.4: p-wave Feshbach resonances for (a) $|1\rangle + |1\rangle$, (b) $|1\rangle + |2\rangle$, and (c) $|2\rangle + |2\rangle$ collisions. The resonances were fitted by Lorentzian functions (dotted lines). Adapted from Ref. [133].

and the trapping potential. The second feature is a doublet peak arising from the magnetic dipole-dipole interaction between the atoms' valence electrons, as shown in Fig. 4.5 [134]. In contrast to the s-wave case, two fermions scattered through the p-wave channel experience a non-vanishing dipole-dipole interaction in lowest order, which can split the FR into distinct resonances based on their partial-wave projection onto the quantization axis, i.e., the magnetic quantum number $m_\ell = 0$ or $m_\ell = \pm 1$. Therefore, splitting of the p-wave FR offers a means to tune separately the p-wave interaction in different m_ℓ states. A typical experiment data [134] indicating this splitting is shown in Fig. 4.5. Notice that the splitting between $m_\ell = 0$ and $|m_\ell| = \pm 1$ can reach 1 G at low temperatures, which is about twice

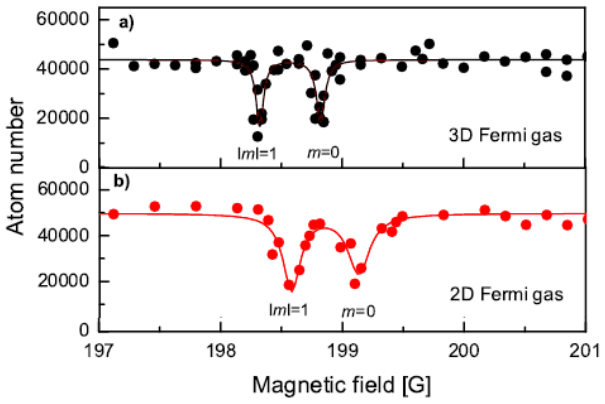

Figure 4.5: Atom loss measurements of the p-wave FR for ^{40}K atoms held in a crossed-beam optical dipole trap. Adapted from Ref. [134].

the width of each FR peak.

The finite separation of p-wave FRs in different "spin" and m_ℓ states may allow the selectively tuning of interactions in specific channels. This possibility is even more dramatic in comparison to s-wave Fermi condensates, since one may control not only how strongly the fermions are attracted, but also in which additional channels they interact. Thus, p-wave Fermi condensates are ideal candidates for investigations of triplet superfluidity. In the rest part of this chapter, I will focus on the time evolution and matter-wave interference of p-wave Fermi condensates in the BEC regime, show some of their distinctive properties, and compare them to the s-wave Fermi condensates.

4.2 Hamiltonian and Effective Action

In order to investigate the dynamics of a p-wave Fermi condensate, I consider a dilute Fermi gas of fermions with mass m in two hyperfine states (pseudospins), labeled by greek indices $\alpha = 1, 2$. The Fermi gas is assumed to be confined in a harmonic trap at low temperatures. Using natural units with $\hbar = k_B = 1$, the Hamiltonian in the Heisenberg picture is given by

$$\begin{aligned}\mathcal{H}(t) &= \int d\mathbf{r}\Bigg\{ c_\alpha^\dagger(\mathbf{r},t)\left[-\frac{\nabla_{\mathbf{r}}^2}{2m} + U_{\text{ext}}(\mathbf{r},t)\right] c_\alpha(\mathbf{r},t) \\ &\quad + \int d\mathbf{r}'\left[c_\alpha^\dagger(\mathbf{r},t)c_\beta^\dagger(\mathbf{r}',t)V_{\alpha\beta\gamma\delta}(\mathbf{r}-\mathbf{r}')c_\gamma(\mathbf{r}',t)c_\delta(\mathbf{r},t)\right]\Bigg\}, \qquad (4.5)\end{aligned}$$

where repeated greek indices indicate summation, $c_\alpha^\dagger$ and c_α are creation and annihilation operators of fermions in state α, respectively, and $V_{\alpha\beta\gamma\delta}(\mathbf{r}-\mathbf{r}')$ is the interparticle interaction potential. The harmonic trapping potential can be written as

$$U_{\text{ext}}(\mathbf{r},t) = \sum_{j=x,y,z} m\omega_j(t) r_j^2/2, \tag{4.6}$$

where $\omega_j(t)$ describes the time dependence of the potential.

Since one is interested in the dynamics of this Fermi system, the analysis should be different from the previous chapters since the system is not at *equilibrium* state. In *nonequilibrium* many-body theory, the complete description of a system with a time-dependent Hamiltonian $\mathcal{H}(t)$ is given by the many-particle density matrix $\rho(t)$, which satisfies the Heisenberg equation of motion $i\partial_t\rho(t) = [\mathcal{H}(t), \rho(t)]$ with initial condition $\rho(t_0) = \rho_0$. The average value of any operator $\hat{O}$ can be calculated as follows:

$$\langle \hat{O}(t) \rangle = \frac{\text{Tr}\rho(t)\hat{O}}{\text{Tr}\rho(t)} = \frac{\text{Tr}\rho_0 \hat{\mathcal{U}}^\dagger(t-t_0)\hat{O}\hat{\mathcal{U}}(t_0,t)}{\text{Tr}\rho(t)}, \tag{4.7}$$

where

$$\hat{\mathcal{U}}(t_2,t_1) \equiv \hat{T}_c \exp\left[-i\int_{t_1}^{t_2} \mathcal{H}(t)dt\right] \tag{4.8}$$

is the evolution operator and $\hat{T}_c$ means chronological ordering. Calculation of these averages can be reformulated in a more compact way by introducing the generating functional [215]

$$\mathcal{Z}(t) = \text{Tr}\hat{\mathcal{U}}^\dagger(t,t_0) \exp\left[-\beta(\mathcal{H}(t_0) - \mu_\alpha N_\alpha)\right] \hat{\mathcal{U}}(t,t_0), \tag{4.9}$$

where $N_\alpha \equiv c_\alpha^\dagger c_\alpha$ is the number operator for fermions of type α, μ_α is the corresponding chemical potential, and $\beta = 1/T$. In order to get this expression, it is assumed that the trapping potential $U_{\text{ext}}(\mathbf{r},t)$ is independent of time for $t < t_0 = 0$, such that the initial condition of $\rho(t)$ corresponds to thermal equilibrium. This assumption is directly related to experiments where the traps are effectively static before the cloud release. Therefore, the generating functional at $t = t_0$ can be written as $\mathcal{Z}(t_0) = \text{Tr}\exp\left[-\beta(\mathcal{H}(t_0) - \mu_\alpha N_\alpha)\right]$.

By introducing a complex time τ, the generating functional Eq. (4.9) can be written as

$$\mathcal{Z}(t) = \int_{\text{BC}} \Pi_\alpha D[c_\alpha^\dagger, c_\alpha] \exp\left\{-[S_2(c_j^\dagger, c_j) + S_4(c_j^\dagger, c_j)]\right\}, \tag{4.10}$$

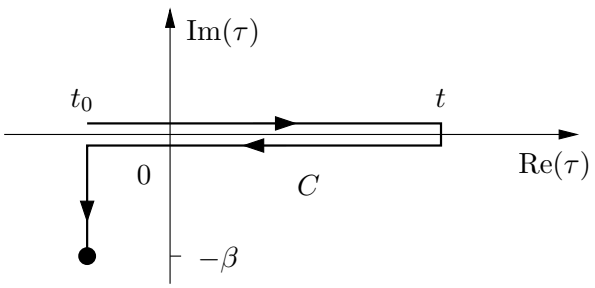

Figure 4.6: Integration contour C used in Eq. (4.11). Adapted from Ref. [204].

where the boundary condition (BC) of the functional integral is $c_\alpha(\mathbf{r}, t_0 - i/T) = -c_\alpha(\mathbf{r}, t_0)$. The quadratic term is

$$S_2(c_j^\dagger, c_j) = \int_C d\tau \int d\mathbf{r} c_\alpha^\dagger(\mathbf{r}, \tau) \hat{\mathcal{L}}_\alpha(\mathbf{r}, \tau) c_\alpha(\mathbf{r}, \tau), \tag{4.11}$$

where the integration contour C is shown in Fig. 4.6 [215], and the one-particle operator $\mathcal{L}_\alpha$ is defined as

$$\hat{\mathcal{L}}_\alpha(\mathbf{r}, \tau) = -i\partial_\tau - \frac{\nabla^2}{2m} + U_{\text{ext}}(\mathbf{r}, \tau) - \mu_\alpha. \tag{4.12}$$

The second term $S_4(c_j^\dagger, c_j)$ in the action of Eq. (4.10) corresponds to the contribution of interaction Hamiltonian in Eq. (4.5).

To derive the effective field theory and calculate the effective action of the system, one writes the interacting potential with weak spin-orbit coupling in the triplet channel as in Eq. (2.35),

$$V_{\alpha\beta\gamma\delta}(\boldsymbol{\rho}) = -V(\boldsymbol{\rho}) \mathbf{v}_{\alpha\beta} \cdot \left(\mathbf{v}^\dagger\right)_{\gamma\delta}, \tag{4.13}$$

where the spin matrices $(v_j)_{\alpha\beta} \equiv (i\sigma_j\sigma_y)_{\alpha\beta}$ and σ_j are Pauli matrices.

Next, the field $\mathbf{B}^\dagger(\mathbf{r}, \mathbf{r}', \tau) = c_\alpha^\dagger(\mathbf{r}, \tau) \mathbf{v}_{\alpha\beta} c_\beta^\dagger(\mathbf{r}', \tau)$ is introduced and the corresponding Hubbard–Stratonovich auxiliary field $\mathbf{d}(\mathbf{r}, \mathbf{r}', \tau)$ is used to integrate out the fermions. The vector nature of the order parameter $\mathbf{d}$ can be understood from the spin structure of the pair wave function Eq. (2.29) and its matrix representation Eq. (2.30). Therefore, the direction of $\mathbf{d}$ determines the amplitude of the pair wavefunction in each of the pseudospin triplet channels $|11\rangle$, $|12\rangle + |21\rangle$, and $|22\rangle$.

The quadratic part $S_{\text{eff}}^{(2)}$ of the effective action can be obtained from the corresponding

Feynman diagram similar to that in Fig. 3.9, leading to

$$S_{\text{eff}}^{(2)} = \frac{1}{2}\int_C d\tau d\tau' \int d\mathbf{r}_1 d\mathbf{r}_2 d\mathbf{r}_1' d\mathbf{r}_2' \Big[\mathbf{d}^\dagger(\mathbf{r}_1,\mathbf{r}_2,\tau)\cdot \mathbf{v}_{\alpha\beta}^\dagger K_{0,\alpha\beta}\mathbf{v}_{\beta\alpha}\cdot \mathbf{d}(\mathbf{r}_1',\mathbf{r}_2',\tau') + 2V(\mathbf{r}_1-\mathbf{r}_2)\delta_C(\tau-\tau')\delta(\mathbf{r}_1-\mathbf{r}_1')\delta(\mathbf{r}_2-\mathbf{r}_2')\mathbf{d}^\dagger(\mathbf{r}_1,\mathbf{r}_2,\tau)\cdot\mathbf{d}(\mathbf{r}_1',\mathbf{r}_2',\tau')\Big]. \quad (4.14)$$

The bare two-particle Green's function

$$K_{0,\alpha\beta}(\mathbf{r}_1,\mathbf{r}_2,\tau;\mathbf{r}_1',\mathbf{r}_2',\tau') = V(\mathbf{r}_1-\mathbf{r}_2)G_\alpha(\mathbf{r}_1,\tau;\mathbf{r}_1',\tau')G_\beta(\mathbf{r}_2,\tau;\mathbf{r}_2',\tau')V(\mathbf{r}_1'-\mathbf{r}_2'), \quad (4.15)$$

where, $\delta_C(\tau-\tau')$ is the delta function on the contour C. The fermionic Green's function $G_\alpha(\mathbf{r},\tau;\mathbf{r}',\tau')$ is defined as the inverse of the one-particle operator $\mathcal{L}_\alpha$ in Eq. (4.12),

$$\mathcal{L}_\alpha(\mathbf{r},\tau)G_\alpha(\mathbf{r},\tau;\mathbf{r}',\tau') = \delta(\mathbf{r}-\mathbf{r}')\delta_C(\tau-\tau'). \quad (4.16)$$

The quadratic effective action Eq. (4.14) can be simplified in the special case where the two fermionic hyperfine states are equally populated with $N_1 = N_2 = N$ and $\mu_1 = \mu_2 = \mu$. In such case, the fermionic Green's function $G_1 = G_2 = G$, and $K_{0,\alpha\beta}$ and $K_{\alpha\beta}$ are spin independent. Therefore, the trace of spin matrices can be performed separately leading to

$$S_{\text{eff}}^{(2)} = -\int_C d\tau d\tau' \int d\mathbf{r}_1 d\mathbf{r}_2 d\mathbf{r}_1' d\mathbf{r}_2' \mathbf{d}^\dagger(\mathbf{r}_1,\mathbf{r}_2,\tau)\cdot(K^{-1}-K^{-1}K_0K^{-1})\mathbf{d}(\mathbf{r}_1',\mathbf{r}_2',\tau'), \quad (4.17)$$

where the bare two-particle Green's function K_0 can be related to the full two-particle Green's function K via the Dyson's equation

$$K = K_0 - K_0\Sigma K = K_0 - K_0\Sigma K + K_0\Sigma K_0\Sigma K_0 - \cdots. \quad (4.18)$$

Here, the self energy Σ as the difference between the vertex function for the interacting and non-interacting systems is just the interaction $V(\boldsymbol{\rho})$. The full two-particle Green's function $K(\mathbf{r}_1,\mathbf{r}_2,\tau;\mathbf{r}_1',\mathbf{r}_2',\tau')$ can be found as a solution to the following equation:

$$\left[i\partial_\tau + \frac{\nabla_{\mathbf{r}_1}^2}{2m} + \frac{\nabla_{\mathbf{r}_2}^2}{2m} - U_{\text{ext}}(\mathbf{r}_1,\tau) - U_{\text{ext}}(\mathbf{r}_2,\tau) + V(\mathbf{r}_1-\mathbf{r}_2) + 2\mu\right]K = \delta(\mathbf{r}_1-\mathbf{r}_1')\delta(\mathbf{r}_2-\mathbf{r}_2')\delta_C(\tau-\tau'). \quad (4.19)$$

Since the external trapping potential U_{ext} is harmonic, the expression in square brackets in Eq. (4.19) can be rewritten as a function of the center-or-mass $\mathbf{R} = \mathbf{r}_1 + (\mathbf{r}_2)/2$ and the

relative $\boldsymbol{\rho} = \mathbf{r}_1 - \mathbf{r}_2$ coordinates, leading to

$$K^{-1} = i\partial_\tau + \frac{\nabla^2_{\mathbf{R}}}{4m} + \frac{\nabla^2_{\boldsymbol{\rho}}}{m} - U_{\text{ext}}(\mathbf{R}+\boldsymbol{\rho}/2,\tau) - U_{\text{ext}}(\mathbf{R}-\boldsymbol{\rho}/2,\tau) + V(\boldsymbol{\rho}) + 2\mu. \quad (4.20)$$

The simplified form of $S^{(2)}_{\text{eff}}$ in Eq. (4.17) can also be obtained in another case where only one hyperfine state is populated. In such a spin-polarized case, only one spin label α is relevant and the chemical potential in Eqs. (4.19) and (4.20) is $\mu = \mu_\alpha$.

Since the $\mathbf{d}$ field depends on two spatial variables $\mathbf{r}$ and $\mathbf{r}'$, it can also be transformed into center-of-mass $\mathbf{R}$ and relative $\boldsymbol{\rho}$ coordinates:

$$\mathbf{d}(\mathbf{r},\mathbf{r}',\tau) = \sum_{n,\ell,m_\ell} \mathbf{D}_{n,\ell,m_\ell}(\mathbf{R},\tau)\eta_{n,\ell,m_\ell}(\boldsymbol{\rho}). \quad (4.21)$$

Here, the expansion basis functions $\eta_{n,\ell,m_\ell}(\boldsymbol{\rho})$ are eigenfunctions of the reduced two-body Hamiltonian $\mathcal{H}_2 = -\nabla^2_\rho/m - V(\boldsymbol{\rho})$, satisfying

$$\left[-\frac{\nabla^2_{\boldsymbol{\rho}}}{m} - V(\boldsymbol{\rho})\right]\eta_{n,\ell,m_\ell}(\boldsymbol{\rho}) = -\varepsilon_{n,\ell,m_\ell}\eta_{n,\ell,m_\ell}(\boldsymbol{\rho}). \quad (4.22)$$

Therefore, substitution of the expansion Eq. (4.21) into Eq. (4.17) leads to

$$S^{(2)}_{\text{eff}} = -\int_C d\tau \sum_{qn,qn'} \int d\mathbf{R}\mathbf{D}^\dagger_{qn}(\mathbf{R},\tau)\cdot\langle\eta_{qn}|K^{-1} - K^{-1}K_0K^{-1}|\eta_{qn'}\rangle\mathbf{D}_{qn'}(\mathbf{R},\tau), \quad (4.23)$$

where the set of quantum numbers is $qn = \{n,\ell,m_\ell\}$ and $qn' = \{n',\ell',m'_\ell\}$.

From now on, I will concentrate on p-wave superfluids at the BEC side of FRs. For isotropic interaction potential $V(\boldsymbol{\rho})$, the lowest eigenvalue of the two-particle Schrodinger equation (4.22) for the p-wave channel is $-\varepsilon_{2,1,m_\ell}$, corresponding to the ground state with $n = 2$ and $\ell = 1$. This state is three-fold degenerate which are labeled by $m_\ell = -1, 0, 1$, with corresponding wave functions $Y_{1m_\ell}(\hat{\boldsymbol{\rho}})$. However, since the p-wave Feshbach resonances have finite separation between $m_\ell = 0$ and $m_\ell = \pm 1$ states [131, 134], the interaction potential $V(\boldsymbol{\rho})$ for different $|m_\ell|$ values can be tuned independently. Therefore, the three-fold degeneracy of the state ($n = 2$, $\ell = 1$) is broken, leading to a ground state with no degeneracy ($m_\ell = 0$) or with two-fold degeneracy ($m_\ell = \pm 1$). In the latter case ($m_\ell = \pm 1$), the ground state wave function can be any linear combination of $\eta_{2,1,1}$ and $\eta_{2,1,-1}$. In a superfluid, since all Cooper pairs are in a coherent state, then the internal degree of freedom

wave function of each pair takes a specific form $\eta_{2,1,\pm1} = c_1\eta_{2,1,1} + c_2\eta_{2,1,-1}$, where c_1 and c_2 are constants. Therefore, at low temperatures where the excited states contribution is negligible, the effective action Eq. (4.23) becomes

$$S_{\rm eff}^{(2)} \approx -\int_C d\tau \int d\mathbf{R}\mathbf{D}_{2,1,0}^{\dagger}(\mathbf{R},\tau)\cdot\langle\eta_{2,1,0}|K^{-1}-K^{-1}K_0K^{-1}|\eta_{2,1,0}\rangle\mathbf{D}_{2,1,0}(\mathbf{R},\tau) \quad (4.24)$$

when $(n=2,\ell=1,m_\ell=0)$ is the ground state, and

$$S_{\rm eff}^{(2)} \approx -\int_C d\tau \int d\mathbf{R}\mathbf{D}_{2,1,\pm1}^{\dagger}(\mathbf{R},\tau)\cdot\langle\eta_{2,1,\pm1}|K^{-1}-K^{-1}K_0K^{-1}|\eta_{2,1,\pm1}\rangle\mathbf{D}_{2,1,\pm1}(\mathbf{R},\tau) \quad (4.25)$$

when $(n=2,\ell=1,m_\ell=\pm1)$ is the ground state.

Using the explicit form of K^{-1} in Eq. (4.20) and Eq. (4.22), and the representation of spherical harmonics in terms of linear functions of the unit vector $\hat{\boldsymbol{\rho}}$

$$\begin{aligned} Y_{11}(\hat{\boldsymbol{\rho}}) &\sim \hat{\rho}_x + i\hat{\rho}_y, \\ Y_{10}(\hat{\boldsymbol{\rho}}) &\sim \hat{\rho}_z, \\ Y_{1-1}(\hat{\boldsymbol{\rho}}) &\sim \hat{\rho}_x - i\hat{\rho}_y, \end{aligned} \quad (4.26)$$

one obtains the matrix element

$$\langle\eta_{2,1,|m_\ell|}|K^{-1}|\eta_{2,1,|m_\ell|}\rangle = i\partial_\tau + \frac{\nabla_{\mathbf{R}}^2}{4m} - 2U_{\rm ext}(\mathbf{R},\tau) + 2\mu + \varepsilon_{2,1,|m_\ell|}. \quad (4.27)$$

In the derivation of Eq. (4.27), I use the fact that the wave function $\eta_{2,1,|m_\ell|}$ is localized on the length scale of a_0, satisfying the condition $a_0 \ll L$ where L is the characteristic length scale of the external trapping potential $U_{\rm ext}$.

The additional contribution of the type $\langle\eta_{2,1,|m_\ell|}|K^{-1}K_0K^{-1}|\eta_{2,1,|m_\ell|}\rangle$ describe corrections to Eq. (4.27). In the BEC regime, these terms are small since they contain a factor $K_0 \sim 1/|\mu| \sim 2/\varepsilon_{2,1,|m_\ell|}$, which is the smallest parameter of the theory. Therefore, the low energy contribution to the quadratic part of the effective action takes the form

$$S_{\rm eff}^{(2)} = -\int_C d\tau \int d\mathbf{R}\mathbf{D}^{\dagger}(\mathbf{R},\tau)\cdot\left[i\partial_\tau + \frac{\nabla_{\mathbf{R}}^2}{2M} - 2U_{\rm ext}(\mathbf{R},\tau) + \mu_B\right]\mathbf{D}(\mathbf{R},\tau), \quad (4.28)$$

where $\mu_B = 2\mu + \varepsilon_{2,1,|m_\ell|}$. In Eq. (4.28), I have dropped the subscript of $\mathbf{D}$ to simplify notation. Notice that the expression above has a similar form to the action of an ideal

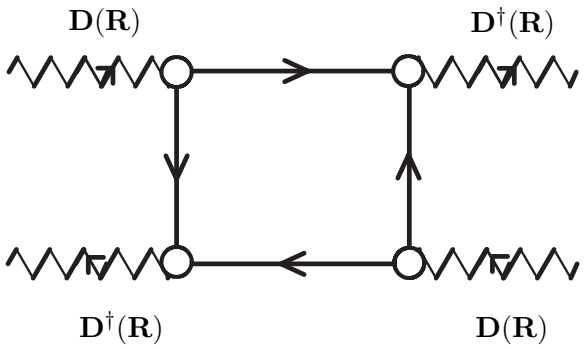

Figure 4.7: Diagrammatic representation of the fourth-order effective action in the strong coupling limit.

gas of vector Bose particles with the mass $M = 2m$ and the chemical potential μ_B in the presence of the effective time-dependent external potential $2U_{\rm ext}(\mathbf{R}, t)$.

The fourth-order term of the effective action can be obtained from a Feynman diagram similar to that of in Fig. 3.13(a). However, in the BEC regime, the diagram can be transformed into the form shown in Fig. 4.7. In this diagram, wavy lines represent the center-of-mass portion $\mathbf{D}(\mathbf{r}, t)$ of the bosonic field $\mathbf{d}(\mathbf{r}, \mathbf{r}', t)$, and the circles are boson-fermion vertices $\Omega_{qn,\alpha\beta}$ or $\Omega^\dagger_{qn,\alpha\beta}$, which depend only on the relative coordinate $\boldsymbol{\rho}$

$$\begin{aligned}\Omega_{\{2,1,|m_\ell|\},\alpha\beta}(\boldsymbol{\rho}) &= V(\boldsymbol{\rho})\eta_{2,1,|m_\ell|}(\boldsymbol{\rho})\mathbf{v}_{\alpha\beta} \\ &= \left[-\frac{\nabla^2_{\boldsymbol{\rho}}}{m} + \varepsilon_{2,1,|m_\ell|}\right]\eta_{2,1,|m_\ell|}(\boldsymbol{\rho})\mathbf{v}_{\alpha\beta}. \end{aligned} \tag{4.29}$$

The main contribution to the internal integrals in the diagram of Fig. 4.7 comes from the high energy region of the fermionic propagator [215]. Therefore, the effects of inhomogeneity and deviations from equilibrium of the bare fermionic Green's function G are irrelevant for the calculation of the quartic terms. To the leading order in the BEC regime the coefficients of the forth-order term coincide with those obtained in the equilibrium theory. By substituting the fermionic Green's functions G into the diagram of Fig. 4.7 and performing the spin labels trace and Matsubara summation, the forth-order term of effective action can be written as

$$S^{(4)}_{\rm eff} = \int dt \int d\mathbf{R}\left[g_0\left(\mathbf{D}^\dagger\cdot\mathbf{D}\right)^2 - \frac{g_0}{2}\left(\mathbf{D}^\dagger\cdot\mathbf{D}^\dagger\right)(\mathbf{D}\cdot\mathbf{D})\right], \tag{4.30}$$

where the coefficient g_0 represent the effective interaction of the $\mathbf{D}$ fields.

In conclusion, the effective action of triplet Fermi condensates in strongly coupling limit becomes

$$\begin{aligned} S_{\text{eff}} &= -\int_C d\tau \int d\mathbf{R}\mathbf{D}^\dagger(\mathbf{R},\tau)\cdot\left[\hat{\mathcal{K}}\mathbf{D}(\mathbf{R},\tau)\right] \\ &\quad \int dt \int d\mathbf{R}\frac{g_0}{2}\left[2|\mathbf{D}(\mathbf{R},t)|^4 - |\mathbf{D}^2(\mathbf{R},t)|^2\right], \end{aligned} \tag{4.31}$$

where the operator $\hat{\mathcal{K}} = i\partial_\tau - 2U_{\text{ext}}(\mathbf{R},\tau) + \nabla^2_{\mathbf{R}}/(4m)$ corresponds to the action of an ideal non-equilibrium gas of Bose particles with mass $M = 2m$.

4.3 Equation of Motion and Time Evolution of a Single Cloud

This action in Eq. (4.31) leads to the equation of motion

$$i\partial_t D_j = \left[-\frac{\nabla^2_{\mathbf{R}}}{2M} + 2U_{\text{ext}}(\mathbf{R},t) + 2g_0|\mathbf{D}|^2\right] D_j - g_0\left(\mathbf{D}\cdot\mathbf{D}\right) D_j^\dagger. \tag{4.32}$$

Notice that this expression is different from the time-dependent Gross-Pitaevskii (TDGP) equation for an atomic vector Bose system.

Equation (4.32) can be simplified to the TDGP form in two special cases. First, if the atomic hyperfine states $|1\rangle$ and $|2\rangle$ are equally populated with $N_1 = N_2 = N$ ($\mu_1 = \mu_2 = \mu$) and $\mathbf{D}$ is unitary, then $\mathbf{D}$ is a real vector with an overall phase, leading to the equation of motion

$$i\partial_t D_j = \left[-\frac{\nabla^2_{\mathbf{R}}}{2M} + 2U_{\text{ext}}(\mathbf{R},t) + g_0|\mathbf{D}|^2\right] D_j. \tag{4.33}$$

Second, if only one atomic hyperfine state is populated, then $\mathbf{D}$ is non-unitary and $\mathbf{D} = A(1,\pm i,0)$, where A is a complex constant. Thus, the last term $\mathbf{D}\cdot\mathbf{D}$ in Eq. (4.32) vanishes, and the equation of motion is identical to Eq. (4.33), with $g_0 \to 2g_0$. In the following lines, I will discuss only these two special cases.

For this purpose, a solution of the general equation of motion (4.33) is required. However, such a solution is not easy to obtain, due to the non-linear nature of this equation. To obtain an approximate solution to Eq. (4.33), I consider here a trapped gas at $t < 0$, where the trapping potential U_{ext} is time-independent with $\omega_j(t<0) = \omega_j$ =constants.

Thus, for $t < 0$, the system is in thermodynamic equilibrium state and can be described by

$$\mu_0 D_j(\mathbf{R}) = \left[-\frac{\nabla^2_{\mathbf{R}}}{2M} + 2U_{\rm ext}(\mathbf{R}) + g|\mathbf{D}(\mathbf{R})|^2 \right] D_j(\mathbf{R}), \tag{4.34}$$

where μ_0 is the effective boson chemical potential, and $g = g_0$ ($g = 2g_0$) when $\mathbf{D}$ is unitary (non-unitary). In the regime where the effective boson interactions are dominant, a Thomas–Fermi approximation is valid where the kinetic energy term is neglected, leading to

$$|\mathbf{D}(\mathbf{R},0)| = \begin{cases} g^{-1/2}[\mu_0 - 2U_{\rm ext}(\mathbf{R})]^{1/2}; & \text{for } \mu_0 \geq 2U_{\rm ext}(\mathbf{R}) \\ 0; & \text{otherwise.} \end{cases} \tag{4.35}$$

When this approximation fails the initial condition for the time evolution can be obtained by solving Eq. (4.34) numerically. However, the Thomas–Fermi approximation cannot be directly applied to the equation of motion (4.33), since the kinetic energy may not be negligible any more in a time dependent system. To treat the expansion of a cloud, Kagan, Surkov, and Shlyapnikov [194], as well as Castin and Dum [195] introduced a unitary transformation and a scaling process which approximately describe the time dependence for a scalar Bose system. Here, I generalize this method and apply it to triplet Fermi condensates in the BEC regime.

For $t > 0$, I introduce the transformation $R_j(t) = b_j(t)R_j(0)$, where the scaling factors $b_j(t)$ satisfy [194, 195]

$$\frac{d^2 b_j(t)}{dt^2} = \frac{\omega_j^2}{A(t)b_j(t)} \tag{4.36}$$

with $A(t) = b_x(t)b_y(t)b_z(t)$ and initial conditions $b_j(0) = 1$. The three coupled equations for $b_j(t)$ are ordinary differential equations hence can be solved numerically by standard methods.

First, I consider a dilute Fermi gas trapped in an isotropic harmonic potential with $\omega_x(t) = \omega_y(t) = \omega_z(t) = \omega(t)$. In this case the equations for b_j reduce to,

$$\frac{d^2 b(t)}{dt^2} = -\omega^2(t)b(t) + \frac{\omega^2(0)}{b^4(t)}. \tag{4.37}$$

Consider a sudden change of trapping potential at $t = 0$, i.e., $\omega(t < 0) = \omega$ and $\omega(t > 0) = \omega'$ are constants, the equation above can be solved numerically. The results for different values

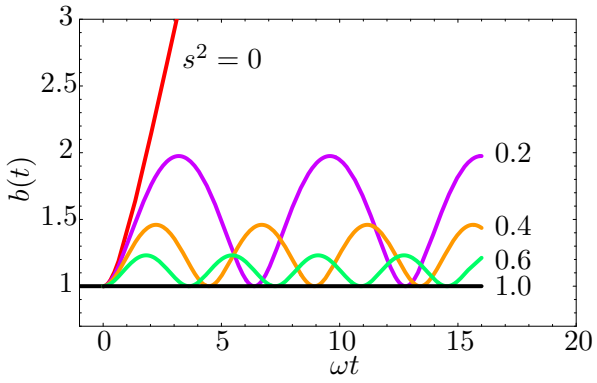

Figure 4.8: Time evolution of scaling factor $b(t)$ for a sudden change of isotropic harmonic potential at $t = 0$. Cases with different values of $s \equiv \omega'/\omega$ are considered. The $s = 0$ case corresponds to a complete shut-down of the potential, and $s = 1$ indicates no change is applied.

of $s \equiv \omega'/\omega$ are shown in Fig. 4.8. Notice that for the special case where the trapping potential is completely shut down at $t = 0$ (i.e., $s = \omega'/\omega = 0$), the scaling factor $b(t)$ behaves almost linearly when $\omega t > 1$. Since the experimental value for ω is about several kHz, we can approximate $b(t) = 1 + a\omega t$ whenever $t > 1$ ms, where a is a dimensionless constant. Consider that observations in most experiments [201, 202] are usually taken at around 10-100 ms after shutting down the potential, thus such approximation is valid. A numerical calculation gives the value of $a \approx 0.8165$.

Another important case is that of an axially symmetric trapping potential with respect to the z axis and with $\omega_\perp(t) \equiv \omega_x(t) = \omega_y(t) \gg \omega_z(t)$. The equipotential surface of this trap is cigar shaped with the longest axis being z. In this case Eq. (4.36) becomes

$$\frac{d^2 b_\perp(t)}{dt^2} = -\omega_\perp^2(t) b_\perp(t) + \frac{\omega_\perp^2(0)}{b_\perp^3(t) b_z(t)}, \tag{4.38}$$

$$\frac{d^2 b_z(t)}{dt^2} = -\omega_z^2(t) b_z(t) + \frac{\omega_z^2(0)}{b_\perp^2(t) b_z^2(t)}, \tag{4.39}$$

where $b_\perp \equiv b_x = b_y$. For a sudden change of the trapping potential from ω_j for $t < 0$ to ω_j' for $t > 0$, a numerical solution can also be obtained. In Fig. 4.9, I show the solutions of $b_\perp$ and b_z as a function of dimensionless time $\tau = \omega_\perp t$, with $\epsilon = \omega_z/\omega_\perp = 0.1$, and $\omega_\perp' = \omega_z' = 0$. Notice that when τ is large, both $b_\perp$ and b_z depend linearly on τ, with $b_\perp \approx 1 + a_\perp \tau$ and $b_z \approx 1 + a_z \tau$. The coefficients $a_\perp \approx 0.9944 > a_z \approx 0.01492$ indicates that the cloud expands

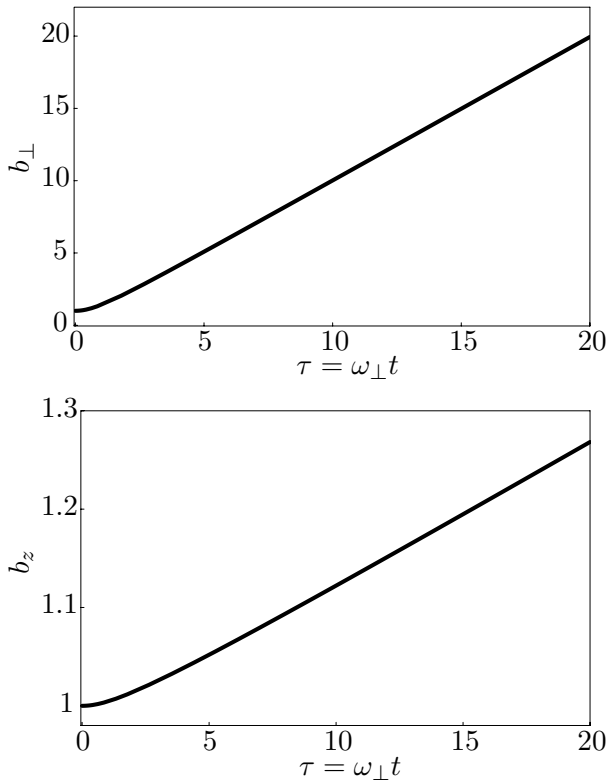

Figure 4.9: Time evolution of scaling factors $b_\perp$ and b_z for a sudden change of a cigar-shaped anisotropic potential starting at $t = 0$. Parameters used in these figures are $\omega_j' = 0$ (complete shut-down), and $\epsilon = \omega_z/\omega_\perp = 0.1$.

faster along the radial direction in comparison with the axial direction. The aspect ratio of the cloud $r_{xz} = L_\perp/L_z = \epsilon b_\perp/b_z$ as a function of τ is shown in Fig. 4.10, where $L_\perp$ and L_z are the cloud lengths along the radial and axial directions, respectively. Notice that r_{xz} increases from 0.1 to 6.665, indicating that the cloud changes from cigar-shape to disk-shape. It should be emphasized that this anisotropy inversion is a direct consequence of the anisotropy of trapping potential. From a classical point of view, particles tend to move faster along the radial directions upon release from the trap, because the cloud is strongly confined along the radial direction. This effect presents in Bose [92] and s-wave Fermi [199] condensates.

In addition to numerical solutions, an approximated analytic solutions can also be obtained as a power expansion of $\epsilon = \omega_z/\omega_\perp$ for the specific case of $\omega_j' = 0$, which corresponds

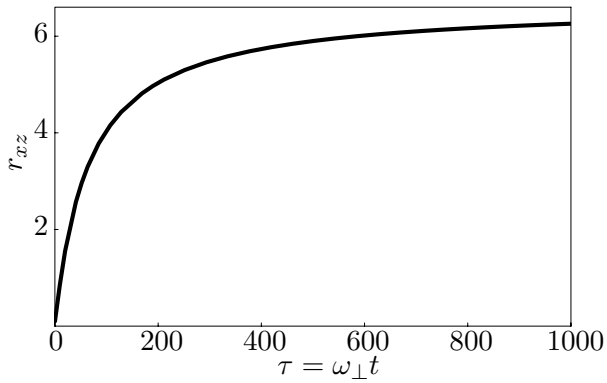

Figure 4.10: Time dependence of the aspect ratio $r_{xz} = L_\perp/L_z$. Parameters used in this plot are same as in Fig. 4.9.

to a complete shut-down of the trapping potential. The scaling coefficients are

$$b_\perp(t) = (1+\tau^2)^{1/2}, \tag{4.40}$$

$$b_z(t) = 1 + \epsilon^2\Big[\tau\tan^{-1}(\tau) - \frac{1}{2}\ln(1+\tau^2)\Big] + \mathcal{O}(\epsilon^4), \tag{4.41}$$

which are in agreement with Castin and Dum [195]. Therefore, for this cigar-shaped trapping potential, $D_j(\mathbf{R},t)$ becomes

$$D_j(\mathbf{R},t) = \frac{\exp[i\theta(\mathbf{R},t)]}{\sqrt{1+\omega_\perp^2 t^2}} D_j(\overline{\mathbf{R}},0), \tag{4.42}$$

where $\overline{R}_k = R_k/b_k(t)$ are scaled coordinates, and the phase factor is

$$\begin{aligned}\theta(t) \approx & -\frac{\tan^{-1}(\tau)}{\omega_\perp\tau}\mu + M\frac{\omega_\perp\tau}{1+\tau^2}(R_x^2+R_y^2) \\ & + \frac{\epsilon^2\mu}{\omega_\perp}\theta_{02}(\tau) + \epsilon^2 M\left[\omega_\perp\tan^{-1}(\tau)\right]R_z^2.\end{aligned} \tag{4.43}$$

Here

$$\theta_{02}(\tau) = \int_0^\tau \frac{2\tau_1\tan^{-1}(\tau_1) - \ln(1+\tau_1^2)}{2(1+\tau_1^2)} d\tau_1. \tag{4.44}$$

Notice that $\theta_{02} \sim \ln\tau$ as $t\to\infty$, hence the third term in Eq. (4.43) becomes comparable to the first one when $t\ln(\tau) \sim \epsilon^2$. Since the experimental parameters $\epsilon \sim 10^{-2}$, $\omega_\perp \sim 10^3$ Hz, this condition is satisfied only when $t \sim 10^2$ s, which is several orders of magnitude larger than any time scales in experiments [201, 202]. Therefore, I neglect the θ_{02} term in the following discussions.

4.4 Matter-wave Interference and Polarization Effect

Next, I consider the matter-wave interference of two spatially separated condensates such that the energy barrier between them is large enough to neglect the tunneling effect. For these two condensates, the number of particles in each trap is fixed. Thus, one may write down the total wave function naively as a product Fock state as

$$\Phi_{\rm tot}(\mathbf{R},t) \propto \Phi_{\rm L}(\mathbf{R},t)\Phi_{\rm R}(\mathbf{R},t).$$

However, a direct application of this wave function to explain experimental results for s-wave Fermi and Bose systems does not work. This disagreement originates from the fact that condensates are pure coherent states, and that two condensates are not coherent in an ensemble average, but couple for each trial. Therefore, any single-run interference of these two-cloud systems need to be described by a coherent superposition wave function

$$\Phi_{\rm tot}(\mathbf{R},t) = \Phi_{\rm L}(\mathbf{R},t) + \Phi_{\rm R}(\mathbf{R},t), \tag{4.45}$$

which in the p-wave case can be written in terms of the $\mathbf{D}$ vector as $\Phi_{\rm P} \propto i\sum_j D_{j,{\rm P}}\sigma_j\sigma_y$, denoting the pair wave function of Fermi condensates in the left [P = L(+)] or right [R(−)] traps. The trap centers lie at $(\mp W/2, 0, 0)$ where W is the distance between traps.

Now I consider the case of two identical axially symmetric Fermi condensates with $\omega_\perp \gg \omega_z$. In this case, the time evolution of each cloud is described by Eq. (4.42):

$$D_{j,{\rm P}}(\mathbf{R},t) = \frac{\exp[i\theta(\mathbf{R}\pm W\hat{\mathbf{x}}/2,t)]}{\sqrt{1+\tau^2}} D_{j,{\rm P}}(\overline{\mathbf{R}\pm W\hat{\mathbf{x}}/2},0),$$

Thus, for a single run of the experiment, the particle density $n(\mathbf{R},t) \equiv |\Phi_{\rm tot}(\mathbf{R},t)|^2$ is

$$\begin{aligned} n(\mathbf{R},t) \quad \propto \quad & \mathbf{D}_{\rm L}^\dagger(\mathbf{R},t)\cdot\mathbf{D}_{\rm L}(\mathbf{R},t) + \mathbf{D}_{\rm R}^\dagger(\mathbf{R},t)\mathbf{D}_{\rm R}(\mathbf{R},t) \\ & + 2{\rm Re}\frac{\mathbf{D}_{\rm L}^\dagger(\overline{\mathbf{R}+W\hat{\mathbf{x}}/2},0)\cdot\mathbf{D}_{\rm R}(\overline{\mathbf{R}-W\hat{\mathbf{x}}/2},0)e^{i\chi}}{A(\tau)}, \end{aligned} \tag{4.46}$$

where the phase $\chi(\mathbf{R},t) = \theta(\mathbf{R}+W\hat{\mathbf{x}}/2,t) - \theta(\mathbf{R}-W\hat{\mathbf{x}}/2,t) + \chi_0$, and χ_0 is the initial relative phase of the two clouds.

When each cloud has only one hyperfine state occupied (e.g. $\Psi_{\rm pair} = h_{11}|11\rangle$) the $\mathbf{D}$ vectors in each cloud have the fixed form $A(1,i,0)$ and fringes are present in all experimental

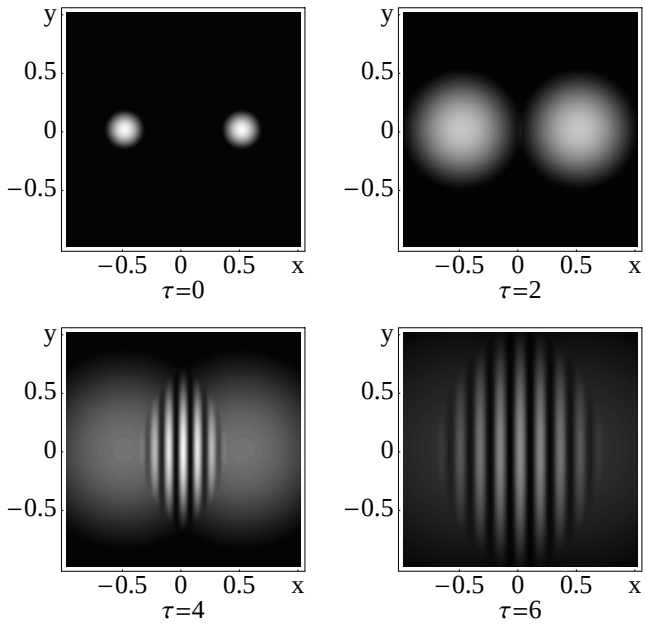

Figure 4.11: Interference pattern versus dimensionless time $\tau = \omega_\perp t$ for p-wave Fermi condensates in the BEC limit with $\omega_z/\omega_x = 0.1$, assuming $|\mathbf{D}_{\rm L}^\dagger \cdot \mathbf{D}_{\rm R}|$ is maximal. The plots include only the superfluid part, and show columnar density versus x, y coordinates in units of the initial clouds separation W. The patterns are similar to those of atomic scalar bosons, and s-wave paired Fermions.

realizations. This result is similar to the s-wave case where the order parameter is a complex scalar. However, when both Fermi condensates are in unitary states, $\mathbf{D}$ is essentially a real vector with an overall phase, and $n(\mathbf{R}, t)$ shows an angular dependence controlled by the dot product in Eq. (4.46). When the two order parameters are parallel, this term is maximal and the interference pattern is most visible (Fig. 4.11). But if the $\mathbf{D}$ vectors are perpendicular, fringes are absent at all times (Fig. 4.12). Therefore, in the unitary case the existence and intensity of interference fringes are very sensitive to the relative orientation of the $\mathbf{D}$ vectors.

Since the interference pattern depends crucially on $\mathbf{D}_{\rm L}$ and $\mathbf{D}_{\rm R}$, it is important to understand how these vectors can be controlled experimentally. Recall that experimental results for p-wave Feshbach resonances (FR) show a finite separation in different channels [133] implying different interactions in "spin" space. Therefore, one can tune the interaction in a specific channel to control the $\mathbf{D}$ vector to a certain degree. For example, a set of p-wave

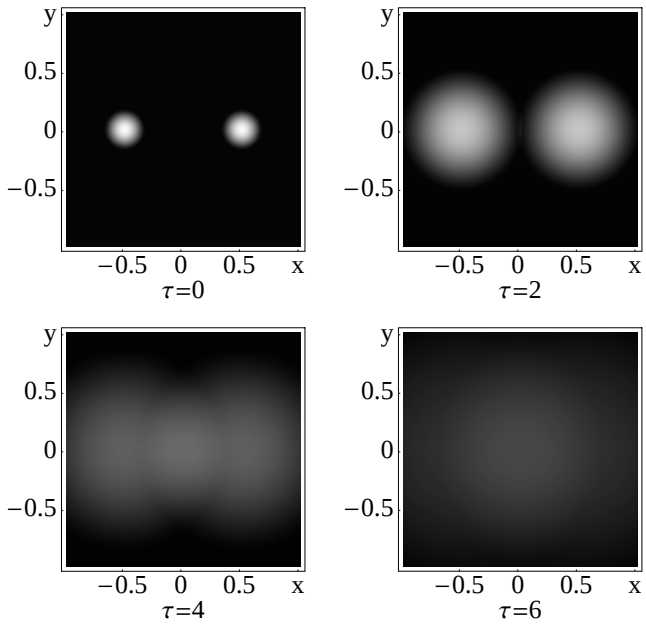

Figure 4.12: Interference pattern versus dimensionless time $\lambda = \omega_\perp t$ for p-wave Fermi condensates in the BEC limit with $\omega_z/\omega_x = 0.1$, assuming $|\mathbf{D}_{\rm L}^\dagger \cdot \mathbf{D}_{\rm R}| = 0$. The plots include only the superfluid part, and show columnar density versus x, y coordinates in units of the initial clouds separation W.

FRs for ^{6}Li occur at 159 G (width 0.4 G), 185G (width 0.2 G) and 215 G (width 0.4 G) for the $|11\rangle$, $|12\rangle$ (or $|21\rangle$), and $|22\rangle$ channels, respectively. By applying a constant plus a gradient magnetic field, one can in principle tune the local field at the left (L) cloud to be 216 G, and at right (R) cloud to be 214 G, which are above and below the $|22\rangle$ resonance, respectively. Thus, a sweep down of the constant magnetic field part by 30G makes the L cloud cross the $|22\rangle$ but not the $|12\rangle$ resonance, while it makes the R cloud cross only the $|12\rangle$ resonance. In this case, the L cloud is in the BEC regime of the $|22\rangle$ channel, with $\Psi_{\rm pair,L} \approx h_{22,\rm L}|22\rangle$ or $\mathbf{D}_{\rm L} = h_{22,\rm L}(1/2, -i/2, 0)$. However, the R cloud is in the BEC regime of the $|12\rangle$ channel, with $\Psi_{\rm pair,R} \approx h_{12,\rm R}(|12\rangle + |21\rangle)$ or $\mathbf{D}_{\rm R} = h_{12,\rm R}(0, 0, 1)$. Therefore, $\mathbf{D}_{\rm L}^\dagger \cdot \mathbf{D}_{\rm R} = 0$ and the interference pattern is that of Fig. 4.12. More generally, however, the preparation of pair wave functions (or $\mathbf{D}$-vectors) in each cloud can be controlled by tuning the constant and gradient magnetic fields, as well as the separation between the two clouds.

The polarization effect also manifests itself in the Josephson tunneling between the two traps. By considering a tunneling process across the energy barrier, the left and right

condensates can be described by the modified equation of motion

$$\begin{aligned} i\partial_t D_{\mathrm{L},j} &= \left[-\frac{\nabla^2_{\mathbf{R}}}{2M} + 2U_{\mathrm{ext}}(\mathbf{R}) + g|\mathbf{D}_{\mathrm{L}}|^2\right] D_{\mathrm{L},j} \\ &\quad + \sum_k \int d\mathbf{R}' T_{kj}(\mathbf{R},\mathbf{R}') D_{\mathrm{R},j}(\mathbf{R}'), \qquad (4.47a) \\ i\partial_t D_{\mathrm{R},j} &= \left[-\frac{\nabla^2_{\mathbf{R}}}{2M} + 2U_{\mathrm{ext}}(\mathbf{R}) + g|\mathbf{D}_{\mathrm{R}}|^2\right] D_{\mathrm{R},j} \\ &\quad + \sum_k \int d\mathbf{R}' T^*_{jk}(\mathbf{R},\mathbf{R}') D_{\mathrm{L},j}(\mathbf{R}'), \qquad (4.47b) \end{aligned}$$

where $T_{jk}(\mathbf{R},\mathbf{R}') \equiv T_c + T_s$ is the tunneling matrix, with T_c and T_s are the "spin"-conserving and non-conserving portions, respectively. In the case where the trapping potential is much smaller than the energy difference between the two hyperfine states, or the time scale of experiments is much shorter than the lifetime of each hyperfine state, the non-conserving tunneling process is negligible, leading to $T_{jk} = T(\mathbf{R},\mathbf{R}')\delta_{jk}$.

Multiplying Eq. (4.47a) by $D^\dagger_{\mathrm{L},j}$ and subtracting the Hermitian conjugate, one obtains

$$\begin{aligned} i\partial_t |D_{\mathrm{L},j}(\mathbf{R})|^2 &= \frac{1}{2}\Bigg[\int d\mathbf{R}' T(\mathbf{R},\mathbf{R}') D^\dagger_{\mathrm{L},j}(\mathbf{R}) D_{\mathrm{R},j}(\mathbf{R}') \\ &\quad - D^\dagger_{\mathrm{L},j}(\mathbf{R}) \frac{\nabla^2_{\mathbf{R}}}{2M} D_{\mathrm{L},j}(\mathbf{R})\Bigg] - \mathrm{H.C.} \qquad (4.48) \end{aligned}$$

After summing over j and integrating over the spatial coordinate $\mathbf{R}$ in the left half space $LS = \{\mathbf{R} : R_x < 0\}$, the left hand side of Eq. (4.48) is proportional to the derivative of number of particles in the left trap. An application of the divergence theorem to the spatial gradient terms,

$$\partial_t n_{\mathrm{L}} = \mathrm{Im} \int_{LS} d\mathbf{R} \int d\mathbf{R}' T(\mathbf{R},\mathbf{R}') \mathbf{D}^\dagger_{\mathrm{L}}(\mathbf{R}) \cdot \mathbf{D}_{\mathrm{R}}(\mathbf{R}'). \qquad (4.49)$$

Therefore, if $\mathbf{D}^\dagger_{\mathrm{L}}(\mathbf{R}) \cdot \mathbf{D}_{\mathrm{R}}(\mathbf{R}') = 0$ for all $\mathbf{R}$ and $\mathbf{R}'$, there is no Josephson tunneling between the two condensates.

4.5 Anisotropic Free Expansion

Up to now, I discuss p-wave Fermi condensates trapped in a harmonic potential only in the BEC limit. In this limit, fermions form tightly bounded molecules with the average pair size much smaller than the inter-molecular spacing. Thus, the internal degrees of freedom

of the fermion pairs are not important, and have negligible effects on physical properties of the condensates. However, if one moves away from the BEC limit, the average pair size increases with decreasing interaction strength, and the detailed structure of fermion pairs can dramatically change the condensate properties when the pair size becomes comparable to the inter-molecular spacing.

Next, I discuss corrections to the expansion of a harmonically trapped p-wave Fermi condensate when one moves away from the BEC limit, but remains on the BEC side of the Feshbach resonance. In such case, the method used in Section. 4.2 to derive the effective action (4.31) is not directly applicable, since the internal-degree-of-freedom wave function $\eta_{0,1,|m_\ell|}(\boldsymbol{\rho})$ is no longer localized within a small volume. However, if the trapping potential $U_{\rm ext}$ varies slowly in comparison with other length scales including the coherence length and the average pair size, a semiclassical approximation can be applied. Within this approximation, one can first derive the effective action in a free space (without trapping potential), and add the potential afterwards. Again, I consider here only "spin"-polarized systems consisting of fermions in a single hyperfine state, and unitary cases where fermions in two hyperfine states are equally populated.

For such a system, the quadratic term of the effective action takes the form [216]

$$S^{(2)}_{\rm eff} = -\int dt \int d\mathbf{R} \mathbf{D}^\dagger_{m_\ell}(\mathbf{R},t) \cdot \left[a_{m_\ell} - \sum_{ij} c^{ij}_{m_\ell} \frac{\nabla_i \nabla_j}{4m} + 2U_{\rm ext}(\mathbf{R}) + i d_{m_\ell} \partial_t \right] \mathbf{D}_{m_\ell}(\mathbf{R},t), \tag{4.50}$$

where it is assumed that only one of the spherical harmonics Y_{1,m_ℓ} is dominant and characterizes the order parameter. The coefficients a, c^{ij}, and d in Eq. (4.50) can be obtained by considering the free space problem and transforming it into momentum space [217]. It should be emphasized that the coefficient c^{ij} is in general anisotropic, taking the form

$$c^{ij}_{m_\ell} = \sum_{\mathbf{k}} \left\{ \left[\frac{X(\mathbf{k})}{4E^2(\mathbf{k})} - \frac{\beta Y(\mathbf{k})}{16 E(\mathbf{k})} \right] \delta_{ij} + \kappa^{ij}_{m_\ell} \frac{\beta^2 \mathbf{k}^2 X(\mathbf{k}) Y(\mathbf{k})}{32 m E(\mathbf{k})} \right\} \phi^2(k), \tag{4.51}$$

where $E(\mathbf{k}) = \xi_{1,\mathbf{k}} + \xi_{2,\mathbf{k}}$, $\xi_{\alpha,\mathbf{k}} = \mathbf{k}^2/2m - \mu_\alpha$, $X(\mathbf{k}) = \tanh(\beta\xi_{1,\mathbf{k}}/2) + \tanh(\beta\xi_{2,\mathbf{k}}/2)$, and $Y(\mathbf{k}) = \mathrm{sech}^2(\beta\xi_{1,\mathbf{k}}/2) + \mathrm{sech}^2(\beta\xi_{2,\mathbf{k}}/2)$. The symmetry function $\phi(k)$ is defined as in Section 2, by $V(\mathbf{k},\mathbf{k}') = \int d\mathbf{x} V(\mathbf{x}) \exp[i(\mathbf{k}-\mathbf{k}')\cdot\mathbf{x}] = V\phi(k)\phi(k') Y_{1,m_\ell}(\hat{\mathbf{k}}) Y^*_{1,m'_\ell}(\hat{\mathbf{k}}')$, and the

angular average is

$$\kappa_{m_\ell}^{ij} = \int d\hat{\mathbf{k}} \hat{k}_i \hat{k}_j Y_{1,m_\ell}(\hat{\mathbf{k}}) Y_{1,m_\ell}^*(\hat{\mathbf{k}}) = \kappa_{m_\ell}^{ii} \delta_{ij}. \tag{4.52}$$

For the case where $m_\ell = 0$, this angular average is anisotropic with $\kappa_0^{yy} = \kappa_0^{zz} = 1/10$, and $\kappa_0^{xx} = 3/5$. Here, I choose the x direction to be the quantization axis. Therefore, the coefficient c_0^{ij} (which is directly related to the Ginzburg-Landau coherence length ξ_{ij}) is anisotropic, thus acquiring a mass anisotropy $M_{ij} = 2m/c_0^{ij}$. This mass anisotropy reflects the higher angular momentum (p-wave) nature of the order parameter for paired fermions, and it is absent for s-wave Fermi and atomic Bose condensates.

This effective mass anisotropy has a non-trivial influence on the time evolution of condensates after release from the trap. As an example, I consider a p-wave Fermi condensate in an axially symmetric trap where $\omega_x = \omega_y \gg \omega_z$, with a magnetic field applied along $\hat{\mathbf{x}}$ (chosen as the quantization axis) to tune through the Feshbach resonance (see Fig. 4.13). Since the resonances for different m_ℓ states are split in ^{40}K [131, 134], it may be possible to adjust the magnetic field such that fermions are paired in the $m_\ell = 0$ (p_x) state only. In this case, the p-wave interaction leads to the formation of p_x symmetry pairs, which are more strongly correlated along the x direction ($\xi_x > \xi_y = \xi_z$ or $M_x < M_y = M_z$). Thus, in the xy plane the cloud expands faster along the x-direction corresponding to the lighter effective mass M_x, hence breaking the axial symmetry. This anisotropic expansion due to p-wave interactions also occurs for a completely isotropic trap, and it is very different from the anisotropy inversion (in the xz and yz planes) found in axially symmetric traps for s-wave Fermi condensates [199]. As discussed in Section 4.3, the anisotropy inversion is related only to the anisotropy of the trapping potential, while the anisotropic expansion discussed here is due to anisotropic interactions.

In Fig. 4.14, I show the cloud anisotropy ratio $r_{xy} = L_x/L_y$ as a function of the effective mass anisotropy ratio $r_M = M_y/M_x = \xi_x^2/\xi_y^2$. The anisotropy effect disappears in the BEC limit, as the effective masses become isotropic, however towards unitarity the anisotropic expansion become more evident. The values of r_M change as a function of the scattering volume a_p, and vary from $r_M = 1$ in the BEC limit ($a_p \to 0^+$), to $r_M = 3$ in the BCS limit ($a_p \to 0^-$). Since our theory is valid only on the BEC side where the fermion chemical

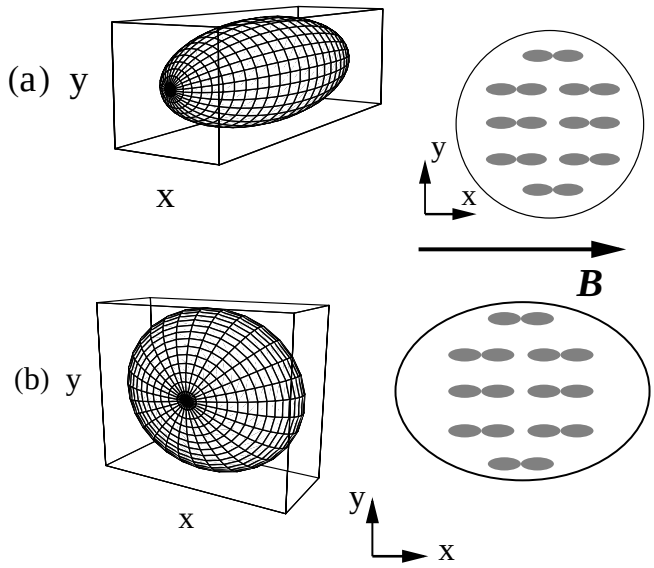

Figure 4.13: p-wave Fermi condensate of p_x-symmetry ($m_\ell = 0$) (a) in an axially symmetric trap and (b) upon release from trap. Notice that the axial symmetry is lost in the xy plane due to the anisotropic effective mass (interaction).

potential $\mu < 0$, the maximal theoretical anisotropy is reached near $\mu = 0$ (which is also close to the unitarity limit $a_p \to \pm\infty$ [140]), leading to a 10% anisotropy ($r_M \approx 1.1$) for trapped ^{40}K in the p_x-state ($m_\ell = 0$). Investigations on the BCS side ($\mu > 0$) and near unitarity require the inclusion of Landau damping which leads to the decay of Cooper pairs, and are beyond the scope of the present theory [218].

4.6 Summary

In conclusion, I considered in this chapter a Fermi condensate consisting of fermions in two hyperfine states with p-wave interactions, and derived the equation of motion in a vector boson representation near the BEC limit. For the spin-polarized case where the superfluid consists of fermions in one single hyperfine state, and the unitary case where two hyperfine states are equally populated, the equation of motion can be simplified and have a similar form to the time dependent Gross-Pitaevskii (TDGP) equation for vector atomic Bose systems. Within the two special cases, I described the time evolution of the vector order parameter approximately by scaling the spatial coordinate, and found that p-wave Fermi condensates behave very differently from s-wave Fermi condensates in the following

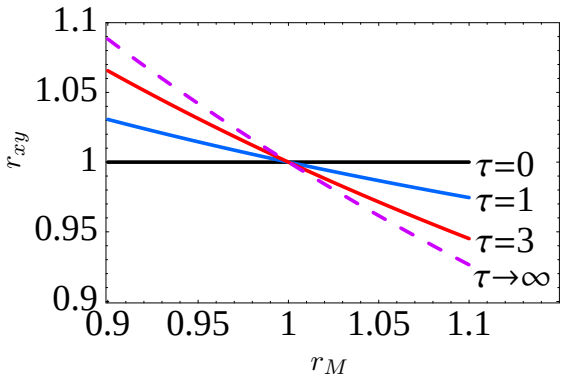

Figure 4.14: Cloud anisotropy ratio $r_{xy} = L_x/L_y$ as a function of effective mass anisotropy ratio $r_M = M_x/M_y$ at time τ (Solid lines). Dashed line indicate the saturated behavior at $\tau \to \infty$.

aspects:

1. The quantum interference of two p-wave Fermi condensates has an angular effect due to the vector nature of the order parameter. When the dot product of the vector order parameters of the left and right condensates reaches its maximum, the interference pattern is most visible; while the dot product of vector order parameters is zero, the interference pattern disappears. This effect is absent in the BEC limit of s-wave Fermi superfluids, as well as in scalar Bose systems. It was also proposed that the relative orientation of order parameters of two condensates can be controlled to a certain degree by applying a constant plus a gradient magnetic field to cross different Feshbach resonances.

2. Furthermore, towards unitarity, an anisotropic p-wave interaction leads to anisotropic effective masses for a given orbital symmetry. As a result, for a cigar-shaped cloud with axial symmetry, the cloud expansion becomes anisotropic in the axial plane and expands more rapidly along the direction of the smaller effective mass. Thus, the orbital symmetry of the order parameter for p-wave condensates can be directly probed through cloud expansions. This anisotropic expansion is a direct consequence of the anisotropic interaction, hence it is present only in p-wave (and higher angular momentum) Fermi condensates, but not in s-wave Fermi and vector or scalar Bose systems.

CHAPTER V

CONCLUSIONS AND FUTURE TOPICS

In this thesis, I discussed triplet superfluidity in quasi-one-dimensional organic conductors and ultra-cold Fermi gases, and focus on the p-wave case with total angular momentum $L = 1$. Triplet superfluidity is different from the singlet s-wave version in the following aspects: First, the order parameter is a complex vector; Second, the interaction between fermions is in general anisotropic. These two distinctions lead to very different physics in triplet superfluidity as presented in Chapters 3 and 4.

In Chapter 3, I discussed the interplay between triplet superconductivity (TSC) and spin density waves (SDW) in quasi-one-dimensional organic conductors. For a specific material $(TMTSF)_2PF_6$, I proposed a coexistence region of TSC and SDW at low temperatures, such that the critical point is tetracritical. Within this coexistence region, both the TSC and SDW order parameters are non-uniform, having out-of-phase modulations of charge and spin. Furthermore, since the TSC and SDW orders respond differently to a uniform magnetic field, the superconducting state in the coexistence region has an anomalous magnetic field effect. For instance, a sufficiently strong magnetic field pointing along the crystallographic $\mathbf{b}'$ axis may cause a canting transition of the SDW order parameter from the $\mathbf{b}'$ axis to the $\mathbf{a}$-$\mathbf{c}^*$ plane. This canting transition of the SDW order parameter also causes a flop transition of the TSC order parameter, hence it has a non-trivial effect on the superconducting state. In particular, I proposed new magnetic-field versus temperature phase diagrams at fixed pressure, below and above the critical pressure. This anomalous magnetic field effect on the superconducting state is absent in systems having singlet superconductivity.

In Chapter 4, I studied the time evolution and matter-wave interference of p-wave Fermi condensates in the Bose-Einstein condensation (BEC) regime. For a spin-polarized system consisting of fermions in one hyperfine state, and for the unitary case where two hyperfine states are equally populated, the Fermi condensates can be described by an equation of

motion which is similar to the time dependent Gross-Pitaevskii equation for a vector Bose condensate. By solving this equation of motion, I showed that the matter-wave interference of two p-wave Fermi condensates has a polarization effect due to the vector nature of the order parameter. Furthermore, away from the BEC limit towards unitarity, I observed that anisotropic p-wave interactions lead to anisotropic effective masses for a given orbital symmetry. As a consequence, for a cigar-shaped cloud with axial symmetry, the cloud expansion becomes anisotropic in the radial plane and expands more rapidly along the direction of the smaller effective mass. Both these effects are absent in the BEC limit of s-wave Fermi superfluids, as well as in scalar atomic Bose systems.

In the reminder of this chapter I discuss some future topics which I would like to investigate.

- *Upper critical fields of* $(TMTSF)_2PF_6$.

In $(TMTSF)_2PF_6$, the flopping of the TSC order parameter in the coexistence region is proposed by applying a magnetic field pointing along $\mathbf{b}'$ axis. Then it is expected that this flopping transition may change the upper critical field H_{c_2} for $\mathbf{H} \parallel \mathbf{b}'$. A complete understanding of this effect may help us explain the experimental data obtained by Lee *et al.* [41], where an anomalous anisotropy inversion for $H_{c_2}^{\mathbf{a}}$ and $H_{c_2}^{\mathbf{b}'}$ is found in $(TMTSF)_2PF_6$. I expect that this anisotropy inversion is related to the interplay between TSC and SDW orders, since the experiment is done at a pressure of 6 kbar, which is close the SDW phase.

- *Critical phenomena at the tetracritical point.*

In this thesis, I discussed the competition or coexistence of TSC and SDW order parameters in quasi-one-dimensional superconductors within a saddle point approximation. A renormalization group analysis of the Ginzburg–Landau–Wilson functional is necessary to obtain the critical exponents of various thermodynamical properties, and to determine the universality class of the coupled SDW/TSC quasi-one-dimensional system.

- *What is the time evolution of p-wave Fermi condensates at unitarity and the weakly interacting regime?*

The discussion regarding p-wave Fermi condensates in this thesis is confined to the BEC

side of the Feshbach resonances. Thus, the dynamics during free expansion is not strongly affected by collisions, when the density drops and the scattering volume for p-wave is small. Thus, the theory to holds well on the BEC side away from unitarity. However, collisions during free expansion may become important at unitarity where the scattering length are extremely large due to the resonances, and can blur the interference pattern as in Bose systems [218].

Furthermore, the time evolution of p-wave Fermi condensates at the BCS side of the Feshbach resonances is also an interesting problem. It is known that in the BCS regime, the system has Landau damping and large Cooper pairs can decay into two fermions. Therefore, the condensate may lose coherence during the free expansion and the interference pattern could be blurred.

- *What is the effect of population imbalance?*

In Chapter 4, I discussed only the spin-polarized and equally-populated Fermi gases. A more general case is a Fermi gas with population imbalance with $N_1 \neq N_2$ and $\mu_1 \neq \mu_2$, as has been discussed for s-wave Fermi condensates [219, 220, 221, 222]. For p-wave Fermi condensates, the effective action and equation of motion derived in Chapter 4 is no longer valid in a system with population imbalance. Therefore, one has to take into account the chemical potential difference for two hyperfine states, and derive the full theory.

APPENDIX A

SUMMATION OVER SPIN INDICES

Throughout this thesis, a summation over spin indices is often encountered to derive effective action from the corresponding diagrams. The summation takes the form

$$P_{\mathbf{s}} = \sum_{\alpha\beta\gamma\delta} \left[\boldsymbol{\phi}^{\dagger} \cdot \left(\mathbf{s}^{\dagger} \right)_{\alpha\beta} \right] \left[\boldsymbol{\phi} \cdot \mathbf{s}_{\gamma\delta} \right] \delta_{\alpha\delta} \delta_{\beta\gamma} \tag{A.1}$$

for quadratic terms in effective action, where $\mathbf{s}_{\alpha\beta} = \boldsymbol{\sigma}_{\alpha\beta}$ when $\boldsymbol{\phi}$ corresponds to a SDW order parameter $\mathbf{N}$ or a magnetic field $\mathbf{H}$, and $\mathbf{s}_{\alpha\beta} = \mathbf{v}_{\alpha\beta}$ when $\boldsymbol{\phi}$ corresponds to a TSC order parameter $\mathbf{D}$. In this chapter, I perform the summation in Eq. (A.1). The summation for quartic terms have a similar form with four spin matrices, and can be performed using the same method.

First, I discuss the case where $\mathbf{s} = \boldsymbol{\sigma}$. Recall the definition of Pauli matrices ($i = x, y, z$):

$$(\sigma_i) \equiv \begin{pmatrix} \eta_{i,2} & \eta_{i,3} \\ \eta_{i,1} & -\eta_{i,2} \end{pmatrix}, \tag{A.2}$$

where

$$\begin{aligned} \eta_{i,1} &= \delta_{i,x} + i\delta_{i,y}, \\ \eta_{i,2} &= \delta_{i,z}, \\ \eta_{i,3} &= \delta_{i,x} - i\delta_{i,y}. \end{aligned} \tag{A.3}$$

Thus, the dot products in equation (A.1) can be written out explicitly as

$$\begin{aligned} P_{\boldsymbol{\sigma}} &= \sum_{i,j} \phi_i^{\dagger} \phi_j \sum_{\alpha\beta\gamma\delta} (\sigma_i)_{\alpha\beta} (\sigma_j)_{\gamma\delta} \delta_{\alpha\delta} \delta_{\beta\gamma} \\ &= \sum_{i,j} \phi_i^{\dagger} \phi_j \mathrm{Tr} \left[\begin{pmatrix} \eta_{i,2} & \eta_{i,3} \\ \eta_{i,1} & -\eta_{i,2} \end{pmatrix} \begin{pmatrix} \eta_{j,2} & \eta_{j,3} \\ \eta_{j,1} & -\eta_{j,2} \end{pmatrix} \right]. \end{aligned} \tag{A.4}$$

Notice that the trace of the two spin matrices product in Eq. (A.4) is

$$\begin{aligned}
&\mathrm{Tr}\begin{pmatrix} \eta_{i,2}\eta_{j,2}+\eta_{i,3}\eta_{j,1} & \eta_{i,2}\eta_{j,3}-\eta_{i,3}\eta_{j,2} \\ \eta_{i,1}\eta_{j,2}-\eta_{i,2}\eta_{j,1} & \eta_{i,1}\eta_{j,3}+\eta_{i,2}\eta_{j,2} \end{pmatrix} \\
&\quad = 2\eta_{i,2}\eta_{j,2}+\eta_{i,3}\eta_{j,1}+\eta_{i,1}\eta_{j,3} \\
&\quad = 2\delta_{i,x}\delta_{j,x}+2\delta_{i,y}\delta_{j,y}+2\delta_{i,z}\delta_{j,z}=2\delta_{i,j}. \qquad \text{(A.5)}
\end{aligned}$$

Therefore, equation (A.4) becomes $S = 2\sum_{i,j}\phi_i^\dagger\phi_j\delta_{i,j} = 2\boldsymbol{\phi}^\dagger\cdot\boldsymbol{\phi}$, hence acquires the dot product form.

For the case where $\mathbf{s}_{\alpha\beta} = \mathbf{v}_{\alpha\beta}$, the summation (A.1) becomes

$$\begin{aligned}
P_{\mathbf{v}} &= \sum_{i,j}\phi_i^\dagger\phi_j\sum_{\alpha\beta\gamma\delta}(\sigma_y\sigma_i)_{\alpha\beta}(\sigma_j\sigma_y)_{\gamma\delta}\,\delta_{\alpha\delta}\delta_{\beta\gamma} \\
&= \sum_{i,j}\phi_i^\dagger\phi_j\mathbf{Tr}\left[\begin{pmatrix} 0 & -i \\ i & 0 \end{pmatrix}\begin{pmatrix} \eta_{i,2} & \eta_{i,3} \\ \eta_{i,1} & -\eta_{i,2} \end{pmatrix}\begin{pmatrix} \eta_{j,2} & \eta_{j,3} \\ \eta_{j,1} & -\eta_{j,2} \end{pmatrix}\begin{pmatrix} 0 & -i \\ i & 0 \end{pmatrix}\right] \\
&= \sum_{i,j}\phi_i^\dagger\phi_j\mathbf{Tr}\left[\begin{pmatrix} -i\eta_{i,1} & i\eta_{i,2} \\ i\eta_{i,2} & i\eta_{i,3} \end{pmatrix}\begin{pmatrix} i\eta_{j,3} & -i\eta_{i,2} \\ -i\eta_{i,2} & -i\eta_{i,1} \end{pmatrix}\right] \\
&= \sum_{i,j}\phi_i^\dagger\phi_j\mathbf{Tr}\begin{pmatrix} \eta_{i,1}\eta_{j,3}+\eta_{i,2}\eta_{i,2} & -\eta_{i,1}\eta_{i,2}+\eta_{i,2}\eta_{i,1} \\ -\eta_{i,2}\eta_{j,3}+\eta_{i,3}\eta_{i,2} & \eta_{i,2}\eta_{i,2}+\eta_{i,3}\eta_{i,1} \end{pmatrix} \\
&= 2\sum_{i,j}\phi_i^\dagger\phi_j\delta_{ij} = 2\boldsymbol{\phi}^\dagger\cdot\boldsymbol{\phi}, \qquad \text{(A.6)}
\end{aligned}$$

hence also has the dot product structure.

APPENDIX B

MATSUBARA FREQUENCY SUMMATION

In addition to the summation over spin indices, one also needs to perform the summation over Matsubara frequency ω_n, which takes the quadratic form

$$A_2 = \sum_{\omega_n} \frac{1}{i\omega_n + pE_1} \frac{1}{i\omega_n + qE_2}, \quad \text{with } p, q = \pm 1; \tag{B.1}$$

or the quartic form

$$A_4 = \sum_{\omega_n} \frac{1}{i\omega_n + pE_1} \frac{1}{i\omega_n + qE_2} \frac{1}{i\omega_n + rE_3} \frac{1}{i\omega_n + sE_4}, \quad \text{with } p, q, r, s = \pm 1. \tag{B.2}$$

Since the summation comes from products of bare fermionic Green's functions, the frequencies ω_n must be Fermi frequencies $\omega_n = (2n+1\pi)/\beta$. Next, I will calculate the second order summation A_2, and use its result to calculate A_4.

In principle, an infinite summation $\sum_{\omega_n} h(\omega_n)$ can be performed using the residue theorem:

$$\lim_{R\to\infty} \oint_{C_R} dz h(z) f(z) = 2\pi i \sum \text{Res}\left[h(z) f(z)\right], \tag{B.3}$$

with an appropriately chosen function $f(z)$ such that ω_n coincide with the singularities of $f(z)$ enclosed by the contour C_R. For the present problem, $h(z) = (z + pE_1)^{-1}(z + qE_2)^{-1}$, and the function $f(z)$ is the Fermi function

$$f(z) = \frac{1}{e^{\beta z} + 1}, \tag{B.4}$$

with singularities at $z_n = i\omega_n$. In addition, the summation on the right hand side of Eq. (B.3) includes two additional singularities of function $h(z)$

$$w_1 = -pE_1 \quad \text{and} \quad w_2 = -qE_2. \tag{B.5}$$

The contour integral Eq. (B.3) vanishes as $R \to \infty$ since $h(z) \approx 1/z^2$ for $|z| \to \infty$.

Therefore, one obtains

$$\begin{aligned} 0 &= \sum \mathrm{Res}\left[h(z)f(z)\right] \\ &= \sum_{i\omega_n} h(i\omega_n)\mathrm{Res}[f(z)]_{i\omega_n} + f(w_1)\mathrm{Res}[h(z)]_{w_1} + f(w_2)\mathrm{Res}[h(z)]_{w_2}. \end{aligned} \tag{B.6}$$

The residue of $h(z)$ at w_1 and w_2 are

$$\mathrm{Res}[h(z)]_{w_1} = \frac{1}{qE_2 - pE_1}, \tag{B.7a}$$

$$\mathrm{Res}[h(z)]_{w_2} = \frac{1}{pE_1 - qE_2}. \tag{B.7b}$$

The residue of $f(z)$ at $i\omega_n$ can be obtained by expanding the denominator of $f(z)$ as

$$\exp(\beta z) + 1 \approx -\beta(z - i\omega_n) + \cdots, \tag{B.8}$$

hence $\mathrm{Res}[f(z)]_{i\omega_n} = -1/\beta$ is a constant.

Substituting Eqs. (B.7) and (B.8) into the residue theorem Eq. (B.6), one obtains

$$\begin{aligned} A_2 &= \sum_{i\omega_n} h(i\omega_n) = \beta\left[\frac{f(-pE_1)}{qE_2 - pE_1} + \frac{f(-qE_2)}{pE_1 - qE_2}\right] \\ &= \frac{\beta}{qE_2 - pE_1}\left[f(qE_2) - f(pE_1)\right] \\ &= \frac{\beta}{2(qE_2 - pE_1)}\left[\tanh\left(\frac{\beta pE_1}{2}\right) - \tanh\left(\frac{\beta qE_2}{2}\right)\right]. \end{aligned} \tag{B.9}$$

Notice that the following identities are used to write the frequency sum A_2 into the expression above:

$$f(-E) = 1 - f(E) \tag{B.10}$$

$$f(E) = \frac{1}{2}\left[1 - \tanh\left(\frac{\beta E}{2}\right)\right], \tag{B.11}$$

In the limiting case where $qE_2 \to pE_1$, one can expand the hyperbolic tangent function in Eq. (B.9) and obtain

$$A_2(qE_2 \to pE_1) = -\frac{\beta^2}{4}\mathrm{sech}^2\left(\frac{\beta pE_1}{2}\right). \tag{B.12}$$

Next, I will use the result for A_2 to derive the fourth-order summation A_4 in Eq. (B.2).

Notice that

$$
\begin{aligned}
A_4 &= \sum_{\omega_n} \frac{1}{i\omega_n + pE_1} \frac{1}{i\omega_n + qE_2} \frac{1}{i\omega_n + rE_3} \frac{1}{i\omega_n + sE_4} \\
&= \sum_{\omega_n} \frac{1}{qE_2 - pE_1} \left[\frac{1}{i\omega_n + pE_1} - \frac{1}{i\omega_n + qE_2} \right] \frac{1}{sE_4 - rE_3} \left[\frac{1}{i\omega_n + rE_3} - \frac{1}{i\omega_n + sE_4} \right] \\
&= \frac{1}{(qE_2 - pE_1)(sE_4 - rE_3)} \sum_{\omega_n} \left[\frac{1}{i\omega_n + pE_1} \frac{1}{i\omega_n + rE_3} \right. \\
&\quad \left. - \frac{1}{i\omega_n + qE_2} \frac{1}{i\omega_n + rE_3} - \frac{1}{i\omega_n + pE_1} \frac{1}{i\omega_n + sE_4} + \frac{1}{i\omega_n + qE_2} \frac{1}{i\omega_n + sE_4} \right]. \quad \text{(B.13)}
\end{aligned}
$$

Each term in the square bracket of Eq. (B.13) has the same form as A_2, hence the Matsubara summation can be performed using the previous result Eq. (B.9). As discussed before, limiting cases such as $qE_2 \to pE_1$ or $sE_4 \to rE_3$ need to be considered by expanding the results into Taylor series and collecting the highest order terms.

REFERENCES

[1] P. Kapitza, "Viscosity of liquid helium below the lambda-point", *Nature* **141**, 74 (1938).

[2] J. F. Allen and A. D. Misener, "Flow of liquid helium II", *Nature* **141**, 75 (1938).

[3] F. London, "The λ-phenomenon of liquid helium and the Bose-Einstein degeneracy", *Nature* **141**, 643 (1938).

[4] S. N. Bose, "Planck's Gesetz und Lichtquantenhypothese", *Z. Phys.* **26**, 178 (1924).

[5] A. Einstein, "Quantentheorie des einatomigen idealen gases", *Sitz. Ber. Preuss. Akad. Wiss. (Berlin)* **22**, 261 (1924).

[6] L. Tisza, "Transport phenomena in Helium II", *Nature* **141**, 913 (1938).

[7] L. Landau, "The theory of superfluidity of Helium II", *J. Phys. (USSR)* **5**, 71 (1941).

[8] N. N. Bogoliubov, "On the theory of superfluidity", *J. Phys. (USSR)* **11**, 23 (1947).

[9] R. P. Feynman and M. Cohen, "Energy spectrum of the excitations in liquid Helium", *Phys. Rev.* **102**, 1189 (1956).

[10] R. P. Feynman, "Application of quantum mechanics to liquid helium", in *Progress in Low Temperature Physics*, edited by C. J. Gorter, Vol. 1, (North-Holland, Amsterdam 1955).

[11] D. D. Oscheroff, R. C. Richardson, and D. M. Lee, "Evidence for a new phase of solid He^3", *Phys. Rev. Lett.* **28**, 885 (1972).

[12] D. D. Oscheroff, W. J. Gully, R. C. Richardson, and D. M. Lee, "New magnetic phenomena in liquid He^3 below 3 mK", *Phys. Rev. Lett.* **29**, 920 (1972).

[13] F. London, *Superfluidity*, Vol. 1 &2, (John Wiley, New York, 1950).

[14] J. Bardeen, L. Cooper, and J. Schrieffer, "Theory of superconductivity", *Phys. Rev.* **108**, 1175 (1957).

[15] N. N. Bogoliubov, "A new method in the theory of superconductivity", *Sov. Phys. JETP* **7**, 41 (1958).

[16] G. R. Stewart, "Heavy-fermion Systems", *Rev. Mod. Phys.* **56**, 755 (1984).

[17] R. Joynt and L. Taillefer, "The superconductivity phases of UPt_3", *Rev. Mod. Phys.* **74**, 235 (2002).

[18] A. P. Mackenzie and Y. Maeno, "The superconductivity of Sr_2RuO_4 and the physics of spin-triplet pairing", *Rev. Mod. Phys.* **75**, 657 (2003).

[19] D. Jérome, A. Mazaud, M. Ribault, and K. Bechgaard, "Superconductivity in a synthetic organic conductor $(TMTSF)_2PF_6$", *J. Phys. (Paris) Lett.* **41**, L95 (1980).

[20] M. Y. Choi, P. M. Chaikin, S. Z. Huang, P. Haen, E. M. Engler, and R. L. Greene, "Effect of radiation damage on the metal-insulator transition and low-temperature transport in the tetramethyltetraselenofulvalinium PF_6 salt $[(TMTSF)_2PF_6]$", *Phys. Rev. B* **25**, 6208 (1982).

[21] R. L. Greene, P. Haen, S. Z. Huang, E. M. Engler, M. Y. Choi, and P. M. Chaikin, "Some properties of the $(TMTSF)_2X$ superconductors", *Mol. Cryst. Liq. Cryst.* **79**, 183 (1982).

[22] S. Bouffard, M. Ribault, R. Brusetti, D. Jérome, and K. Bechgaard, "Low-temperature metallic state and superconductivity in quasi-one-dimensional organic conductors: pressure and irradiation investigations", *J. Phys. C: Solid State Phys.* **15**, 2951 (1982).

[23] S. Tomic, D. Jérome, D. Mailly, M. Ribault, and K. Bechgaard, "Influence of the disorder potential of the anions on the ground state of the organic alloy $(TMTSF)_2(ClO_4)_{1-x}(ReO_4)_x$", *J. Phys. (Paris) Colloq.* **44**, C3 1075 (1983).

[24] C. Coulon, P. Delhaes, J. Amiell, J. P. Manceau, J. M. Fabre, and L. Giral, "Effect of doping $(TMTSF)_2ClO_4$ with TMTTF I. Ambient pressure results: a competition between the different possible ground state", *J. Phys. (Paris)* **43**, 1721 (1983).

[25] A. A. Abrikosov, "Superconductivity in a quasi-one-dimensional metal with impurities", *J. Low Temp. Phys.* **53**, 359 (1983).

[26] L. P. Gorkov and D. Jérome, "Back to the problem of the upper critical fields in organic superconductors", *J. Phys. (Paris) Lett.* **46**, L643 (1985).

[27] R. Brusetti, M. Ribault, D. Jérome, and K. Bechgaard, "Insulating, conducting and superconducting states $(TMTSF)_2ASF_6$ under pressure and magnetid-field", *J. Phys. (Paris)* **43**, 801 (1982).

[28] T. Ishiguro, K. Kajimura, H. Bando, K. Murata, and H. Anzai, "Electronic state of $(TMTSF)_2CLO_4$ in metallic region", *Mol. Cryst. Liq. Cryst.* **119**, 19 (1985).

[29] A. M. Clogston, "Upper limit for the field in hard superconductors", *Phys. Rev. Lett.* **9**, 266 (1962).

[30] B. S. Chandrasekhar, "A note on the maximum critical field of high-field superconductors", *Appl. Phys. Lett.* **1**, 7 (1962).

[31] M. Takigawa, H. Yasuoka, and G. Saito, "Proton spin relaxation in the superconducting state of (TMTSF)2Cl04", *J. Phys. Soc. Jpn.* **56**, 873 (1987).

[32] L. C. Hebel and C. P. Slichter, "Nuclear spin relaxation in normal and superconducting aluminum", *Phys. Rev.* **113**, 1504 (1959).

[33] Y. Hasegawa and H. Fukuyama, "NMR relaxation-time of the anisotropic superconducting state in quasi-one-dimensional systems", *J. Phys. Soc. Jpn.* **56**, 877 (1987).

[34] A. G. Lebed, "Reversible nature of the orbital mechanism for the suppression of superconductivity", *JETP Lett.* **44**, 114 (1986).

[35] L. I. Burlachkov, L. P. Gorkov, and A. G. Lebed, "Identification of the superconductivity type in organic superconductors", *Europhys. Lett.* **4**, 941 (1987).

[36] N. Dupuis, G. Montambaux, and C. A. R. Sá de Melo, "Quasi-one-dimensional superconductors in strong magnetic field", *Phys. Rev. Lett.* **70**, 2613 (1993).

[37] N. Dupuis, "Thermodynamics and excitation spectrum of a quasi-one-dimensional superconductor in a high magnetic field", *Phys. Rev. B* **50**, 9607 (1994).

[38] C. A. R. Sá de Melo, "Paramagnetism and reentrant behavior in quasi-one-dimensional superconductors at high magnetic fields", *Physica C* **260**, 224 (1996).

[39] I. J. Lee, A. P. Hope, M. J. Leone, and M. J. Naughton, "Revisiting the superconducting phase diagram of(TMTSF)2ClO4", *Synth. Metals* **70**, 747 (1995).

[40] O. Fischer, H. W. Meul, M. G. Karkut, G. Remenyi, U. Welp, J. C. Piccoche, and K. Maki, "Antivortex paramagnetism in the magnetic-field-induced superconducting state of $Eu_xSn_{1-x}Mo_6S_8$", *Phys. Rev. Lett.* **55**, 2972 (1985).

[41] I. J. Lee, M. J. Naughton, G. M. Danner, and P. M. Chaikin, "Anisotropy of the Upper Critical Field in $(TMTSF)_2PF_6$", *Phys. Rev. Lett.* **78**, 3555 (1997).

[42] S. Belin and K. Behnia, "Thermal conductivity of superconducting $(TMTSF)_2ClO_4$: Evidence for a nodeless gap", *Phys. Rev. Lett.* **79**, 2125 (1997).

[43] R. A. Klemm, A. Luther, and M. R. Beasley, "Theory of the upper critical field in layered superconductors", *Phys. Rev. B* **12**, 877 (1975).

[44] R. V. Coleman, G. K. Eiserman, S. J. Hillenius, A. T. Mitchell, and J. L. Vicent, "Dimensional crossover in the superconducting intercalated layer compound 2H-TaS_2", *Phys. Rev. B* **27**, 125 (1983).

[45] G. Danner, W. Kang, and P. M. Chaikin, "Measuring the Fermi surface of quasi-one-dimensional metals", *Phys. Rev. Lett.* **72**, 3714 (1994).

[46] M. Tinkham, *Introduction to Superconductivity*, second ed. (McGraw-Hill, New York, 1996).

[47] N. Dupuis and G. Montambaux, "Superconductivity of quasi-one-dimensional conductors in a high magnetic field", *Phys. Rev. B* **49**, 8993 (1994).

[48] A. I. Larkin and Y. N. Ovchinikov, "Inhomogeneous state of superconducts (Production of superconducting state in ferromagnet with Fermi surfaces, examining Green function)", *Sov. Phys. JETP* **20**, 762 (1965).

[49] P. Fulde and R. A. Ferrell, "Superconductivity in a strong spin-exchange superconductors", *Phys. Rev.* **135**, A550 (1964).

[50] A. G. Lebed, "Revival of superconductivity in high magnetic fields and a possible p-wave pairing in $(TMTSF)_2PF_6$", *Phys. Rev. B* **59**, R721 (1999).

[51] I. J. Lee, D. S. Chow, W. G. Clark, M. J. Strouse, M. J. Naughton, P. M. Chaikin, and S. E. Brown, "Evidence from ^{77}Se Knight Shift for triplet superconductivity in $(TMTSF)_2PF_6$", *Phys. Rev. B* **68**, 092510 (2003).

[52] A. G. Lebed, K. Machida, and M. Ozaki, "Triplet electron pairing and anisotropic spin susceptibility in organic superconductors $(TMTSF)_2X$", *Phys. Rev. B* **62**, R795 (2000).

[53] R. D. Duncan, C. D. Vaccarella, and C. A. R. Sá de Melo, "Organic quasi-one-dimensional superconductors: Quasiparticle density of states and spin susceptibility", *Phys. Rev. B* **64**, 172503 (2001).

[54] R. D. Duncan, R. W. Cherng, and C. A. R. Sá de Melo, "Organic quasi-one-dimensional superconductors: quasiparticle density of states and spin susceptibility", *Physica C* **391**, 98 (2003).

[55] I. J. Lee and M. J. Naughton, "Metallic state in $(TMTSF)_2PF_6$ at low pressure", *Phys. Rev. B* **58**, R13343 (1998).

[56] X. Huang and K. Maki, "Upper critical field of organic superconductors", *Phys. Rev. B* **39**, 6459 (1989).

[57] K. Kuroki, R. Arita, and H. Aoki, "Spin-triplet f-wave-like pairing proposed for an organic superconductor $(TMTSF)_2PF_6$", *Phys. Rev. B* **63**, 094509 (2001).

[58] H. Shimahara, "Nodeless d-wave superconductivity in a quasi-one-dimensional organic superconductor under anion order", *Phys. Rev. B* **61**, R14936 (2000).

[59] D. A. Wollman, D. J. Van Harlingen, W. C. Lee, D. M. Ginsberg, and A. J. Leggett, "Experimental determination of the superconducting pairing state in YBCO from the phase coherence of YBCO-Pb dc SQUIDs", *Phys. Rev. Lett.* **71**, 2134 (1993).

[60] D. A. Brawer and H. R. Ott, "Evidence for an unconventional superconducting order parameter in $YBa_2Cu_3O_{6.9}$", *Phys. Rev. B* **50**, 6530 (1994).

[61] A. Mathai, Y. Gim, R. C. Black, A. Amar, and F. C. Wellstood, "Experimental proof of a time-reversal-invariant order parameter with a π shift in $YBa_2Cu_3O_{7-\delta}$", *Phys. Rev. Lett.* **74**, 4523 (1995).

[62] K. Sengupta, I. Zutic, H.-J. Kwon, V. M. Yakovenko, and S. Das Sarma, "Midgap edge states and pairing symmetry of quasi-one-dimensional organic superconductors", *Phys. Rev. B* **63**, 144531 (2001).

[63] C. D. Vaccarella, R. D. Duncan, and C. A. R. Sá de Melo, "Triplet superconductors: Josephson effect in quasi-one-dimensional systems", *Physica C* **391**, 89 (2003).

[64] H. I. Ha, J. I. Oh, J. Moser, and M. J. Naughton, "Zero bias conductance peak in an SNS weak link bicrystal of the triplet superconductor $(TMTSF)_2ClO_4$", *Synth. Metals* **137**, 1215 (2003).

[65] I. J. Lee, S. E. Brown, W. G. Clark, M. J. Strouse, M. J. Naughton, W. Kang, and P. M. Chaikin, "Triplet superconductivity in an organic superconductor probed by NMR Knight shift", *Phys. Rev. Lett.* **88**, 017004 (2002).

[66] L. J. Azevedo, J. E. Schirber, and E. M. Engler, "^{77}Se nuclear magnetic resonance in di-tetramethyltetraselenafulvalene phosphorous hexafluoride [$(TMTSF)_2PF_6$] under pressure", *Phys. Rev. B* **27**, 5842 (1983).

[67] I. J. Lee, P. M. Chaikin, and M. J. Naughton, "Critical field enhancement near a superconductor-insulator transition", *Phys. Rev. Lett.* **88**, 207002 (2002).

[68] T. Vuletić, P. Auban-Senzier, C. Pasquier, S. Tomić, D. Jérome, M. Héritier, and K. Bechgaard, "Coexistence of superconductivity and spin density wave orderings in the organic superconductor $(TMTSF)_2PF_6$", *Eur. Phys. J. B* **25**, 319 (2002).

[69] A. V. Kornilov, V. M. Pudalov, Y. Kitaoka, K. Ishida, G. q. Zheng, T. Mito, and J. S. Qualls, "Macroscopically inhomogeneous state at the boundary between the superconducting, antiferromagnetic, and metallic phases in quasi-one-dimensional $(TMTSF)_2PF_6$", *Phys. Rev. B* **69**, 224404 (2004).

[70] I. J. Lee, S. E. Brown, W. Yu, M. J. Naughton, and P. M. Chaikin, "Coexistence of superconductivity and antiferromagnetism probed by simultaneous nuclear magnetic resonance and electrical transport in $(TMTSF)_2PF_6$ system", *Phys. Rev. Lett.* **94**, 197001 (2005).

[71] D. Podolsky, E. Altman, T. Rostunov, and E. Demler, "SO(4) theory of antiferromagnetism and superconductivity in Bechgaard salts", *Phys. Rev. Lett.* **93**, 246402 (2004).

[72] W. Zhang and C. A. R. Sá de Melo, "Coexistence of antiferromagnetism and triplet superconductivity", *J. Appl. Phys.* **95**, 10B108 (2005).

[73] W. Zhang and C. A. R. Sá de Melo, "Coexistence of triplet superconductivity and spin density waves", *Phys. Rev. Lett.* **97**, 047001 (2006).

[74] A. J. Leggett, "A theoretical description of the new phases of liquid ^{3}He", *Rev. Mod. Phys.* **47**, 331 (1975).

[75] M. H. Anderson, J. R. Ensher, M. R. Matthews, C. E. Wieman, and E. A. Cornell, "Observation of Bose-Einstein condensation in a dilute atomic vapor", *Science* **269**, 198 (1995).

[76] K. B. Davis, M. O. Mewes, M. R. Andrews, N. J. van Druten, D. S. Durfee, D. M. Kurn, and W. Ketterle, "Bose-Einstein condensation in a gas of sodium atoms", *Phys. Rev. Lett.* **75**, 3969 (1995).

[77] D. G. Fried, T. C. Killian, L. Willmann, D. Landhuis, S. C. Moss, D. Kleppner, and T. J. Greytak, "Bose-Einstein condensation of atomic hydrogen", *Phys. Rev. Lett.* **81**, 3811 (1998).

[78] M. Greiner, C. A. Regal, and D. S. Jin, "Emergence of a molecular Bose-Einstein condensate from a Fermi gas", *Nature* **426**, 537 (2003).

[79] S. Jochim, M. Bartenstein, A. Altmeyer, G. Hendl, S. Riedl, C. Chin, J. Hecker Denschlag, and R. Grimm, "Bose-Einstein condensation of molecules", *Science* **302**, 2101 (2003).

[80] M. W. Zwierlein, C. A. Stan, C. H. Schunck, S. M. F. Raupach, S. Gupta, Z. Hadzibabic, and W. Ketterle, "Observation of Bose-Einstein condensation of molecules", *Phys. Rev. Lett.* **91**, 250401 (2003).

[81] T. Bourdel, L. Khaykovich, J. Cubizolles, J. Zhang, F. Chevy, M. Teichmann, L. Tarruell, S. J. J. M. F. Kokkelmans, and C. Salomon, "Experimental study of the BEC-BCS crossover region in Lithium 6", *Phys. Rev. Lett.* **93**, 050401 (2004).

[82] G. B. Partridge, K. E. Strecker, R. I. Kamar, M. W. Jack, and R. G. Hulet, "Molecular probe of pairing in the BEC-BCS crossover", *Phys. Rev. Lett.* **95**, 020404 (2005).

[83] S. Chu, "Nobel Lecture: The manipulation of neutral particles", *Rev. Mod. Phys.* **70**, 685 (1998).

[84] C. N. Cohen-Tannoudji, "Nobel Lecture: Manipulating atoms with photons", *Rev. Mod. Phys.* **70**, 707 (1998).

[85] W. D. Phillips, "Nobel Lecture: Laser cooling and trapping of neutral atoms", *Rev. Mod. Phys.* **70**, 721 (1998).

[86] K. Huang, *Statistical Mechanics*, (John Wiley & Sons, New York, 1987).

[87] C. Cohen-Tannoudji, "Atomic motion in laser light", in *Proceeding of the summer school in Les Houches 1990: Fundamental Processes in Quantum Optics*, edited by J. Dalibard, J. M. Raimond, and J. Zinn-Justin Les Houches, Session LIII, 1990, (Elsevier Science B.V. 1992).

[88] J. F. Annett, *Superconductivity, superfluidis, and condensates*, (Oxford, New York, 2004).

[89] A. J. Leggett, "Bose-Einstein condensation in the alkali gases: Some fundamental concepts", *Rev. Mod. Phys.* **73**, 307 (2001).

[90] W. Petrich, M. H. Anderson, J. R. Ensher, and E. A. Cornell, "Stable, tightly confining magnetic trap for evaporative cooling of neutral atoms", *Phys. Rev. Lett.* **74**, 3352 (1995).

[91] D. E. Pritchard, "Cooling neutral atoms in a magnetic trap for precision spectroscopy", *Phys. Rev. Lett.* **51**, 1336 (1983).

[92] F. Dalfovo, S. Giorgini, L. P. Pitaevskii, and S. Stringari, "Theory of Bose-Einstein condensation in trapped gases", *Rev. Mod. Phys* **71**, 463 (1999).

[93] E. M. Lifshitz and L. D. Landau, *Quantum mechanics: non-relativistic theory*, third ed., (Butterworth-Heinemann, Oxford, 1981).

[94] S. Inouye, M. R. Andrews, J. Stenger, H. J. Miesner, D. M. Stamper-Kurn, and W. Ketterle, "Observation of Feshbach resonances in a Bose-Einstein condensate", *Nature* **392**, 151 (1998).

[95] J. L. Roberts, N. R. Claussen, J. P. Burke Jr., C. H. Greene, E. A. Cornell, and C. E. Wieman, "Resonant magnetic field control of elastic scattering of cold ^{85}Rb", *Phys. Rev. Lett.* **81**, 5109 (1998).

[96] M. Greiner, O. Mandel, T. Esslinger, T. W. Hansch, and I. Bloch, "Quantum phase transition from a superfluid to a Mott insulator in a gas of ultracold atoms", *Nature* **415**, 39 (2002).

[97] B. DeMarco and D. S. Jin, "Onset of Fermi degeneracy in a trapped atomic gas", *Science* **285**, 1703 (1999).

[98] A. G. Truscott, K. E. Strecker, W. I. McAlexander, G. B. Partridge, and R. G. Hulet, "Observation of Fermi pressure in a gas of trapped atoms", *Science* **291**, 2570 (2001).

[99] F. Schreck, L. Khaykovich, K. L. Corwin, G. Ferrari, T. Bourdel, J. Cubizolles, and C. Salomon, "Quasipure Bose-Einstein condensate immersed in a Fermi sea", *Phys. Rev. Lett.* **87**, 080403 (2001).

[100] S. R. Granade, M. E. Gehm, K. M. O'Hara, and J. E. Thomas, "All-optical production of a degenerate Fermi gas", *Phys. Rev. Lett.* **88**, 120405 (2002).

[101] Z. Hadzibabic, C. A. Stan, K. Dieckmann, S. Gupta, M. W. Zwierlein, A. Görlitz, and W. Ketterle, "Two species mixture of quantum degenerate Bose and Fermi gases", *Phys. Rev. Lett.* **88**, 160401 (2002).

[102] G. Roati, F. Riboli, G. Modugno, and M. Inguscio, "Fermi-Bose quantum degenerate ^{40}K-^{87}Rb mixture with attractive interaction", *Phys. Rev. Lett.* **89**, 150403 (2002).

[103] J. Goldwin, S. Inouye, M. L. Olsen, B. Newman, B. D. DePaola, and D. S. Jin, "Measurement of the interaction strength in a Bose-Fermi mixture with ^{87}Rb and ^{40}K", *Phys. Rev. A* **70**, 021601 (2004).

[104] M. Bartenstein, A. Altmeyer, S. Riedl, S. Jochim, C. Chin, J. Hecker Denschlag, and R. Grimm, "Crossover from a molecular Bose-Einstein condensate to a degenerate Fermi gas", *Phys. Rev. Lett.* **92**, 120401 (2004).

[105] M. Köhl, H. Moritz, T. Stöferle, K. Günter, and T. Esslinger, "Fermionic atoms in a three dimensional optical lattice: Observing Fermi surfaces, dynamics, and interactions", *Phys. Rev. Lett.* **94**, 080403 (2005).

[106] C. Ospelkaus, S. Ospelkaus, K. Sengstock, and K. Bongs, "Interaction-driven dynamics of ^{40}K-^{87}Rb fermion-boson gas mixtures in the large-particle-number limit", *Phys. Rev. Lett.* **96**, 020401 (2006).

[107] H. T. C. Stoof, M. Houbiers, C. A. Sackett, and R. G. Hulet, "Superfluidity of spin-polarized ^{6}Li", *Phys. Rev. Lett.* **76**, 10 (1996).

[108] R. Combescot, "Trapped ^{6}Li: A high Tc superfluid?", *Phys. Rev. Lett.* **83**, 3766 (1999).

[109] M. Holland, S. J. J. M. F. Kokkelmans, M. L. Chiofalo, and R. Walser, "Resonance superfluidity in a quantum degenerate Fermi gas", *Phys. Rev. Lett.* **87**, 120406 (2001).

[110] E. Timmermans, K. Furuya, P. W. Milonni, and A. K. Kerman, "Prospect of creating a composite Fermi-Bose superfluid", *Phys. Lett. A* **285**, 228 (2001).

[111] Y. Ohashi and A. Griffin, "BCS-BEC crossover in a gas of Fermi atoms with a Feshbach resonance", *Phys. Rev. Lett.* **89**, 130402 (2002).

[112] M. Houbiers, H. T. C. Stoof, W. I. McAlexander, and R. G. Hulet, "Elastic and inelastic collisions of ^{6}Li atoms in magnetic and optical traps", *Phys. Rev. A* **57**, R1497 (1998).

[113] J. L. Bohn, "Cooper pairing in ultracold ^{40}K using Feshbach resonances", *Phys. Rev. A* **61**, 053409 (2000).

[114] T. Loftus, C. A. Regal, C. Ticknor, J. L. Bohn, and D. S. Jin, "Resonant control of elastic collisions in an optically trapped Fermi gas of atoms", *Phys. Rev. Lett.* **88**, 173201 (2002).

[115] K. M. O'Hara, S. L. Hemmer, S. R. Granade, M. E. Gehm, J. E. Thomas, V. Venturi, E. Tiesinga, and C. J. Williams, "Measurement of the zero crossing in a Feshbach resonance of fermionic ^{6}Li", *Phys. Rev. A* **66**, 041401 (2002).

[116] K. Dieckmann, C. A. Stan, S. Gupta, Z. Hadzibabic, C. H. Schunck, and W. Ketterle, "Decay of an ultracold fermionic lithium gas near a Feshbach resonance", *Phys. Rev. Lett.* **89**, 203201 (2002).

[117] C. A. Regal, C. Ticknor, J. L. Bohn, and D. S. Jin, "Tuning p-wave interactions in an ultracold Fermi gas of atoms", *Phys. Rev. Lett.* **90**, 053201 (2003).

[118] C. A. Regal, C. Ticknor, J. L. Bohn, and D. S. Jin, "Creation of ultracold molecules from a Fermi gas of atoms", *Nature* **424**, 47 (2003).

[119] K. E. Strecker, G. B. Partridge, and R. G. Hulet, "Conversion of an atomic Fermi gas to a long-lived molecular Bose gas", *Phys. Rev. Lett.* **91**, 080406 (2003).

[120] J. Cubizolles, T. Bourdel, S. J. J. M. F. Kokkelmans, G. V. Shlyapnikov, and C. Salomon, "Production of long-lived ultracold Li_2 molecules from a Fermi gas", *Phys. Rev. Lett.* **91**, 240401 (2003).

[121] S. Jochim, M. Bartenstein, A. Altmeyer, G. Hendl, C. Chin, J. Hecker Denschlag, and R. Grimm, "Pure gas of optically trapped molecules created from fermionic atoms", *Phys. Rev. Lett.* **91**, 240402 (2003).

[122] C. A. Regal, M. Greiner, and D. S. Jin, "Lifetime of molecule-atom mixtures near a Feshbach resonance in ^{40}K", *Phys. Rev. Lett.* **92**, 083201 (2004).

[123] M. Bartenstein, A. Altmeyer, S. Riedl, S. Jochim, C. Chin, J. Hecker Denschlag, and R. Grimm, "Collective excitations of a degenerate gas at the BEC-BCS crossover", *Phys. Rev. Lett.* **92**, 203201 (2004).

[124] J. Kinast, S. L. Hemmer, M. E. Gehm, A. Turlapov, and J. E. Thomas, "Evidence for superfluidity in a resonantly interacting Fermi gas", *Phys. Rev. Lett.* **92**, 150402 (2004).

[125] J. Kinast, A. Turlapov, and J. E. Thomas, "Breakdown of hydrodynamics in the radial breathing mode of a strongly interacting Fermi gas", *Phys. Rev. A* **70**, 051401 (2004).

[126] C. A. Regal, M. Greiner, S. Giorgini, M. Holland, and D. S. Jin, "Momentum distribution of a Fermi gas of atoms in the BCS-BEC crossover", *Phys. Rev. Lett.* **95**, 250404 (2005).

[127] J. Kinast, A. Turlapov, J. E. Thomas, Q. J. Chen, J. Stajic, and K. Levin, "Heat capacity of a strongly interacting Fermi gas", *Science* **307**, 1296 (2005).

[128] C. Chin, M. Bartenstein, A. Altmeyer, S. Riedl, S. Jochim, J. H. Denschlag, and R. Grimm, "Observation of the pairing gap in a strongly interacting Fermi gas", *Science* **305**, 1128 (2004).

[129] M. Greiner, C. A. Regal, and D. S. Jin, "Probing the excitation spectrum of a Fermi gas in the BCS-BEC crossover regime", *Phys. Rev. Lett.* **94**, 070403 (2005).

[130] M. Zwierlein, J. Abo-Shaeer, A. Schirotzek, C. Schunck, and W. Ketterle, "Vortices and superfluidity in a strongly interacting Fermi gas", *Nature* **435**, 1047 (2005).

[131] C. Ticknor, C. A. Regal, D. S. Jin, and J. L. Bohn, "Multiplet structure of Feshbach resonances in nonzero partial waves", *Phys. Rev. A* **69**, 042712 (2004).

[132] J. Zhang, E. G. M. van Kempen, T. Bourdel, L. Khaykovich, J. Cubizolles, F. Chevy, M. Teichmann, L. Tarruell, S. J. J. M. F. Kokkelmans, and C. Salomon, "p-wave Feshbach resonances of ultracold ^{6}Li", *Phys. Rev. A* **70**, 030702(R) (2004).

[133] C. H. Schunck, M. W. Zwierlein, C. A. Stan, S. M. F. Raupach, W. Ketterle, A. Simoni, E. Tiesinga, C. J. Williams, and P. S. Julienne, "Feshbach resonances in fermionic ^{6}Li", *Phys. Rev. A* **71**, 045601 (2005).

[134] K. Günter, T. Stöferle, H. Moritz, M. Köhl, and T. Esslinger, "p-wave interactions in low-dimensional fermionic gases", *Phys. Rev. Lett.* **95**, 230401 (2005).

[135] S. S. Botelho and C. A. R. Sá de Melo, "Quantum phase transition in the BCS-to-BEC evolution of p-wave Fermi gases", *J. Low. Temp. Phys.* **140**, 409 (2005).

[136] V. Gurarie, L. Radzihovsky, and A. V. Andreev, "Quantum phase transitions across a p-wave Feshbach resonance", *Phys. Rev. Lett.* **94**, 230403 (2005).

[137] C.-H. Cheng and S.-K. Yip, "Anisotropic Fermi superfluid via p-wave Feshbach resonance", *Phys. Rev. Lett.* **95**, 070404 (2005).

[138] T.-L. Ho and R. B. Diener, "Fermion superfluids of nonzero orbital angular momentum near resonance", *Phys. Rev. Lett.* **94**, 090402 (2005).

[139] Y. Ohashi, "BCS-BEC crossover in a gas of Fermi atoms with a p-wave Feshbach resonance", *Phys. Rev. Lett.* **94**, 050403 (2005).

[140] M. Iskin and C. A. R. Sá de Melo, "Evolution from BCS to BEC superfluidity in p-wave Fermi gases", *Phys. Rev. Lett.* **96**, 040402 (2006).

[141] V. L. Berezinskii, "Destruction of long-range order in one-dimensional and two-dimensional systems possessing a continuous symmetry group .2. Quantum systems", *Sov. Phys. JETP* **34**, 610 (1972).

[142] J. M. Kosterlitz and D. J. Thouless, "Long-range order and metastability in 2-dimensional solids and superfluids", *J. Phys. C: Solid State Physics* **5**, L124 (1972).

[143] J. M. Kosterlitz and D. J. Thouless, "Ordering, metastability and phase transitions in 2-dimensional systems", *J. Phys. C: Solid State Physics* **6**, 1181 (1973).

[144] L. N. Cooper, "Bound electron pairs in a degenerate Fermi gas", *Phys. Rev.* **104**, 1189 (1956).

[145] J. B. Ketterson and S. N. Song, *Superconductivity*, (Cambridge Univeristy Press, Cambridge, U.K., 1999).

[146] V. P. Mineev and K. V. Samokhin, *Introduction to Unconventional Superconductivity*, (Gordon and Breach, Amsterdam, 1999).

[147] P. W. Anderson and W. F. Brinkman, "Theory of anisotropic superfluidity in ^{3}He", in *The Helium Liquids*, edited by J. G. M. Armitage and I. E. Farquhar, (Academic Press, New York, 1975).

[148] J. W. Negele and H. Orland, *Quantum many-particle systems*, (Westview Press, Boulder, 1998).

[149] G. D. Mahan, *Many-Particle Physics*, third ed., (Plenum, New York, 2000).

[150] R. L. Stratonovich, "A method for the computation of quantum distribution functions", *Dokl. Akad. Nauk SSSR* **115**, 1097 (1957).

[151] J. Hubbard, "Calculation of partition functions", *Phys. Rev. Lett.* **3**, 77 (1959).

[152] N. Goldenfeld, *Lectures on Phase Transitions and the Renormalization Group*, (Perseus Books, MA, 1992).

[153] E. Dagotto, "Correlated electrons in high-temperature superconductors", *Rev. Mod. Phys.* **66**, 763 (1994).

[154] Y. Maeno, H. Hashimoto, K. Yoshida, S. Nishizaki, T. Fujita, J. G. Bednorz, and F. Lichtenberg, "Superconductivity in a layered Perovskite without copper", *Nature* **372**, 532 (1994).

[155] C. Pfleiderer, M. Uhlarz, S. M. Hayden, R. Vollmer, H. V. Lohneysen, N. R. Bernhoeft, and G. G. Lonzarich, "Coexistence of superconductivity and ferromagnetism in the d-band metal $ZrZn_2$", *Nature (London)* **412**, 58 (2001).

[156] S. S. Saxena, P. Agarwal, K. Ahilan, F. M. Grosche, R. K. W. Haselwimmer, M. J. Steiner, E. Pugh, I. R. Walker, S. R. Julian, P. Monthoux, G. G. Lonzarich, A. Huxley, I. Sheikin, D. Braithwaite, and J. Flouquet, "Superconductivity on the border of itinerant-electron ferromagnetism in UGe_2", *Nature (London)* **406**, 587 (2000).

[157] L. Balicas, K. Behnia, W. Kang, E. Canadell, P. Auban-Senzier, D. Jérome, M. Ribault, and J. M. Fabre, "Superconductivity and magnetic-field-induced spin-density waves in the $(TMTTF)_2X$ family", *J. Phys. I (Paris)* **4**, 1539 (1994).

[158] J. F. Kwak, J. E. Schirber, R. L. Greene, and E. M. Engler, "Magnetic quantum oscillations in Tetramethyltetraselenafulvalenium Hexafluorophosphate $[(TMTSF)_2PF_6]$", *Phys. Rev. Lett.* **46**, 1296 (1981).

[159] G. Saito and S. Kagoshima, *The Physics and Chemistry of Organic Superductors*, (Springer-Verlag, Berlin, 1990).

[160] T. Osada, A. Kawasumi, S. Kagoshima, N. Miura, and G. Saito, "Commensurability effect of magnetoresistance anisotropy in the quasi-one-dimensional conductor tetramethyltetraselenafulvalenium perchlorate, $(TMTSF)_2ClO_4$", *Phys. Rev. Lett.* **66**, 1525 (1991).

[161] T. Osada, S. Kagoshima, and N. Miura, "Third angular effect of magnetoresistance in quasi-one-dimensional conductors", *Phys. Rev. Lett.* **77**, 5261 (1996).

[162] M. J. Naughton, I. J. Lee, P. M. Chaikin, and G. M. Danner, "Critical fields and magnetoresistance in the molecular superconductors $(TMTSF)_2X$", *Synth. Metals* **85**, 1481 (1997).

[163] G. M. Danner, N. P. Ong, and P. M. Chaikin, "Comment on charge localization in $(TMTSF)_2ClO_4$", *Phys. Rev. Lett.* **78**, 983 (1997).

[164] S. P. Strong, D. G. Clarke, and P. W. Anderson, "Magnetic field induced confinement in strong correlated anisotropic materials", *Phys. Rev. Lett.* **73**, 1007 (1994).

[165] T. Ishiguro, K. Yamaji, and G. Saito, *Organic Superconductors*, second ed., (Springer, Berlin, 1998).

[166] C. A. R. Sá de Melo, "Singlet versus triplet superconductivity in quasi-one-dimensional systems: Magnetic field effects", in *The superconducting state in magnetic fields: special topics and new trends*, edited by C. A. R. Sá de Melo, chap. 15, p. 296, (World Scientific, Singapore, 1998).

[167] C. S. Jacobsen, D. B. Tanner, and K. Bechgaard, "Optical and infrared properties of tetramethyltetraselenafulvalene $[(TMTSF)_2X]$ and tetramethyltetrathiafulvalene $[(TMTTF)_2X]$ compounds", *Phys. Rev. B* **28**, 7019 (1983).

[168] N. Thorup, G. Rindorf, H. Soling, and K. Bechgaard, "The structure of di(2,3,6,7-tetramethyl-1,4,5,8-tetraselenafulvalenium) hexafluorophosphate, $(TMTSF)_2PF_6$, the first superconducting organic solid", *Acta. Cryst. B* **37**, 1236 (1981).

[169] G. Rindorf, H. Soling, and N. Thorup, "The structure of di(2,3,6,7-tetramethyl-1,4,5,8-tetraselenafulvalenium) perrhenate, $(TMTSF)_2ReO_4$, and perchlorate, $(TMTSF)_2ClO_4$", *Acta. Cryst. B* **38**, 2805 (1982).

[170] Z. Tešanović, M. Rasolt, and L. Xing, "Quantum limit of a flux lattice: Superconductivity and magnetic field in a new relationship", *Phys. Rev. Lett.* **63**, 2425 (1989).

[171] M. R. Norman, H. Akera, and A. H. MacDonald, "Landau quantization and superconductivity at high magnetic fields", in *Physical Phenomena in High Magnetic Fields*, edited by E. Manousakis, P. Schlottmann, P. Kumar, K. Bedell, and F. Mueller, (Addison-Wesley, New York, 1992).

[172] A. K. Rajagopal and R. Vasudevan, "Superconducting state of an electron gas in a homogeneous magnetic field", *Phys. Lett.* **20**, 585 (1966).

[173] L. W. Gruenberg and L. Gunther, "Effect of orbital quantization on the critical field of type-II superconductors", *Phys. Rev.* **176**, 606 (1968).

[174] K. Murata, H. Anzai, K. Kajimura, T. Ishiguro, and G. Saito, "Superconducting transition of $(TMTSF)_2ClO_4$ in magnetic fields", *Mol. Cryst. Liq. Cryst.* **79**, 283 (1982).

[175] K. Murata, M. Tokumoto, H. Anzai, K. Kajimura, and T. Ishiguro, "Upper critical field of the anisotropic organic superconductors, $(TMTSF)_2ClO_4$", *Jpn. J. Appl. Phys.* **26**, 1367 (1987).

[176] P. M. Chaikin, T. Tiedje, and A. N. Bloch, "Sound-velocity measurements on $(TMTSF)_2PF_6$", *Solid State Commun.* **41**, 739 (1982).

[177] D. U. Gubser, W. W. Fuller, T. O. Poehler, J. Stokes, D. O. Cowan, M. Lee, and A. N. Bloch, "Resistive and magnetic-susceptibility transitions in superconducting $(TMTSF)_2CLO_4$", *Mol. Cryst. Liq. Cryst.* **79**, 225 (1982).

[178] P. M. Chaikin, M. Y. Choi, and R. L. Greene, "Superconductivity and metal-insulator transition in $(TMTSF)_2X$", *J. Magn. Magn. Mater.* **31-34**, 1268 (1983).

[179] Y. N. Ovchinnikov and V. Z. Kresin, "Recovery of superconductivity and the critical field in layered superconductors", *Phys. Rev. B* **54**, 1251 (1996).

[180] G. Kotliar and C. M. Varma, "Low-temperature upper-critical-field anomalies in clean superconductors", *Phys. Rev. Lett.* **77**, 2296 (1996).

[181] T. Takahashi, H. Kawamura, T. Ohyama, Y. Maniwa, K. Murata, and G. Saito, "Pressure dependence of SDW properties in the organic conductor $(TMTSF)_2PF_6$", *J. Phys. Soc. Jpn.* **58**, 703 (1989).

[182] L. J. Azevedo, J. E. Schirber, and E. M. Engler, "^{13}C nuclear magnetic resonance in bis-tetramethyltetraselenafulvalenium hexafluorophosphide $[(TMTSF)_2PF_6]$ under pressure", *Phys. Rev. B* **29**, 464 (1984).

[183] F. Creuzet, C. Bourbonnais, L. G. Caron, D. Jérome, and A. Moradpour, "^{77}Se NMR spin-lattice relaxation rate properties in the $(TMTSF)_2X$ series under pressure: cooperative phenomena and SDW transition", *Synth. Metals* **19**, 277 (1987).

[184] S. Valfells, P. Kuhns, A. Kleinhammes, J. S. Brooks, W. Moulton, S. Takasaki, J. Yamada, and H. Anzai, "Spin-density-wave in $(TMTSF)_2PF_6$: A ^{77}Se NMR study at high magnetic fields", *Phys. Rev. B* **56**, 2585 (1997).

[185] D. Podolsky, E. Altman, T. Rostunov, and E. Demler, "Competition between triplet superconductivity and antiferromagnetism in quasi-one-dimensional electron systems", *Phys. Rev. B* **70**, 224503 (2004).

[186] M. Tinkham, *Group Theory and Quantum Mechanics*, (McGraw-Hill, New York, 1964).

[187] C. Herring, "Exchange interactions among itinerant electrons", in *Magnetism IV*, edited by G. T. Rado and H. Suhl, (Academic Press, New York, 1966).

[188] R. M. White, *Quantum Theory of Magnetism*, second ed., (Springer-Verlag, Belin, 1983).

[189] J. Solyom, "The Fermi gas model of one-dimensional conductors", *Adv. Phys.* **28**, 201 (1979).

[190] K. Mortensen, Y. Tomkiewicz, T. D. Schultz, and E. M. Engler, "Antiferromagnetic ordering in the organic conductor bis-tetramethyltetraselenafulvalene-Hexafluorophosphate $(TMTSF)_2PF_6$", *Phys. Rev. Lett.* **46**, 1234 (1981).

[191] P. M. Chaikin and T. C. Lubensky, *Principles of Condensed Matter Physics*, (Cambridge University Press, Cambridge, U.K., 1997).

[192] J. M. Delrieu, M. Roger, Z. Toffano, A. Moradpour, and K. Bechgaard, "NMR proton lineshape in $(TMTSF)_2X$: Incommensurability of nesting vector and order parameter", *J. Phys. (Paris)* **47**, 839 (1986).

[193] T. Takahashi, Y. Maniwa, H. Kawamura, and G. Saito, "Determination of SDW characteristics in $(TMTSF)_2PF_6$ by H-1-NMR analysis", *J. Phys. Soc. Jpn.* **55**, 1364 (1986).

[194] Y. Kagan, E. L. Surkov, and G. V. Shlyapnikov, "Evolution of a Bose-condensed gas under variations of the confining potential", *Phys. Rev. A* **54**, R1753 (1996).

[195] Y. Castin and R. Dum, "Bose-Einstein condensates in time dependent traps", *Phys. Rev. Lett.* **77**, 5315 (1996).

[196] F. Dalfovo, C. Minniti, and L. P. Pitaevskii, "Frequency shift and mode coupling in the nonlinear dynamics of a Bose-condensed gas", *Phys. Rev. A* **56**, 4855 (1997).

[197] M. J. Holland, D. Jin, M. L. Chiofalo, and J. Cooper, "Emergence of interaction effects in Bose-Einstein condensation", *Phys. Rev. Lett.* **78**, 3801 (1997).

[198] M. Brewczyk, K. Rzazewski, and C. W. Clark, "Strong-field driving of a dilute atomic Bose-Einstein condensate", *Phys. Rev. A* **57**, 488 (1998).

[199] C. Menotti, P. Pedri, and S. Stringari, "Expansion of an interacting Fermi gas", *Phys. Rev. Lett.* **89**, 250402 (2002).

[200] M. R. Andrews, C. G. Townsend, H. J. Miesner, D. S. Durfee, D. M. Kurn, and W. Ketterle, "Observation of interference between two Bose condensates", *Science* **275**, 637 (1997).

[201] Y. Shin, M. Saba, T. A. Pasquini, W. Ketterle, D. E. Pritchard, and A. E. Leanhardt, "Atom interferometry with Bose-Einstein condensates in a double-well potential", *Phys. Rev. Lett.* **92**, 050405 (2004).

[202] T. Schumm, S. Hofferberth, L. M. Andersson, S. Wildermuth, S. Groth, I. Bar-Joseph, J. Schmiedmayer, and P. Kruger, "Matter-wave interferometry in a double well on an atom chip", *Nature Physics* **1**, 57 (2005).

[203] S. Fölling, F. Gerbier, A. Widera, O. Mandel, T. Gericke, and I. Bloch, "Spatial quantum noise interferometry in expanding ultracold atom clouds", *Nature* **434**, 481 (2005).

[204] C. A. R. Sá de Melo, M. Randeria, and J. R. Engelbrecht, "Crossover from BCS to Bose superconductivity: Transition temperature and time-dependent Ginzburg-Landau theory", *Phys. Rev. Lett.* **71**, 3202 (1993).

[205] U. Fano, "Effects of configuration interaction on intensities and phase shifts", *Phys. Rev.* **124**, 1866 (1961).

[206] H. Feshbach, "A unified theory of nuclear reactions II", *Ann. Phys.* **19**, 287 (1962).

[207] W. C. Stwalley, "Stability of spin-aligned hydrogen at low temperatures and high magnetic fields: New field-dependent scattering resonance and predissociations", *Phys. Rev. Lett.* **37**, 1628 (1976).

[208] E. Tiesinga, B. J. Verhaar, and H. T. C. Stoof, "Threshold and resonance phenomena in ultracold ground-state collisions", *Phys. Rev. A* **47**, 4114 (1993).

[209] C. A. Regal, "Experimental realization of BCS-BEC crossover physics with a Fermi gas of atoms", *PhD Thesis, University of Colorado* (2005).

[210] M. H. Szymánska, K. Góral, T. Köhler, and K. Burnett, "Conventional character of the BCS-BEC crossover in ultracold gases of ^{40}K", *Phys. Rev. A* **72**, 013610 (2005).

[211] K. Góral, T. Köhler, S. A. Gardiner, E. Tiesinga, and P. S. Julienne, "Adiabatic association of ultracold molecules via magnetic-field tunable interactions", *J. Phys. B* **37**, 3457 (2004).

[212] R. G. Newton, *Scattering theory of waves and particles*, (Springer, New York, 1982).

[213] B. DeMarco, J. L. Bohn, J. P. Burke Jr., M. Holland, and D. S. Jin, "Measurement of p-wave threshold law using evaporatively cooled fermionic atoms", *Phys. Rev. Lett.* **82**, 4208 (1999).

[214] H. R. Sadeghpour, J. L. Bohn, M. J. Cavagnero, B. D. Esry, I. I. Fabrikant, J. H. Macek, and A. R. P. Rau, "Collisions near threshold in atomic and molecular physics", *J. Phys. B* **33**, R93 (2000).

[215] I. V. Tokatly, "Bose representation for a strongly coupled nonequilibrium fermionic superfluid in a time-dependent trap", *Phys. Rev. A* **70**, 043601 (2004).

[216] W. Zhang and C. A. R. Sá de Melo, "Time evolution and matter wave interference in Fermi condensates", *cond-mat/0603561* (2006).

[217] M. Iskin and C. A. R. Sá de Melo, "Nonzero orbital angular moemtnum superfluidity in ultracold Fermi gases", *cond-mat/0602157* (2006).

[218] M. Naraschewski, H. Wallis, A. Schenzle, J. I. Cirac, and P. Zoller, "Interference of Bose condensates", *Phys. Rev. A* **54**, 2185 (1996).

[219] T. N. De Silva and E. J. Mueller, "Surface tension in unitary Fermi gases with population imbalance", *Phys. Rev. Lett.* **97**, 070402 (2006).

[220] M. Iskin and C. A. R. Sá de Melo, "Two-species fermion mixtures with population imbalance", *cond-mat/0604184* (2006).

[221] C. C. Chien, Q. Chen, Y. He, and K. Levin, "Intermediate temperature superfluidity in an atomic Fermi gas with population imbalance", *cond-mat/0605039* (2006).

[222] G. D. Lin, W. Yi, and L. M. Duan, "Superfluid shells for trapped fermions with mass and population imbalance", *cond-mat/0607664* (2006).

VITA

Wei Zhang was born on January, 1980 in the city of Tianjin, which is about 100 miles south-east to Beijing, China. He grew up in Tianjin and attended Yaohua High School in 1992, where he spent five years of study with unforgettable happiness. Upon graduation from high school in 1997 he left his hometown and enrolled at the Peking University at Beijing to begin his study of Physics. In the four years of study in Peking, he was very active in both the Department of Physics and the Society of Physics Students. He was also an active participant in experimental condensed matter research starting from his junior year, while in the same year he became a recipient of Guanghua Scholarship. Under the guidance and mentorship of Dr. Han Zhang, he studied electrical and thermal transport properties of high temperature superconductors. It was these research experience stimulated his interests in condensed matter physics, especially in superconductivity and superfluidity. After graduating from Peking University in 2001, he enrolled at Georgia Institute of Technology to pursue his Ph.D. degree in Physics. In 2002, he passed the comprehensive examination for Ph.D. candidacy and received the Henry S. Valk award, which honors the attendee with the highest score. After that, he began his doctoral thesis work in theoretical condensed matter physics, and became a Gilbert F. Amelio fellow in 2005. In addition, he also gained great interests in Mathematics, and received his M.S. degree in Mathematics under the mentorship of Dr. Stavros Garoufalidis in 2006.